Synergistic Effect of Hemodynamic Environment and Dyslipidemia on Endothelial Biomechanics

BY

ELIZABETH LYNN LE MASTER
B.S., Bioengineering, University of Illinois at Chicago, 2009
B.S., Learning Behavior Specialist, Illinois State University, Normal, 2001

THESIS
Submitted as partial fulfillment of the requirements
for the degree of Doctor of Philosophy in Bioengineering
in the Graduate College of the
University of Illinois at Chicago, 2017
Chicago, Illinois

Defense Committee:

Irena Levitan, Chair and Advisor
Richard Minshall, Co-advisor, Pharmacology
David Eddington
James Lee
Yun Fang, University of Chicago

ACKNOWLEDGEMENTS

First and foremost I want to thank my advisor Dr. Irena Levitan for her support and guidance throughout my PhD studies. She has helped me develop my critical thinking skills and my ability to design and conduct meaningful research plans. I am grateful to have her as an advisor, as she is an excellent example of a successful woman scientist and professor. I am also thankful to have such a knowledgeable, accessible and diverse thesis committee: Dr. Richard Minshall, Dr. David Eddington, Dr. Yun Fang and Dr. James Lee. I appreciate all of the time and guidance they have all given to make this research project possible.

I would also like to thank the staff, faculty and fellow graduate students from both the Bioengineering department and the Pulmonary Critical Care division for their support in my academic research studies. They have helped to ensure that I have fulfilled all of the requirements necessary to make the completion of this PhD possible.

Last but not least, I would like to thank my family and friends for all their love and encouragement throughout my PhD research studies and my life in general. I would especially like to thank my grandpa and my mom for fostering a love of science at a young age and for my dad who keeps encouraging me to fulfill my goals.

TABLE OF CONTENTS

LIST OF FIGURES

LIST OF ABBREVIATIONS

7KC	7-ketocholesterol
AFM	Atomic force microscopy
A-P	Athero-protective
Cav1	Caveolin-1 protein
DiI-oxLDL	1,1'-dioctadecyl-3,3,3',3'-tetramethyl-indocarboncyanine perchlorate oxLDL
DF	Disturbed flow
EC	Endothelial cell
eNOS	Endothelial nitric oxide synthase
GP	General polarization value
HAEC	Human aortic ECs
HMVEC	Human microvascular ECs
KO	Knockout
LF	Laminar flow
LDL	Low density lipoprotein
MMVEC	Mouse microvascular ECs
MP	Multi-photon microscope
MLCP	Myosin light chain phosphatase
NO	Nitric oxide
OF	Oscillatory flow
OxLDL	Oxidized low density lipoprotein
OxPCs	Oxidized phosphatidylcholines
P-A	Pro-atherogenic
PDMS	Polydimethysiloxane
PGPC	1-palmitoyl-2-glutaroyl-sn-glycero-3-phosphocholine
POVPC	1-palmitoyl-2-(5-oxovaleroyl)-sn-glycero-3-phosphocholine
ROCK	Rho Kinase
ROS	Reactive oxygen species
SMC	Smooth muscle cell
SEM	Sub-endothelial extracellular matrix

SUMMARY

The onset and progression of atherosclerosis is due to the combination of several different factors. Plaque development at its nascent stage begins at the endothelial monolayer lining the inner arterial surface. Disturbed flow is well-known to induce endothelial dysfunction and combined with plasma dyslipidemia facilitate atherosclerotic plaque formation. Specifically, it has been shown that atherosclerosis develops in the vascular regions exposed to recirculating disturbed flow patterns and patients with cardiovascular disease have increased plasma levels of pro-atherogenic low density lipoprotein and its oxidized form. Little research, though, has focused on the combined impact of disturbed flow and dyslipidemia on endothelial biomechanical properties. In this dissertation, the overall goal was to determine the impact of disturbed flow on endothelial stiffness and the role of oxidized LDL/dyslipidemia in this process. We provide evidence that oxLDL uptake into endothelial cells is enhanced under disturbed flow, a process that is mediated by oxLDL receptor CD36, but not Lox1, and endocytotic caveolae. Furthermore, this increase in oxLDL uptake resulted in cellular stiffening *in vitro* and *ex vivo* measurements show enhanced stiffness in the pro-atherogenic disturbed flow regions of the aortic arch in WT mice, an effect that is abolished in mice globally deficient in CD36 and caveolin1 protein. This observation persisted even when challenged with a high fat diet.

In summary, the results provided in this dissertation provide substantial evidence that plasma dyslipidemia results in endothelial stiffening at the pro-atherogenic region of the aortic arch, and demonstrate that this effect is mediated by oxLDL uptake, the oxLDL receptor CD36 and endocytotic caveolae. We propose, therefore, that increased uptake of oxLDL and endothelial stiffening in the athero-prone regions of the aorta are important factors in the local disruption of the endothelial permeability barrier and the onset of the inflammatory response.

CHAPTER 1: Introduction

1.1 Atherosclerosis:

Cardiovascular disease is a class of diseases involving the heart and blood vessels, such as hypertension, aortic aneurisms, heart attacks and stroke. Cardiovascular disease is the leading cause of mortality and morbidity in the United States and other western societies. Hypercholesterolemia is a condition characterized by pathologically high levels of cholesterol in the blood plasma which is a key risk factor for cardiovascular disease. Low density lipoprotein (LDL), the main cholesterol carrier in plasma, is primarily comprised of cholesterol ester, phospholipids and free cholesterol [reviewed by (Levitan et al., 2010)]. A healthy level of LDL in an individual is typically less than 100 mg/dL, whereas pathological levels of LDL are considered by to be above 150 mg/dL [reviewed by (Youngblom et al., 1993)]. Although cholesterol is a necessary component of healthy cellular structure (Ikonen, 2008), lowering the levels of plasma LDL is one of the main courses in the treatment and management of cardiovascular disease.

Atherosclerotic plaque formation is a characteristic of cardiovascular disease and is defined as the accumulation of lipids and inflammatory cells in the inner lining of the arteries, hyper-proliferation of smooth muscle cells, increased deposition of calcium deposits, cell death, and the development of lipid-laden foam cells. The core of the plaque is typically comprised of foam cells with a fibrotic cap. Although plaque composition is heterogeneous, there are three main cellular components: (1) hypocellular fibrosis area, defined as an area of decreased cellular composition and increased scarring of connective tissue; (2) hypercellular fibrosis area, defined as an area of fibrosis comprised of smooth muscle cell (SMC) migrated from the inner medial layer; and a (3) lipid rich area, defined as either macrophage derived foam cell-rich region or an extracellular lipid-rich region (Tracqui et al., 2011).

Plaque development at its nascent stage begins at the endothelial monolayer lining the inner arterial surface, which provides the main barrier between the flowing blood and the surrounding vascular tissue. Atherogenesis is characterized by increased adhesion and chemotactic molecule expression which facilities the capture and internalization of pro-inflammatory leukocytes (including monocytes) into the intimal and medial layers directly underneath the endothelial cells [reviewed by (Libby et al., 2011)]. The endothelial barrier becomes compromised which also allows the entry of LDL into the arterial wall. As shown in Figure 1.1, the LDL particles become trapped in the sub-endothelial extracellular matrix (SEM) through its binding to proteoglycans [reviewed by (Maiolino et al., 2013)]. The monocytes in the arterial wall differentiate into macrophages which stimulate pro-inflammatory reactive oxygen species (ROS) generation and the oxidation of LDL. These macrophages recognize, bind to and engulf both the native and oxidized LDL particles through species specific receptors and through this process become lipid-laden foam cells. SMCs from the medial layer are recruited to the SEM due to the foam cells' production of platelet derived growth factors. The extracellular matrix molecules (collagen and elastin) produced by the SMCs combine with the apoptotic foam cells to become atherosclerotic lipid-laden plaques with a fibrous cap. Excess LDL in the blood plasma, or hyperlipidemia, exacerbates and often accelerates this process [reviewed by (Libby et al., 2011; Maiolino et al., 2013)].

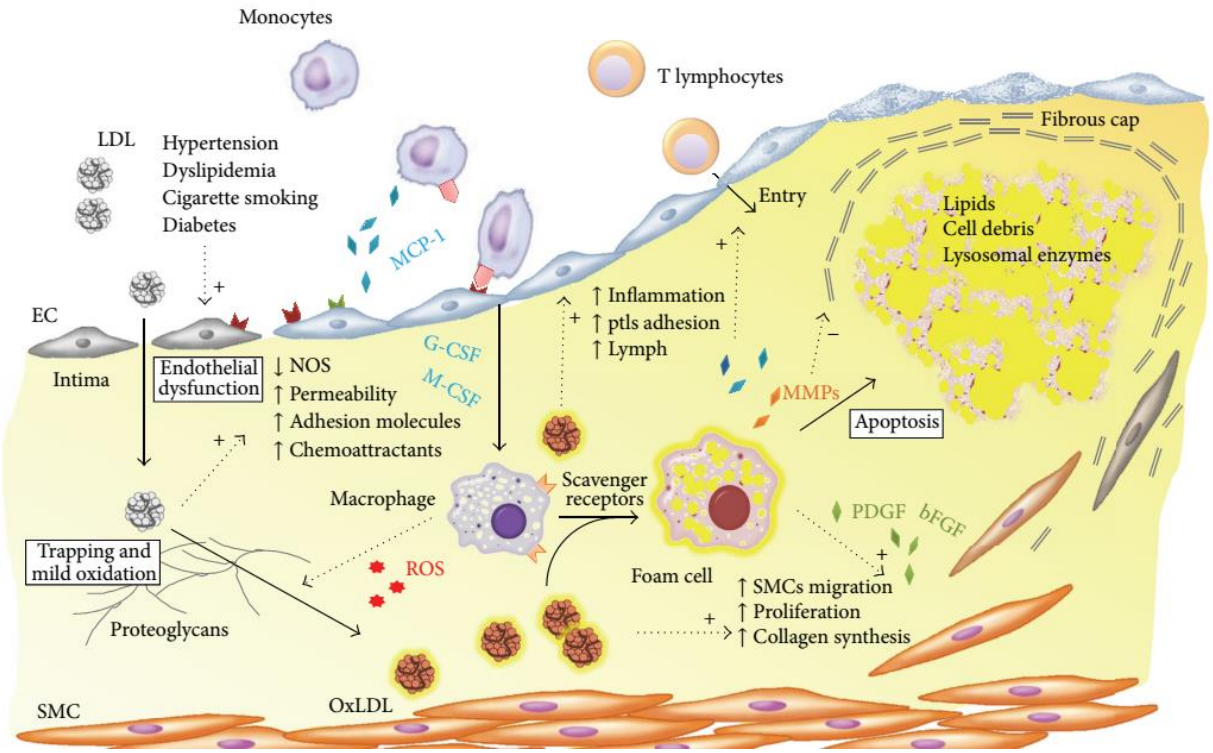

Figure 1.1: Atherosclerotic disease progression on the endothelial and sub-endothelial extracellular matrix.
This schematic view describes the binding of monocytes and entry of LDL to the endothelium. In the sub-endothelial layer, macrophages engulf oxLDL and smooth muscles proliferate, which combine and form a lipid laden plaque with a fibrous cap.
Reprinted with permission (Maiolino et al., 2013).

1.2 OxLDL:

OxLDL, the oxidized form of LDL, is also a major factor in atherosclerosis. There are two main categories of oxLDL: minimally modified oxLDL and fully or extensively oxidized LDL. Minimally modified LDL is comprised mainly of oxidized phosphatidylcholines (oxPCs) and is recognized by the cellular LDL receptor [reviewed by (Goldstein and Brown, 2009)]. Fully oxidized LDL is primarily comprised of oxysterols and becomes bound to a different set of receptors known as scavenger receptors, such as LOX1, CD36 and SRA [reviewed by (Levitan et al., 2010)]. Several studies have shown that mouse models of genetic knockout of LDL and scavenger receptors confer protection against atherosclerotic lesion formation [reviewed by (Goyal et al., 2012; Park, 2014; Pirillo et al., 2013)]. Elevated levels of oxLDL have been found in plaques in both animal and human models of atherosclerosis (Ehara et al., 2001; Yla-Herttuala et al., 1989). Additionally, an increased level of oxLDL in the plasma has been shown in patients with hypercholesterolemia (van Tits et al., 2003), acute myocardial infarction (Ehara et al., 2001) and coronary heart disease [reviewed by (Itabe et al., 2011)]. Several mechanisms have been proposed for the oxidation modification of LDL *in vivo*, including the enzymes 12/15-lipoxygenase and myeloperoxidase, which is secreted by monocytes/macrophages, and several ROS including peroxides and superoxide anions [reviewed by (Maiolino et al., 2013)].

Much research shows that oxLDL has many pro-inflammatory properties, including the impairment of the essential vasodilator nitric oxide (NO), increased ROS, monocyte adhesion molecule expression, activating the NF-KB inflammatory signaling pathway, cytokine production and cytotoxicity to endothelial cells inducing EC apoptosis [reviewed by (Levitan et al., 2010; Lubrano and Balzan, 2014; Maiolino et al., 2013)], though some studies suggest that certain bioactive components of oxLDL have anti-inflammatory properties [reviewed by (Birukov, 2006)]. It has also been shown that oxLDL increases endothelial cell (EC) injury and barrier permeability *in vitro* (May and Qu, 2010) and *in vivo* (Rangaswamy et al., 1997). The disruption

of the EC barrier has been attributed to oxLDL's ability to activate the Rho/RhoA Kinase (ROCK) pathway and inhibit myosin light chain phosphatase (MLCP) (Essler et al., 1999). Activating this pathway enhances transendothelial migration of leukocytes [commentary by (Schaefer and Hordijk, 2015)] leading to foam cell formation and eventually plaque development.

1.3 Hemodynamics:

Although pro-inflammatory LDL and oxLDL are major factors in the development of atherosclerosis, another main component is the hemodynamic environment the endothelial monolayer experiences. Atherosclerotic plaques characteristically form at vascular bifurcations, stenosis and curvatures where blood flow patterns change (VanderLaan et al., 2004). These hemodynamic changes are the result of various factors including arterial geometry, compliance and shear stress value. Shear stress is the frictional fluid force onto a solid surface, such as the EC monolayer. High shear stress unidirectional laminar blood flow (LF) is athero-protective and is found in straight blood vessels with uniform circumference such as the descending and abdominal aortas. Low shear stress bi-directional or recirculating disturbed flow (DF) is pro-atherogenic and is found at bifurcations, stenosis and curvatures, such as the aortic arch, carotid sinus, and femoral veins [reviewed by (Chiu and Chien, 2011)]. It is well-known that LF promotes wound repair and vasodilation and reduces ROS production, adhesion molecule expression and platelet aggregation. DF increases adhesion molecule expression, inflammatory and chemokine genes and promotes an environment of sustained oxidative stress. Additionally, DF decreases nitric oxide production, the expression of antioxidant genes and reduces EC regeneration [reviewed by (Chiu and Chien, 2011)].

Mechanotransduction is the term used to explain how cells respond and adapt to their constant environmental mechanical stimuli. ECs respond to mechanical stimuli such as shear stress through a variety of means, for example the PECAM1/VE-Cadherin/VEGRF complex (Tzima et al., 2005), glycocalyx (Tarbell and Pahakis, 2006), caveolin1 protein (Rizzo et al., 2003), integrins (Katsumi et al., 2004) and endothelial ion channels (Olesen et al., 1988) to name a few. These putative ‘shear stress sensors’ transduce mechanical fluid force through signaling pathways, including the RhoA/ROCK/myosin pathway which inhibits actin polymerization and inactivates MLCP. This inactivation leads to enhanced acto-myosin contraction which impairs

EC barrier functioning leading to leukocyte transendothelial migration [commentary by (Schaefer and Hordijk, 2015)].

Although it is well-known that while disturbed flow by itself causes EC dysfunction and pre-disposes a local region to plaque formation, it is the combination of disturbed flow and hyperlipidemia that leads to the development of atherosclerotic plaques. Only a scarce amount of research, though, has been devoted to the mechanisms of the synergetic effects of DF and hyperlipidemia on endothelial properties. This research shows how oxLDL and hyperlipidemia in combination with DF *in vitro* and *in vivo* contributes to an increase in endothelial stiffening.

1.4 Role of cellular biomechanical properties in EC functioning:

Endothelial dysfunction has been shown in patients with atherosclerosis, coronary arterial disease, heart failure and peripheral arterial occlusive disease (Daiber et al., 2016) and is recognized to be a key factor in the initiation of atherosclerosis. Cellular biomechanics describes the changing physical properties in cells, such as stiffness, contractility and cell membrane fluidity. It is becoming more widely recognized that biomechanics is a driving force in cell development, phenotype and organogenesis: spring forces modify the uncoiling of cytoskeletal actin; osmotic pressure regulates ion channels; tensional forces are required for cell stability; and hemodynamic shear stress is a fluid force on the endothelial monolayer [reviewed by (Mammoto and Ingber, 2010)].

Quantification of the cellular biomechanical property of stiffness can be measured on a micro- or nano-scale using various techniques such as permanent ceramic magnet, pulsatile magnetic tweezers (Collins et al., 2014), micropipette aspiration and atomic force microscopy (Oh et al., 2016). It has been previously shown in our lab that oxLDL induces endothelial stiffness and contractility and that this stiffness can be reversed by the addition of excess cholesterol (Byfield et al., 2006). Although it is a well-known that atherosclerosis is characterized by macroscale stiffness of whole vessels, the stiffness of the endothelial cell monolayer is less defined.

Several factors have been shown to modify endothelial stiffness *in vitro*: cell growth on stiffer 2D substrates or within 3D gels (Byfield et al., 2009), magnetic force applied to a bead coated cell surface (Collins et al., 2012; Collins et al., 2014) and uni-directional laminar flow compared to a static control environment (Sato and Ohashi, 2005). Our previous studies show that the lipid composition of the cell membrane affects endothelial biomechanical properties. Specifically, cells stiffen with exposure to oxLDL and certain oxysterols, such as 7-ketocholesterol (7KC) and 7α-hydroxycholesterol, and by cholesterol depletion (Byfield et al., 2004; Shentu et al., 2012), and is correlated with a decrease in the ordering of lipid membrane domains (Shentu et al.,

2010). Additionally, we have shown that oxLDL exposure in ECs enhanced stress-fiber formation (Kowalsky et al., 2008), which is presumed to increase EC stiffness (Sato and Ohashi, 2005). A recent study from our group has shown that oxLDL exposure also activates this RhoA/ROCK/MLCP pathway leading to increased endothelial stiffening and contractile forces (Oh et al., 2016).

Little is known, though, on the effect of laminar versus disturbed flow on EC biomechanical properties, especially ECs in intact vessels. One recent study showed enhanced endothelial cell responsiveness to pulsatile magnetic tweezers in the DF region of the aortic arch as compared to the LF region of the descending aorta in WT mice (Collins et al., 2014), an effect that was attributed to the increased fibronectin accumulation in the SEM of the arch. Another study showed that the endothelial cells from intact rabbit vessels are stiffer in the pro-atherogenic region of the medial common iliac artery (CIA) as compared to the athero-protective region of the lateral CIA (Miyazaki and Hayashi, 1999). In this study, we show that disturbed flow facilitates endothelial CD36/Cav1-dependent uptake of oxidized lipids causing a local increase in EC stiffness in the athero-prone regions of the aorta, an effect which is exacerbated by a high fat diet.

CHAPTER 2: Materials and Methods

2.1 Cellular models:

HAECs (human aortic endothelial cells, Lonza, Allendale, NJ) and HMVECs (human microvascular endothelial cells, Lonza) were grown using Endothelial Cell Growth Medium (EGM-2, Lonza) supplemented with the EGM^{TM}-2 BulletKit^{TM} (Lonza) plus 10 μg/mL penicillin/streptomycin (Gibco; Grand Island, NY) and 2% FBS (fetal bovine serum, Invitrogen). Both human cell types were used between passages 4-12. WT (wild type), Cav1 KO, eNOS/Cav1 DKO (double knockout)-Cav1-YFP (Cav1 tagged with yellow fluorescent protein) MMVECs (mouse microvascular endothelial cells) and BAECs (bovine aortic endothelial cells) were grown in DMEM (Deballco's modified endothelial cell medium, Gibco) with 4.5 g/L D-glucose, L-glutamine and 100mg/L sodium pyruvate (Gibco), 1% pen/strep, 0.1 mmol/L non-essential amino acids (Gibco) and 10% FBS. MMVECs were used in experiments between passages 10-20. All cells were fed every 2-3 days, split every 3-7 days, and maintained in a humidified incubator at 37°C with 5% CO_2. All experiments adhered to protocols approved by the Institutional Biosafety Committee (Protocols 09-038, 12-032, 15-024).

2.2 Mouse models:

WT (C57BL/6) male mice were purchased from Charles River and Jackson Laboratory. CD36 KO (B6.129S1-Cd36^{tm1Mfe}), Cav1 KO (B6.Cg-Cav1 tm1/nls), ApoE KO (B6.129P2-Apoe^{tm1Unc}) breeding pairs were purchased from Jackson Laboratory and bred in-house. All mice were housed in pathogen-free conditions under a 12 hour light/dark schedule and fed a regular chow diet unless otherwise stated. All animal protocols adhered to the established guidelines by UIC's Institutional Animal Care and Use Committee (Protocols 10-218, 13-209, 16-183). All mice were euthanized by CO_2 followed by cervical dislocation, except for the experiments involving blood collection. In the later experiments, the mice were sedated using isoflurane,

decapitated and exsanguinated. The blood was chilled on ice for approximately a half hour followed by centrifugation at 4°C for ten minutes at 1500 rpm. The plasma's top layer was collected for further analysis.

Diet-induced hyperlipidemia

We used two different diet-induced hyperlipidemic models. The first diet was used because it is a well-established diet-induced model of endothelial dysfunction and dyslipidemia in WT mice [reviewed by (Collins et al., 2004)]. Eight to ten week old WT, CD36 KO and Cav1 KO male mice were fed a short-term high fat, high cholesterol diet (Harlan, TD.88137) for one month. This diet consisted of 0.2% total cholesterol and 21% total fat of which more than 60% are saturated (425 kcal from fat). Control and HFD fed mice were weighed at the start and end of the diet period. The second high fat, high cholesterol diet (MP Biomedicals, 960404) was used as it was shown to induce atherosclerotic lesion formation in mice (Paigen et al., 1985). This diet was administered to two month old ApoE KO male mice until 5-6 months of age. This diet consisted of 1.25% total cholesterol and 15% total fat.

Measuring LDL and oxLDL in mouse blood plasma

The quantification of total LDL and cholesterol in the mouse plasma was determined by a standard lipid profile analysis performed by IDEXX. OxLDL quantification was performed in-house using a sandwich ELISA (Elabscience Biotech) following the manufacturer's protocol.

Mouse vessel extraction

Following euthanasia, the mouse descending aorta and the aortic arch were extracted, cut longitudinally to expose the endothelial monolayer and gently washed to remove excess blood particles. The live tissue samples adhered to the glass coverslip, endothelial side up, using double sided tape and maintained in Hank's buffering solution (ThermoFisher). The endothelial cell surface was then measured for elastic modulus values using atomic force microscopy

(AFM). In select experiments, the samples were fixed, washed and stained for endothelial junctional marker, PECAM1.

Removal of the endothelial monolayer (denuding)

To test the elastic modulus of the sub-endothelial layer, we used a denuding technique as previously described (Peloquin et al., 2011). In brief, cotton tipped applicator was wetted with Hank's buffering solution and gently rubbed over the endothelial monolayer ~10 times, then gently washed with Hank's solution to remove any excess debris. In select experiments, the sub-endothelial layer was fixed, washed and stained for PECAM1 to ensure the ECs were removed.

Bone marrow transfer

Two to three month old recipient WT and CD36 KO male mice were exposed to 10 Gy radiation followed by bone marrow transfer of macrophages from WT donor mice with a Ly5.1 marker 4-6 hours later. Mice were monitored either every day or twice per week following the standard post-bone marrow transfer (BMT) protocol. One month post-BMT, blood from each mouse was collected and used to determine the degree of donor macrophage incorporation into each recipient mouse, using flow cytometry. Stiffness measurements were performed on the recipient mice two months post-BMT, using atomic force microscopy.

Mass Spectrometric Analysis

Mass spectrometric results were provided by Evgeny Berdyshev, PhD at the National Jewish Health Hospital in Denver Colorado as previously described (Oh et al., 2016). In brief, sterols and oxysterols were quantified using an EST-LC-MS/MS approach using AB Sciex 6500 QTRAP mass spectrometer. Internal deuterated cholesterol and oxysterol standards were used. Cholesterol and oxysterols compositions were quantified using an isotope dilution approach.

2.3 Isolation and oxidation of LDL:

Isolation of LDL and its oxidation were performed as previously described (Oh et al., 2016). In brief, human blood plasma from healthy volunteers was purchased from Life Source (Chicago, IL). Isolation of LDL from the plasma was made possible by repeated centrifugations at $4^{o}C$ using KBr (1.019 - 1.063 g/mL). The KBr was removed from LDL through three rounds of dialysis in a 10 mmol/L Tris/HCl buffer ($4^{o}C$). LDL was oxidized by 25 μmol/L copper sulfate for 16 hours. EDTA (1 mmol/L) was added to stop the oxidation process and a TBARs (thiobarbituric acid-reactive substance) assay (ZeptoMetrix, Buffalo, NY) was performed to measure the degree of oxidation. A TBARs value of 12-25 was used in all experiments performed.

2.4 Flow apparatus:

<u>Parallel plate flow machine</u>

The parallel plate flow apparatus (Ibidi, Integrated Biodiagnostic, Munchen, Germany) consists of an air pressure pump, syringes containing the flow medium and tubing to connect the microfluidic chambers (Ibidi) which contain a seeded monolayer of cells. The apparatus' switching mechanism creates uninterrupted unidirectional laminar flow and bi-directional oscillatory flow (direction of flow switching every half second). The pressure pump can create pressures between 5 kPa and 95 kPa, which correspond with physiological shear stress values found in humans (Chiu and Chien, 2011). In this machine, the bidirectional oscillatory flow must be the same shear stress rate as the laminar flow (10 dynes/cm^2). For each flow experiment, the system is maintained in an incubator with 5% CO_2 and $37^{o}C$. The parallel flow apparatus was used for the experiments involving the comparison of laminar versus oscillatory flow changes in endothelial cells and laminar versus disturbed flow created by the microfluidic step barrier chamber.

Flow chamber with step barrier

A microfluidic flow chamber with a step barrier was used to mimic the recirculating disturbed flow that occurs *in vivo* (DePaola et al., 1992).

Computational modeling

Computational fluid dynamic simulations were employed to modify the earlier design in order to maximize the region of low shear stress recirculating disturbed flow based on the height of the step barrier. Computational distributions of the fluid's shear stress patterns were obtained using the microfluidic module of Comsol Multiphysics 5.1 (Comsol Inc, Burlington, MA) for a normal grid mesh and an inlet pressure of 3400 Pa. The flow medium has a density and viscosity negligibly higher than water. The Reynolds number (Re) based on the cross section of the step is predicted to be:

$$Re = \frac{uD_h}{v} = 216.22$$

Where u is the average velocity of the flow, D_h is the hydraulic diameter of the channel (which is proportional to the channel's cross section divided by the perimeter), and υ is the dynamic velocity. This relatively low Reynold's number, which is consistent with studies of the carotid arteries in normal volunteers (Holdsworth et al., 1999), dictates that there will be laminar flow throughout the chamber, but unstable fluid flow after the step where recirculation occurs. The computer aided design (CAD) image of the chamber was generated using AutoCAD software (Autodesk Inc, San Rafael, CA).

Microfabrication

The flow chamber with the step barrier was fabricated at UIC's Microfabrication Foundry (PI: David Eddington, PhD) using polydimethysiloxane (PDMS, Ellsworth Adhesives, Germantown, WI) using photolithography, a well-established material and method for engineering patterned microfluidic devices for use in biological applications. The photomasks used to fabricate the

molds for the photolithographic process were made to order from Fineline Imaging (Colorado Springs, CO).

A subsequent design has a coverslip #1 bottom instead of PDMS in order to permit imaging with a confocal microscope. In this design, the PDMS step barrier and coverglass were plasma treated to bond the step and top chamber to the coverglass. In both designs, the endothelial cells were exposed to physiological flow patterns for 48 hours: 10 – 20 dynes/cm^2 in the laminar regions and low (0 – 5 dynes/cm^2) recirculating flow in the disturbed flow regions immediately following the step barrier.

Cone and plate device

We also used a cone and plate apparatus that generates physiologically relevant pulsatile flow patterns (Dai et al., 2004; Wu et al., 2015). Athero-protective laminar flow (A-P) waveforms mimicking the shear stress patterns in the human distal internal carotid artery and pro-atherogenic disturbed flow (P-A) waveforms modeling the flow in the carotid sinus were simulated using a dynamic *in vitro* flow system developed by Dai *et al* (Dai et al., 2004). In brief, the flow device consists of a computerized stepper motor UMD-17 (Arcus Technology, Livermore, CA) and a stainless steel cone (tapered at 1°). The flow devices were kept in a humidified incubator (37° C) with 5% CO_2. HAECs were grown to 100% confluence in 6-well plates and subjected to the experimentally prescribed 24 or 48 hours of A-P or P-A flow. During flow, cells are maintained in EGM-2 media containing 4% high molecular weight dextran (Sigma).

2.5 Atomic force microscopy microindentation:

Cell stiffness was assessed by measuring Young's elastic modulus using atomic force microscopy, AFM (Novascan Technologies, Ames, IA; Asylum MFP-3D-Bio, Santa Barbara, CA), as previously described (Shentu et al., 2012; Shentu et al., 2010). The AFM measures the tension of the cortex of the cell by deforming the cell's surface (0.5-1 μm indentation depth

which corresponds to ~10-15% of the cell's total height). This deformation is measured as the laser's deflection on the cantilever tip (cantilever descent velocity of 2 μm/s till the trigger force is 3 nN) in order to produce quantifiable force-distance curves. These curves were obtained and analyzed using the Hertz model:

$$F = \frac{4}{3} \frac{E}{(1-\nu^2)} \delta^{3/2} \sqrt{R}$$

Where F is the loading force, E is the local Young's elastic modulus, v is the cellular Poisson's ratio (assumed to be 0.5), δ is the indentation depth and R is the radius of the spherical indenter (5 μm, Novascan AFM). The Asylum brand of AFM (Asylum Research, Goleta, CA) used a silicon nitride cantilever with a 35° cone tip with a spring constant of 0.08-0.24 N/m. A bi-domain polynomial model was used to fit the experimental force-distance curve using a least-square minimization algorithm.

AFM measurements on cultured ECs

Cellular stiffness measurements were taken between the cell's edge and nucleus in order to avoid the peri-nuclear space. ECs were either seeded on untreated glass coverslips (semi-confluent) for static experiments or into the 0.2% gelatin (Sigma, 2 μg/mL) treated microfluidic PDMS chamber [except those comparing ECs on a collagen (Corning, 40 μg/mL) versus fibronectin (10 μg/mL) coating, as previously described (Collins et al., 2014)] until confluency prior to flow treatment. To access the flow treated ECs, the upper panel of the chamber was removed following flow cessation to allow the AFM tip access to the cell surface. Regions treated with laminar versus disturbed flow were identified by their proximity to the step barrier: cells within two fields of view from the barrier (< 2 mm) were exposed to disturbed flow while those cells 10-20 mm from the step barrier were exposed to laminar flow. Two to four force-distance curves were obtained for each cell and 15-20 cells were taken per condition, per experiment.

AFM measurements of intact aortic endothelial and sub-endothelial denuded monolayers

Cellular stiffness measurements were taken at 6-10 distinct tissue sites on each mouse vessel with 3-9 indentations per site providing a total of 20-90 force-distance curves per condition per experiment. Measurements comparing intact endothelial and denuded sub-endothelial layers were measured on the same day and from the same portion of the descending aorta and aortic arch. Data is presented as a histogram of the elastic modulus value range for each experimental condition.

2.6 Microscopy and immunohistochemistry:

OxLDL uptake

Uptake of oxLDL was quantified by measuring the average cellular fluorescence from the internalized rhodamine tagged oxLDL particles (DiI-oxLDL, Alfa Aesar, Ward Hill, MA). DiI-oxLDL (1 μg/mL) was added to the flow media for the duration of the 48 hour experiment. In all experiments, the media contains lipoprotein deficient serum (LDS, Sigma-Aldrich) instead of FBS. After flow cessation, cells are fixed and washed within the flow chamber. In between the washes with PBS, cells are also washed with an acid wash treatment (0.5 M NaCl, 0.2 M acedic acid, pH 2.5) to remove any DiI-oxLDL particles attached to the cell membrane's surface. Cells exposed to flow in the PDMS microfluidic chamber were imaged with a Ziess Axiovert Fluorescent Microscope with a long-distance 40X lens. In the experiments using glass bottomed microfluidic devices, the cells were imaged with a Ziess Confocal Microscope. Average cellular fluorescence was assessed by outlining 2-7 cells per image, 6-12 images per condition per experiment (ImageJ).

Albumin uptake

Similar to oxLDL uptake, albumin uptake was measured by average fluorescent intensity using a fluorescently tagged particle. Green fluorescent protein-tagged albumin (1 μg/mL, Invitrogen,

Waltham, MA) was added to the flow media (containing LDS instead of FBS) for the duration of the 48 hour experiment. Following flow cessation, cells were fixed, washed (including acid wash), imaged and quantified as previously described for oxLDL uptake.

CD36 Internalization

For this set of experiments, a confluent monolayer of HAECs was treated to the live cells with a rhodamine-tagged plasma membrane marker (Beckmam) overnight, per the manufacturer's protocol. Following several washes with PBS, the cells were serum starved for 3 hours. To achieve staining of the cells for surface expression of CD36, the HAECs were put on ice and washed with 5% bovine serum albumin (BSA, Sigma) blocking solution for 10 minutes. Chilled primary anti-CD36 antibody was applied to the cells for 20 minutes in the cold, followed by washing and the application of FITC-labeled secondary antibody (Invitrogen) for 10 minutes. When cell surface staining of CD36 was desired, the cells were washed and fixed with 0.2% formaldehyde (FA) in the cold for 25 minutes. When CD36 endocytosis was desired, the cells were washed and placed in a 37°C incubator without CO_2 for 30 minutes and then fixed at room temperature with 0.2% formaldehyde for 15 minutes. Cell surface staining and internalization of CD36 was visualized with 0.2 micron z-stack slices using a confocal microscope.

TIRF (total internal reflection fluorescence) microscopy

TIRF microscopy experiments were performed with a motorized Ziess Laser TIRF imaging system with a high-speed EMCCD camera (Quantem 512SC; Photometrics). Images were acquired with a 63x/1.46 NA alpha Plan-Apochromat objective and FITC and rhodamine channels (excitation 488 and 561 nm, respectively). Acquisition time, EMCCD gain and laser intensity was kept constant.

Co-localization

Cav1 and CD36

In the experiments examining CD36/Cav1 co-localization, the flow media contained 1 μg/mL unlabeled oxLDL. Following flow cessation and fixation, HAECs were stained for extracellular CD36 (rhodamine) and Cav1 (green) using immunohistochemistry techniques. Cells were imaged using TIRF and confocal microscopy. In all co-localization experiments, ECs were analyzed using ImageJ software for the degree of co-localization using Mander's correlation.

OxLDL and Cav1

Prior to flow initiation, HAECs were transfected with GFP-Cav1 using Nuclear Factor II/2B kit (Lonza) following the standard protocol. As previously described, GFP-Cav1 HAECs were exposed to 48 hours of laminar and disturbed shear in the glass bottomed microfluidic chamber with a rhodamine tagged oxLDL in the medium. Following flow cessation, cells were fixed and washed, and imaged (x63) in the areas of interest with a Zeiss LSM 710 confocal microscope.

Immunohistochemistry

For all immunohistochemistry, excluding the CD36 internalization experiments, cells were fixed in 3.8% formaldehyde (Fisher) after their experimental treatments, permeabilized (all except those probing for CD36), washed with PBS (Gibco) and blocked with 5% BSA for two hours at room temperature. Cells were then washed and primary antibody (anti-CD36, mouse monoclonal) applied overnight on a slow rocker in 4°C. Following repeated washes, the appropriate secondary antibody (AF-488, donkey anti-mouse, AF-555, donkey anti-mouse, Thermofisher) was added for 1 hour at room temperature on a shaker. Cells were then washed and imaged. All experiments had an IgG control and secondary only control condition. Quantification of average cellular expression was determined using ImageJ software.

Endothelial alignment

EC alignment was measured by analyzing the brightfield images acquired from the Ziess Fluorescent Microscope. Using ImageJ software, the angle of the long axis of the cell was measured, with 0° being the direction of flow. Cell alignment was determined for 3-5 cells per image and 4-5 images per condition for each of the 3-4 analyzed independent experiments.

En face

Following euthanasia, mouse vessels were opened up longitudinally, EC monolayer side up, and affixed to coverslips with double-sided tape, as previously described. Vessels were then fixed in 3.8% formaldehyde for 1-2 hours, washed in PBS several times and non-specific binding was blocked with 5% BSA for 1-2 hours. Primary antibody (anti-CD36, anti-CD31, BD Pharmingen) was applied to the samples overnight on a rocker at 4^oC and then washed several times. Secondary antibody was applied for 1 hour at room temperature. Following several final washes, the samples were mounted for immediate imaging with either a fluorescent or confocal microscope.

2.7 Laurdan multi-photon microscopy:

The physical properties of disordered and ordered cell membrane domains were analyzed using Laurdan dye and a multi-photon (MP) microscope, as described earlier (Gaus et al., 2003; Shentu et al., 2010). In brief, sub-confluent, live bovine aortic endothelial cells were seeded on coverslips and left to adhere overnight. In successive 30 minute intervals, cells were serum starved, treated with (10 μM) POVPC or PGPC (Avanti Lipids), loaded with Laurdan fluorescent dye in DMSO (5 μM, Molecular Probes, Carlsbad, CA) and then washed. Cellular Laurdan fluorescence was excited with a (800 nm) multi-photon laser and imaged with a BioRad MP microscope (63X oil objective). The emitted light was then collected in two distinct wavelength

ranges, 410-490 and 503-553 nm. The general polarization (GP) value is a measure of the relative degree of cell membrane fluidity and was calculated using the following equation:

$$GP = \frac{I_{(410-490\ nm)} - I_{(503-553\ nm)}}{I_{(410-490\ nm)} + I_{(503-553\ nm)}}$$

General polarization was corrected using the G-factor (G):

$$GP = \frac{I_{(410-490\ nm)} - G \times I_{(503-553\ nm)}}{I_{(410-490\ nm)} + G \times I_{(503-553\ nm)}}$$

The G-factor (G) value was calculated using the known GP value for Laurden dye in DMSO at room temperature, GP_{theo}, and from the calculated GP value of our stock solution (500 mM) GP_{exp}, stored at room temperature The G-factor was then calculated by:

$$G = \frac{GP_{theo} + GP_{theo} \times GP_{exp} - 1 - GP_{exp}}{GP_{theo} \times GP_{exp} - GP_{theo} + GP_{exp} - 1}$$

The results of these analyses are pseudo-colored GP images (512 x 512, 32 bits) (ImageJ). Pixel threshold was set to 80-90% of the maximum values calculated from the combined image ($I_{(410\text{-}490\ nm)} + I_{(503\text{-}553\ nm)}$). Background pixel values were set to zero. The GP distribution of disordered and ordered domains was calculated for each cell (12-25 cells per condition per experiment, 3 independent experiments) by fitting the experimental data into two Gaussian curves using a nonlinear fitting algorithm, as previously described (Shentu et al., 2010).

2.8 Real-time PCR, western blot and siRNA:

<u>Real-time PCR</u>

Total RNA was isolated using the mirVana mRNA isolation kit (Life Technologies) or the Direct-zol RNA MiniPrep (Zymo Research, Irvine, CA). Total RNA was reverse transcribed into cDNA using the High Capacity cDNA Reverse Transcription kit (Life Technologies) or the SuperScript III kit (Life Technologies) following the manufacturer's instructions. Absolute quantitative PCR was performed on LightCycler 480 II using the SYBR Green I Master kit from Roche Diagnostics Corporation (Indianapolis, IN). The absolute quantification of CD36 and LOX1 gene expression

was normalized to the geometric mean of the housekeeping genes, GAPDH, B-actin and ubiquitin. The PCR primers are as follows:

CD36 forward, 5'-GCAGCAACATTCAAGTTAAGCA-3';
CD36 reverse, GCTGCAGGAAAGAGACTGTGT-3';
LOX1 forward, 5'-AAGTGGGGAGCCCAAGAAAG-3';
LOX1 reverse, 5'-GGGCCACACATCCCATGATT-3';
GAPDH forward, 5'-TGCACCACCAACTGCTTAGC-3';
GAPDH reverse, 5'-GCATGGACTGTGGTCATGAG-3';
β-actin forward, 5'- TCCCTGGAGAAGAGCTACGA-3';
β-actin reverse, 5'- AGGAAGGAAGGCTGGAAGAG-3';
Ubiquitin forward, 5'-ATTTAGGGGCGGTTGGCTTT-3';
Ubiquitin reverse, 5'-TGCATTTTGACCTGTTAGCGG-3'.

Western Blot

Cells were washed with cold PBS and lysed with a lysis buffer with protease inhibitor cocktail. Cells were briefly sonicated and spun for ten minutes at 14,000 x g at 4°C. The supernatant's protein concentration was measured using a Bio-Rad protein assay reagent. Total protein (30 μg per sample) was separated by 10% SDS-PAGE (sodium dodecyl sulfate-polyacrylamide gel electrophoresis) and then transferred to PVDF (polyvinylidene difluoride) membranes. The membranes were blocked with a Tris-buffered saline solution with 0.1% Tween 20 (TBST) containing 5% BSA and probed with anti-CD36 (Proteintech) or anti-LOX1 (Abcam) antibodies overnight at 4°C. After application of appropriate secondary antibodies, membranes were washed with TBST and developed with enhanced chemiluminescence (Thermo Scientific). Protein quantitative analysis was performed with ImageJ software.

siRNA knockdown of CD36 and Lox1

Cells were seeded and grown to 95 – 100% confluency. Cells were transfected with the FlexiTube Gene Solution for CD36 or ORL1 (LOX1), with All Star Negative siRNA from Quiagen (Hilden, Germany). siRNAs were prepared per the manufacturer's protocol. In brief, a mixture of Lipofectamine RNA mix, RNA max (Invitrogen), OptiMEM and siRNA were mixed together and incubated for 30 minutes at room temperature. The mixture was then added to the cells

(final concentration 50 nmol/L) for 48 hours prior to experimental use. Initially, four siRNAs for CD36 and four siRNAs for LOX1 were tested for maximal reduction in mRNA expression in the cell type to be examined (HAECs). The two siRNAs for each gene with the greatest reduction in mRNA expression (at least 80% reduction) versus scrambled control siRNA was selected for subsequent western blot analysis of protein knockdown.

2.9 Statistical analysis:

One-way ANOVA, analysis of variance, (α = 0.05) was performed to detect the differences between the mouse weights and plasma measurements for total cholesterol, LDL and oxLDL. All other statistical analysis was performed with a two-way ANOVA with replication (α = 0.05) using Excel (Microsoft) to determine statistical significance. Subsequent statistical analysis was done using a standard student's t-test assuming two-tailed distribution with unequal variances. A p-value less than 0.5 was considered statistically significant.

CHAPTER 3: Effect of different shear stress patterns on oxLDL uptake into endothelial cells: Role of CD36, Lox1, Caveolin-1 and eNOS

3.1 Introduction:

Oxidized LDL has been shown to be a major factor in endothelial dysfunction which is an initiating factor in the onset of atherosclerosis. Bi-directional disturbed shear stress patterns found at arterial bifurcations and curvatures are also known to have a causal role in atherosclerotic plaque formation. To better understand the shear stress components responsible for oxLDL uptake, we tested several different flow patterns based on their shear stress value: low (0 – 3 dynes/cm^2) versus high (10 – 20 dynes/cm^2), directionality: uni-directional versus bi-directional and pulsatile versus non-pulsatile flow. Here we show that oxLDL uptake into human aortic ECs (HAECs), human microvascular ECs (HMVECs) and mouse microvascular ECs (MMVECs) increased under low shear stress bi-directional (herein called 'disturbed flow,' DF) conditions and in pulsatile low shear stress bi-directional (herein called 'pro-atherogenic,' P-A) flow as compared to high shear stress athero-protective (A-P) unidirectional laminar flow (LF), but that *high* shear stress bi-directional (herein called 'oscillatory flow,' OF) in ECs has reduced oxLDL uptake compared to laminar flow conditions.

Next, we wanted to understand the mechanisms of this increased oxLDL uptake under disturbed flow. In endothelial cells, extracellular oxLDL binds to and internalizes via two scavenger receptors, CD36 and LOX1, as evidenced by cellular uptake inhibition by using endothelial CD36- and LOX1-blocking antibodies [reviewed by (Febbraio et al., 2001; Lubrano and Balzan, 2014)]. LOX1, or lectin-like oxidized LDL receptor 1, is a scavenger receptor that is found in hematopoietic cells, vascular SMCs, platelets, differentiated macrophages, and ECs and is known to bind with oxLDL, bacteria, leckocytes, fibronectin, and others [reviewed by (Yoshimoto et al., 2011)]. LOX1 has been shown to play a significant role in oxLDL-induced inflammatory processes *in vitro*. Specifically, activation of LOX1 with oxLDL has been shown to

promote EC and vascular SMC hyper-proliferation and induce cell injury and apoptosis in coronary artery ECs [reviewed by (Yoshimoto et al., 2011)]. Cominacini *et al* showed a LOX1-dependent decrease in NO and an increase in ROS formation in bovine aortic ECs due to oxLDL in a dose-dependent manner (Cominacini et al., 2001). Lox1 is believed to be a major receptor in endothelial cells (Lubrano and Balzan, 2014; Pirillo et al., 2013) whereas less is known about the CD36 scavenger receptor in ECs (Silverstein and Febbraio, 2009).

CD36 (cluster of differentiation 36) is a multiple ligand receptor that binds to oxLDL, thrombospondin, long chain fatty acids and collagen. This transmembrane protein is expressed in macrophages, monocytes, adipocytes, smooth muscle cells, microvascular ECs [reviewed by (Kuliczkowska-Plaksej et al., 2006; Park, 2014)] and recently shown to be important in macrovascular EC biomechanics (Oh et al., 2016). CD36 induces inflammatory pathways due to its interaction with oxLDL, which has been shown to enhance cytokine production and recruit immune cells to infiltrate the vascular intima [reviewed by (Park, 2014)]. Uittenbogaard *et al* demonstrated that CD36 is responsible for oxLDL-induced caveolae cholesterol depletion and a reduction in eNOS activation (Uittenbogaard et al., 2000) and that it has anti-angiogenic effects (Dawson et al., 1997). In my study, I show that CD36 was enhanced by and required for disturbed flow induced oxLDL uptake into ECs, but LOX1 had no detectable role.

There are several possible mechanisms of macromolecular uptake in ECs: caveolae and clathrin-mediated endocytosis, phagocytosis and macropinocytosis [reviewed by (Khalil et al., 2006)]. As shown in Figure 3.1 (Parton, 2007), caveolae are small (50-100 nm in diameter) omega-shaped invaginations on the plasma membrane, which are important in cell signaling, lipid metabolism, and macromolecular transport via endocytosis. Caveolae can be found in ECs, SMCs and adipocytes [reviewed by (Kiss, 2012)]. Caveolae form from a lipid raft on the plasma membrane which is comprised of oligermerized caveolin1 protein, phospholipids, sphingolipids, cholesterol, cellular receptors and membrane-bound signaling proteins such as

src-family tyrosine kinases and eNOS [reviewed by (Kiss, 2012; Pavlides et al., 2012)]. Studies from our lab showed that caveolae mediated endocytosis/transcytosis of macromolecules requires an interdependence of many signaling events, including src kinase to regulate Cav1-oligomer stability, nitrosylation of cysteine 156 (Bakhshi et al., 2013), increased filamin A associating with Cav1 (Sverdlov et al., 2009) and phosphorylation of Cav1 on tyrosine 14 (Sverdlov et al., 2007). Several studies have shown that oxLDL internalization into static cultured ECs is caveolae mediated (Kumano-Kuramochi et al., 2013; Lisanti et al., 1994; Sun et al., 2010) yet others show that uptake into other cells types goes through a caveolae-independent mechanism (Collins et al., 2009; Sun et al., 2007; Zeng et al., 2003). This study shows that oxLDL internalization into ECs increases under low shear stress bi-directional ('disturbed') flow and pro-atherogenic waveform conditions, which is found to be dependent upon CD36, eNOS and caveolin1, but not on LOX1.

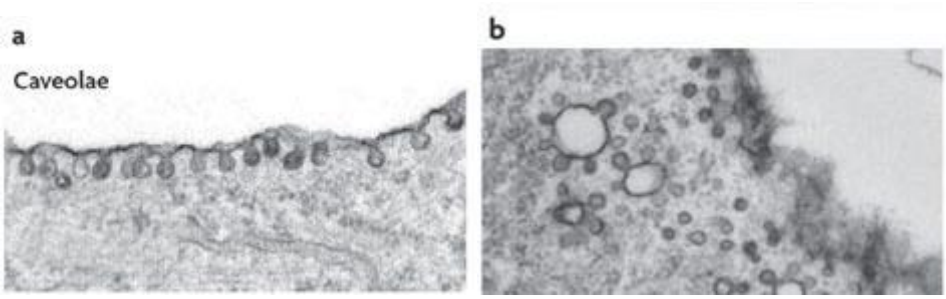

Figure 3.1: Caveolae formation at the plasma membrane.
Budding caveolae at the plasma membrane surface **(A)** and small caveolar clusters as well as pinched off endocytosed caveolae **(B)** are visualized by an electron microscope. Reprinted by permission from Macmillan Publishers Ltd: Nature. (Parton, 2007)

3.2 Results:

Design of the microfluidic chamber with step barrier to mimic disturbed flow

Arterial sites subject to low shear stress, bi-directional disturbed flow are known to be pro-atherogenic. A microfluidic chamber with a step barrier has been shown to mimic DF *in vitro* as well as high shear stress uni-directional laminar flow farther from the step barrier (DePaola et al., 1999). Using computation fluid dynamics (CFD) software (COMSOL Multiphysics), we modified this design in order to create the largest region of recirculating flow following the barrier. Figure 3.2 A [a] shows a sideview of the CFD simulation which depicts the low shear stress region after the step. The step is towards the middle of the chamber ([b] schematic of the design, length 50 mm, width 5 mm, height 0.6 mm) which creates a recirculating region after the step barrier ([c]) with varying directions and speeds ([d] red velocity vectors after the step). Fluorescent microbeads under flow show the recirculation that occurs after the step ([e], left) and the laminar flow 1-2 cm after the step ([e], right). The optimal height of the step was determined through a series of CFD simulations that tested which step height would produce the largest area of recirculation after the step (B): a height of 0.33 mm (55% of the total chamber height) created a recirculating disturbed flow region that extended 2.25 mm following the step.

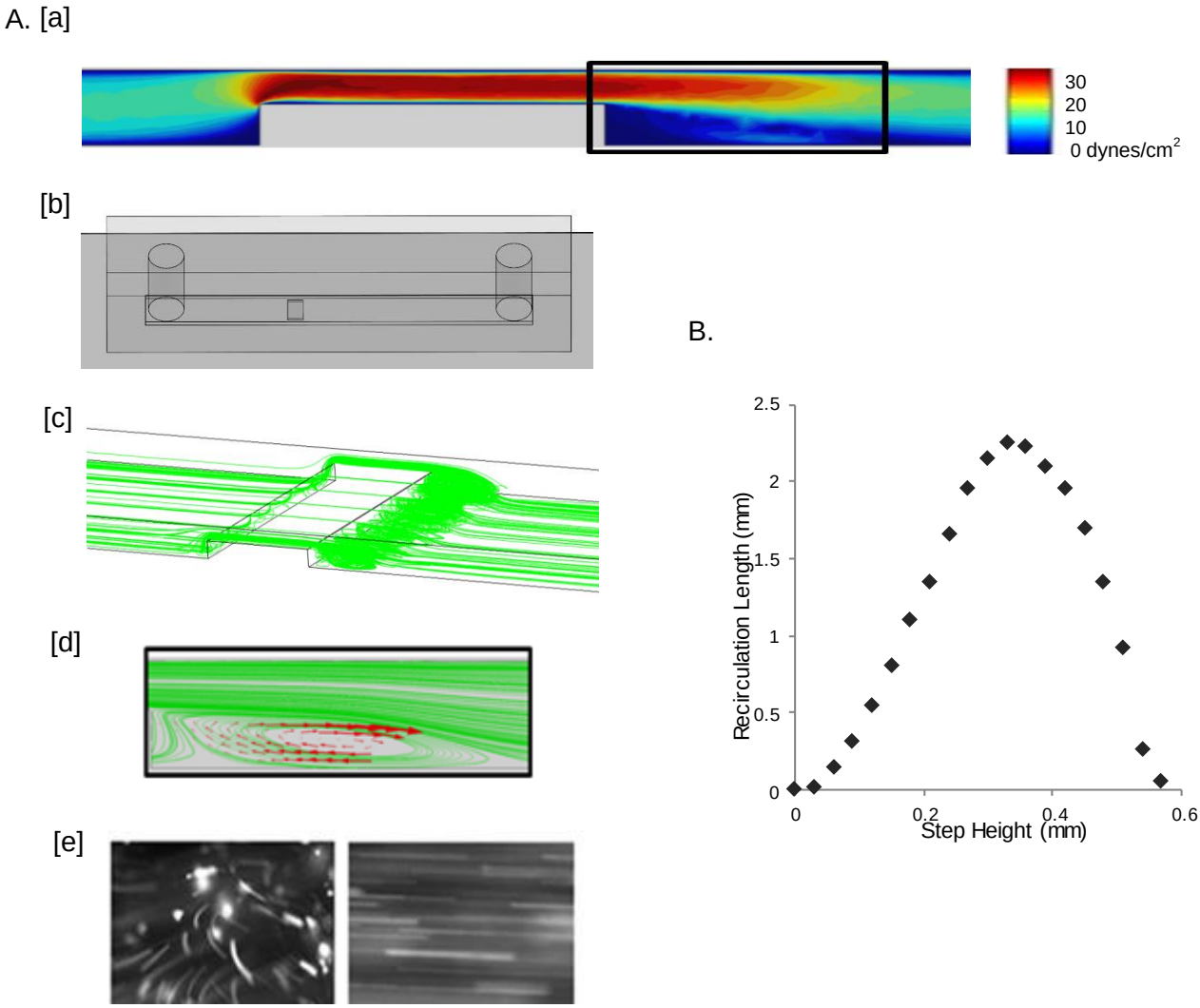

Figure 3.2: Design and validation of a step barrier flow chamber mimicking physiological flow environments. A: [a] Computational fluid dynamics (CFD) simulation of the step barrier microfluidic chamber describing the shear stress values. **[b]** CAD (computer aided design) schematic of the chamber's design. **[c]** CFD simulation depicting the fluid's streamlines of the recirculating disturbed flow (DF) region immediately following the step barrier and unidirectional laminar flow (LF) before and after the step. **[d]** Streamlines (green) and velocity vectors (red) describing the DF after the barrier. **[e]** Fluorescent beads under flow: recirculating DF immediately following the step (left) compared to the LF region 1-2 cm from the step (right). **B:** Fluid's recirculation length after the barrier as a function of the step's height.

To determine the validity of the chamber, we assessed the alignment of three different endothelial types, human aortic, human microvascular and mouse microvascular ECs, in laminar flow as compared to disturbed flow. Endothelial cells are known to align in the direction of flow and elongate under laminar flow, whereas they exhibit a cobblestone appearance under oscillatory or recirculating disturbed flow (DePaola et al., 1999). Following 48 hours of flow, ECs were fixed and imaged with a Ziess Axiovert Microscope with a 10X lens. Using ImageJ, cells were outlined on brightfield images and angular measurements to the direction of flow were calculated. As shown in Figure 3.3, representative images show EC alignment in the direction of flow under laminar conditions and not under disturbed flow conditions. The bell shaped curve in the histograms of the laminar flow conditions (left column) quantitatively indicates alignment to flow, whereas a more plateau-type shape in the histograms of the DF condition (right column) indicate no obvious alignment.

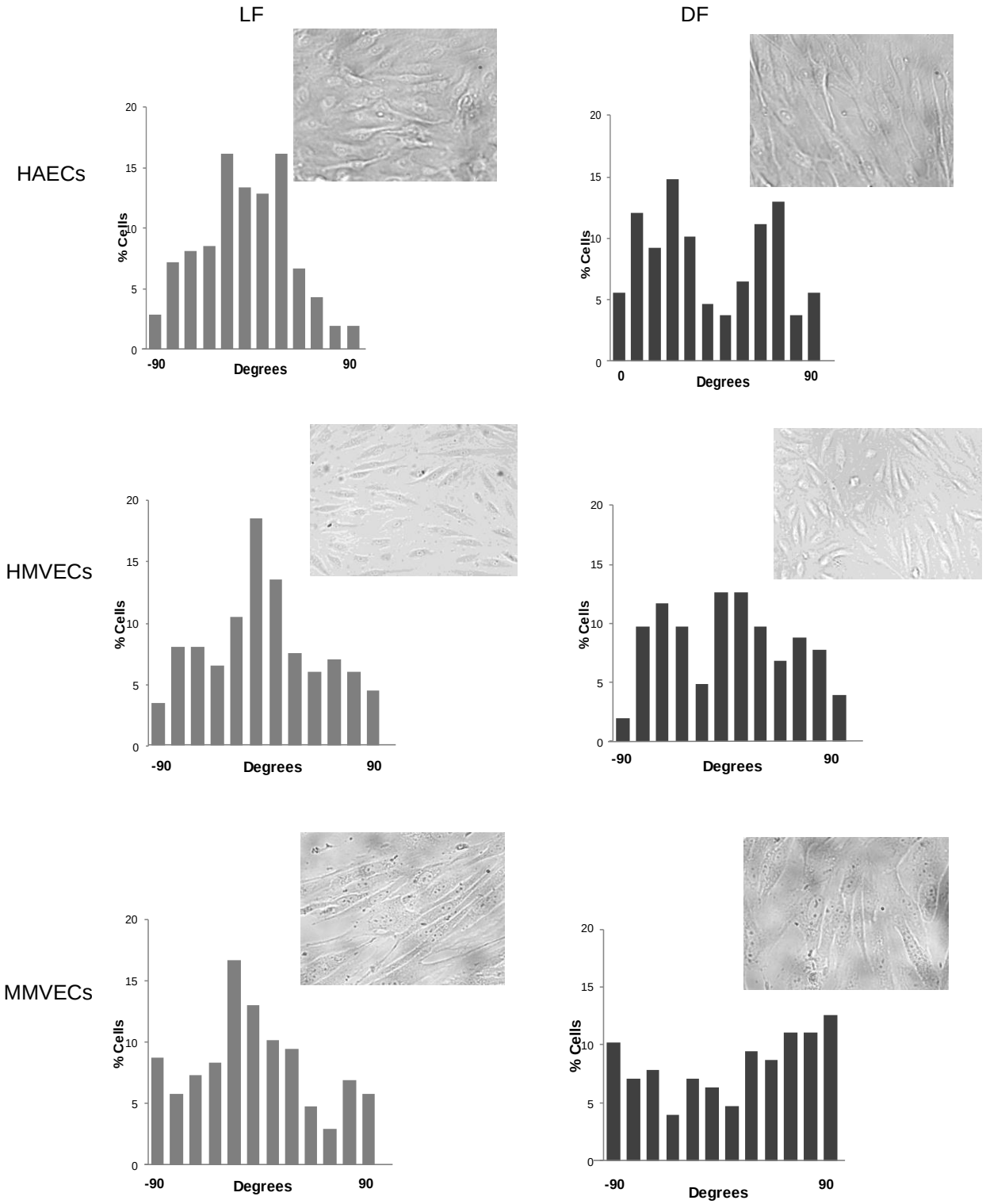

Figure 3.3: Verification of cell alignment under laminar and disturbed flow for three endothelial subtypes. Endothelial cell alignment under laminar flow (left column) and disturbed flow (right column) conditions for human aortic ECs (top row), human microvascular ECs (middle row) and mouse microvascular ECs (bottom row) (20-40 cells per condition per experiment, four independent experiments). The brightfield image insets are representative images of the endothelial subtype under LF (left) and DF (right).

Increased oxLDL uptake in low shear stress bi-directional DF environments

Prior to testing the effect of flow on oxLDL uptake, we assessed the specificity of the rhodamine fluorescently labeled DiI-oxLDL particle. We imaged the average cellular fluorescent intensity in ECs with and without DiI-oxLDL exposure. There was no observable fluorescence in the absence of the DiI-oxLDL particle (Figure 3.4 A, left). More importantly, we did a competition assay which showed that the rhodamine fluorescence of the DiI-oxLDL particle was quenched by the addition of increasing the quantity of non-fluorescent native oxLDL, confirming the specificity of the DiI-oxLDL fluorescent signal (B).

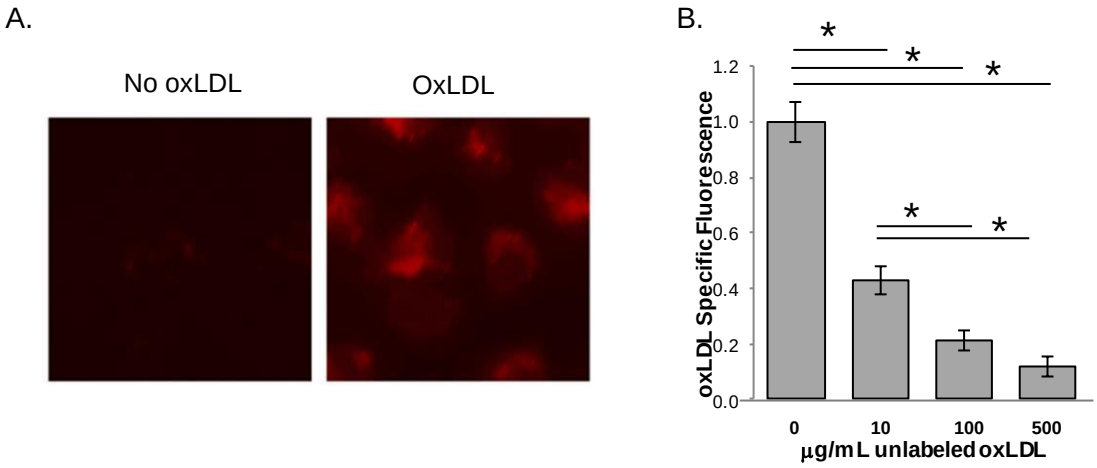

Figure 3.4: Verification of the specificity of rhodamine-tagged DiI-oxLDL. A. Representative fluorescent images of endothelial cells not exposed to rhodamine DiI-oxLDL (left) and ECs with exposure (right). **B.** Relative oxLDL rhodamine fluorescence as a function of increasing amounts of unlabeled oxLDL. n = 3. * $p < 0.05$.

Since atherosclerosis develops in large arteries, we first measured oxLDL uptake into human aortic endothelial cells in regions of disturbed versus laminar flow. OxLDL uptake was quantified in HAECs exposed to physiological shear stress values of 10-12 dynes/cm^2 of laminar or < 3 dynes/cm^2 disturbed flow (Ku et al., 1985) [reviewed by (Chiu and Chien, 2011)] for 48 hours with DiI-oxLDL (1 μg/mL) in the cell medium. OxLDL uptake was measured by quantifying oxLDL specific fluorescence immediately after flow cessation. As shown in Figure 3.5, our data shows that there is increased oxLDL uptake in the disturbed flow region, up to 2 mm following the step, as compared to the laminar regions, 1 – 2 cm before and after the step, in the same microfluidic chamber in the same experiment (A, representative confocal images; B, average oxLDL specific fluorescence).

Then, we checked to see if this increase in DF regions is also observed in other endothelial cell types. We did in fact find that this is a general phenomenon. There is increased oxLDL uptake in HMVECs and MMVECs as well (Figure 3.5 C). Interestingly, our data suggests that there is over two times more oxLDL internalization in human large aortic vessels as compared to microvessels, which may provide some insight into the enhanced oxLDL-induced endothelial dysfunction seen in large vessels as compared to microvessels.

The disturbed flow created by the step barrier in the microfluidic device has two major components: (low, > 3 dynes/cm^2) shear stress and (bi-) directionality. To further analyze these components regarding oxLDL uptake into ECs, we measured uptake under *high* shear stress, bi-directional ‘oscillatory’ flow (OF) as compared to uni-directional laminar flow control.

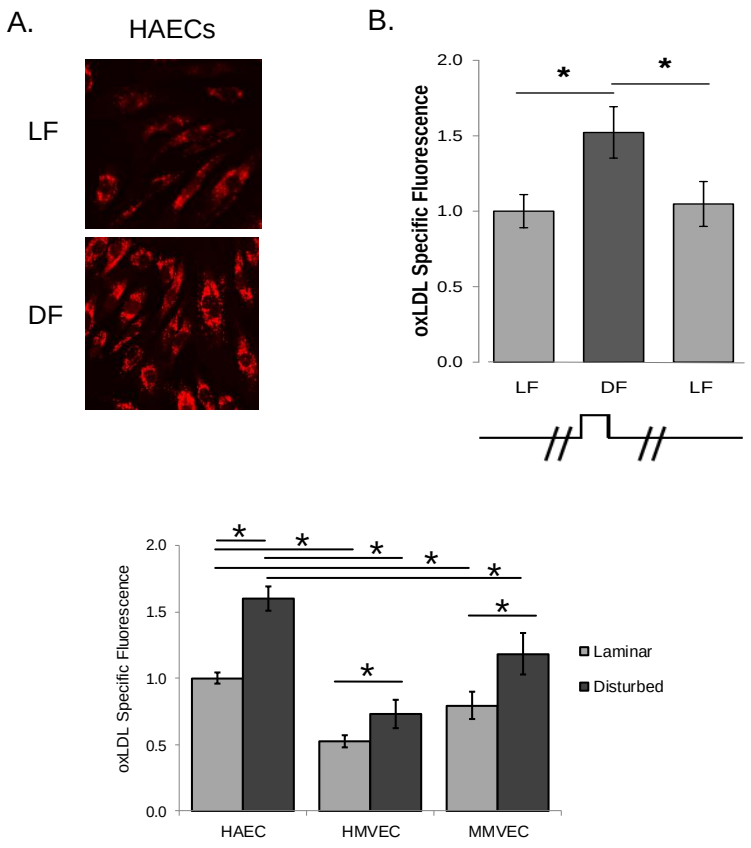

Figure 3.5: Increased oxLDL uptake into ECs under disturbed flow conditions as compared to laminar flow. A. Representative confocal images of oxLDL uptake into HAECs in LF and DF regions. **B.** OxLDL uptake into HAECs in the region immediately following the step barrier (DF) compared to the laminar regions 1-2 cm before and after the step. A graphical sideview of the step chamber with breaklines is shown below. **C.** Comparative analysis of oxLDL uptake under laminar and disturbed flow conditions in HAECs, HMVECs and MMVECs. * $p < 0.05$.

Opposite effect in oxLDL uptake in high shear stress bi-directional OF environments

To mimic the high SS bi-directional oscillatory flow environment compared to uni-directional laminar flow, we used microfluidic chambers without any step barrier. Fluorescent beads under flow in Figure 3.6 A. show that in both high shear stress uni-directional LF and high shear stress bi-directional OF, the fluid streamlines are similar, indicating a similar shear stress value of 10 - 12 dynes/cm^2. In OF conditions, though, the direction of flow changes every half second and there is no lower shear stress recirculation or eddying in the fluid. Endothelial cells (150k) were seeded into Ibidi flow slide (length 50 mm, width 5 mm, height 0.6 mm) and grown to confluency. The bottom of the flow slide is transparent and has a refractive index similar to glass to allow for imaging with a fluorescent or confocal microscope. The ECs are exposed to shear stress, either laminar or oscillatory, for 48 hours with a media that has 1 μg/mL DiI-oxLDL. Following flow, the cells were fixed, washed and imaged with a fluorescent or confocal microscope for uptake of oxLDL.

As shown in Figure 3.6, MMVECs align in the direction of LF as indicated by the bell shaped curve (B, left), but have less alignment in bi-directional OF conditions (B, right). Endothelial endocytosis of oxLDL was determined by average cellular fluorescence. In contrast to disturbed flow, there was decreased uptake in cells exposed to OF as compared to LF (C, representative fluorescent images; D, average oxLDL specific fluorescence) suggesting that the low shear stress component is the major factor in the DF-induced increase in oxLDL uptake into endothelial cells.

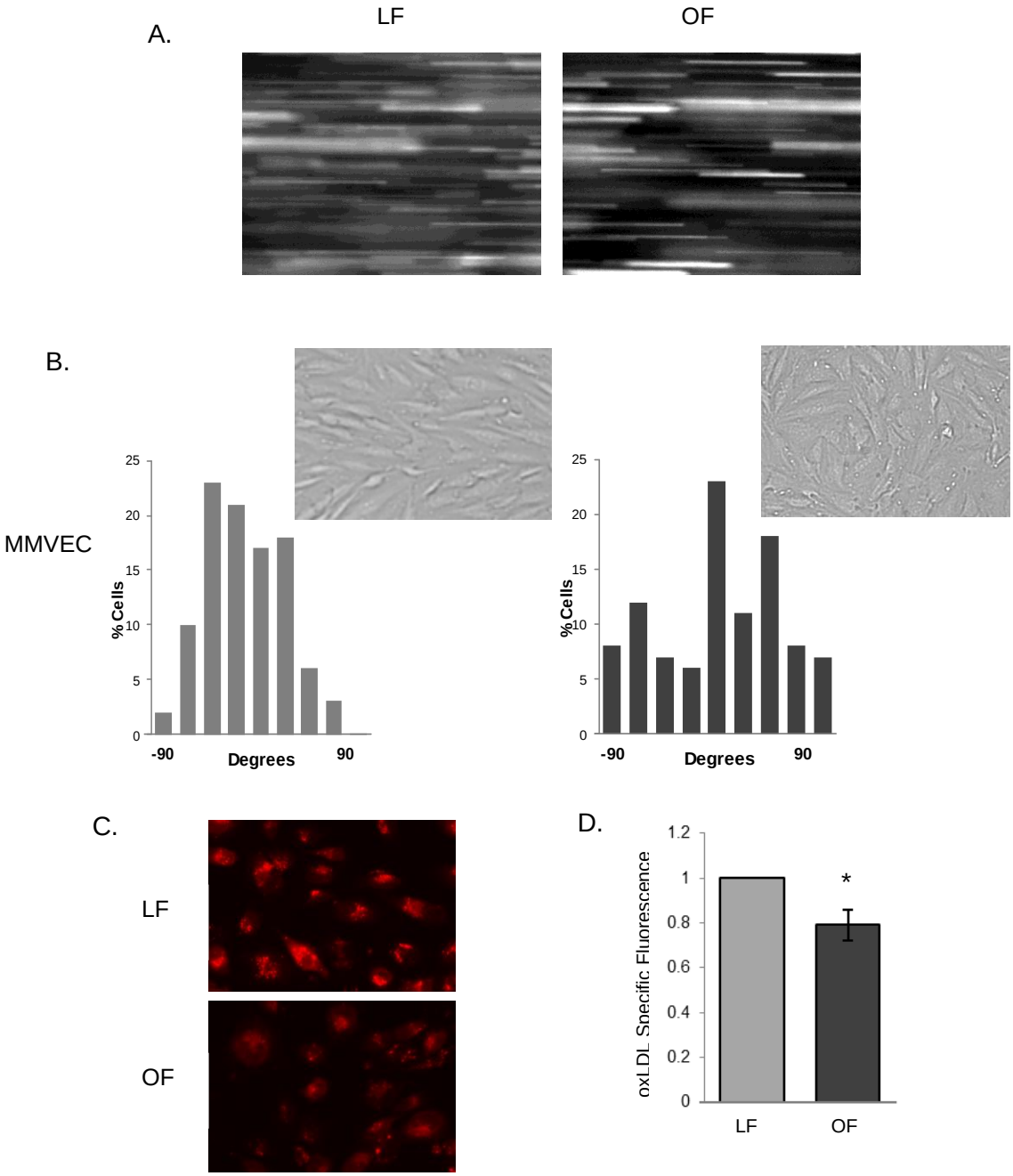

Figure 3.6: Flow induced uptake of oxLDL decreases in high shear stress bi-directional oscillatory flow conditions as compared to laminar flow. A. The trajectories of fluorescent microbeads showing the streamlines created by unidirectional laminar flow (LF, left) and oscillatory flow (OF, right). **B.** Cell alignment to the direction of flow in MMVECs following 48 hours of laminar flow (left) and oscillatory flow (right). 15-30 cells per condition for each experiment, n = 4. Representative brightfield images are shown as insets. **C.** Representative fluorescent images of oxLDL uptake in MMVECs following 48 hours of laminar and oscillatory flow. **D.** Average cellular oxLDL uptake following 48 hours of laminar and oscillatory flow in ECs. 25-40 cells per condition for each experiment, n = 6. * $p < 0.05$.

Pulsatile pro-atherogenic waveform increased endothelial oxLDL uptake

Furthermore, we also tested high shear stress uni-directional athero-protective (A-P) laminar and low shear stress bi-directional pro-atherogenic (P-A) disturbed flow waveforms (Figure 3.7 A) to simulate the pulsatile nature of blood flow using a cone and plate device, as previously described (Wu et al., 2015). As shown by the representative images in Figure 3.7 B (top), cells had a visible alignment in A-P laminar flow (left) but not in P-A disturbed flow (right). Internalization of oxLDL uptake was quantified as in previous experiments. Shear stress was applied to a confluent monolayer of HAECs with a medium containing DiI-oxLDL (1 μg/mL). Cells were fixed immediately after flow cessation, imaged with a fluorescent microscope and average cellular fluorescence was determined using ImageJ software. As shown in Figure 3.7, there is greater oxLDL uptake into cells under pro-atherogenic flow conditions as compared to ECs exposed to the athero-protective waveform (B, bottom; C). Our data shows a general phenomenon of increased oxLDL uptake under lower shear stress pro-atherogenic DF as compared to athero-protective LF. To better understand the mechanism of this phenomenon, we first investigated the role of two oxLDL scavenger receptors, LOX1 and CD36.

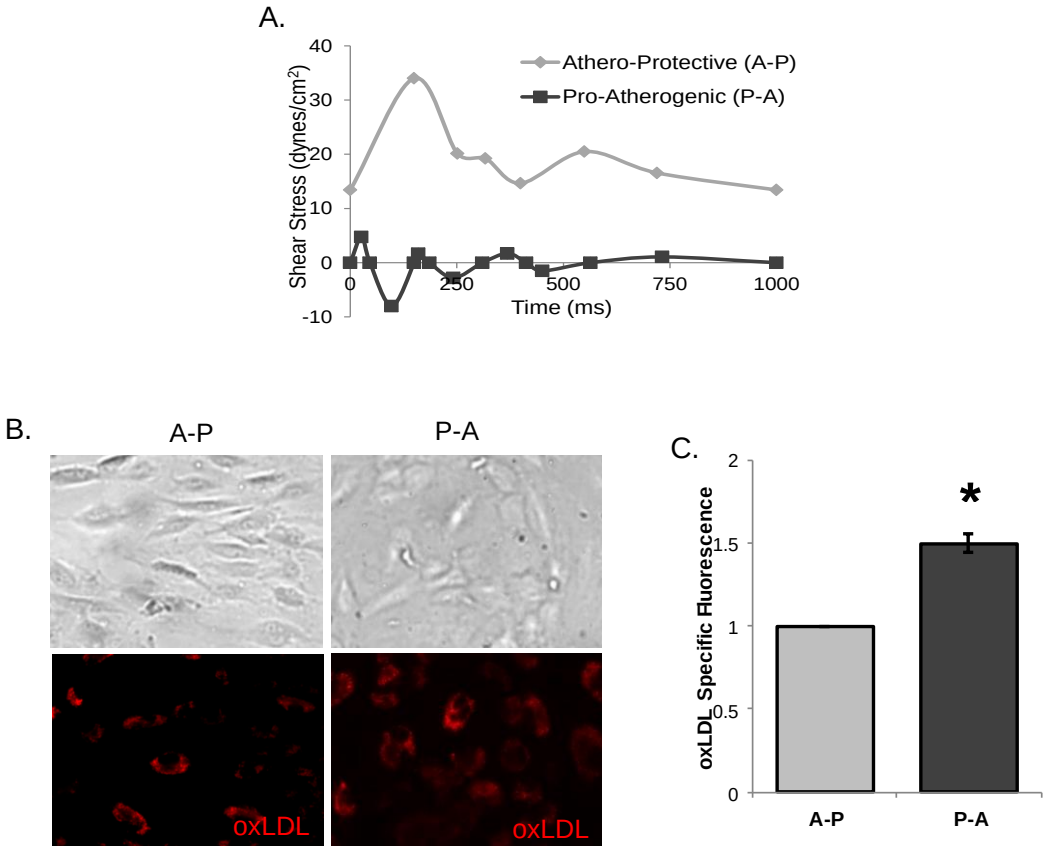

Figure 3.7: Increased oxLDL uptake in ECs exposed to a pro-atherogenic waveform as compared to an athero-protective waveform. A. Fluctuating shear stress values as a function of time to create athero-protective (A-P) laminar and pro-atherogenic (P-A) disturbed flow waveforms. **B.** Representative brightfield (top) and rhodamine (bottom) fluorescent images of HAECs exposed to A-P (left) and P-A (right) waveforms. **C.** Average oxLDL uptake into HAECs exposed to athero-protective and pro-atherogenic waveforms. n = 4. * $p < 0.05$.

Pro-atherogenic disturbed flow increased CD36 expression

We began testing the mRNA expression of LOX-1 and CD36 in HAECs exposed to athero-protective and pro-atherogenic flows for 24 hours. Our results show that under these waveforms there is two-fold increase in CD36 mRNA expression (right) as compared to LOX1 (left) (Figure 3.8 A). Additionally, there is significantly greater mRNA expression under P-A flow as compared to A-P flow for CD36. Since this data shows that CD36 may be the more dominant receptor under these flow waveforms as evidenced by greater relative mRNA expression, we wanted to verify if there was also an increase in protein expression of CD36 under flow. To achieve this aim, we treated HAECs to the LF and DF environments for 48 hours in the microfluidic step barrier chamber in the presence of oxLDL, fixed the cells and performed immunohistochemistry techniques to test for CD36 expression. To test the specificity of the CD36 fluorescence, we tested the relative mRNA and protein knockdown of two CD36-targetting siRNAs compared to control (scrambled siRNA) treated HAECs using PCR and Western Blotting techniques. These candidate siRNAs (siRNA CD36 A and B) were selected based on the PCR results depicting maximal knockdown from an original pool of four CD36-targetting siRNAs. For all experiments, the cells were treated with siRNAs for 48 hours prior to initiating the experiment. There was over 90% reduction in CD36 mRNA expression and ~60% reduction in CD36 protein expression in CD36-targetting siRNA treated ECs as compared to control ECs (Figure 3.8 B). It was important to test two different siRNAs for each scavenger receptor to ensure the knockdown of the receptors would not cause any off-target effects that would skew our results. Now we could determine the CD36 expression in control and CD36-targetting siRNA treated HAECs exposed to 1 μg/mL DiI-oxLDL and 48 hours of LF versus DF in the step barrier chamber using immunohistochemistry techniques. Our data shows that there was greater CD36 expression in HAECs from the disturbed flow regions compared to LF in control HAECs (Figure 3.8: C top row, representative fluorescent images; D, average CD36

specific fluorescence). As expected, there was significantly less CD36 specific fluorescence in the CD36-targeting siRNA treated HAECs (Figure 3.8 C bottom row, D). Additionally, these cells showed no observable difference in CD36 fluorescence under LF versus DF conditions. The increased expression of CD36 under DF in HAECs supports the mRNA expression data as evidence that the scavenger receptor CD36 is significantly up-regulated in ECs from areas of pro-atherogenic disturbed flow as compared to athero-protective laminar flow.

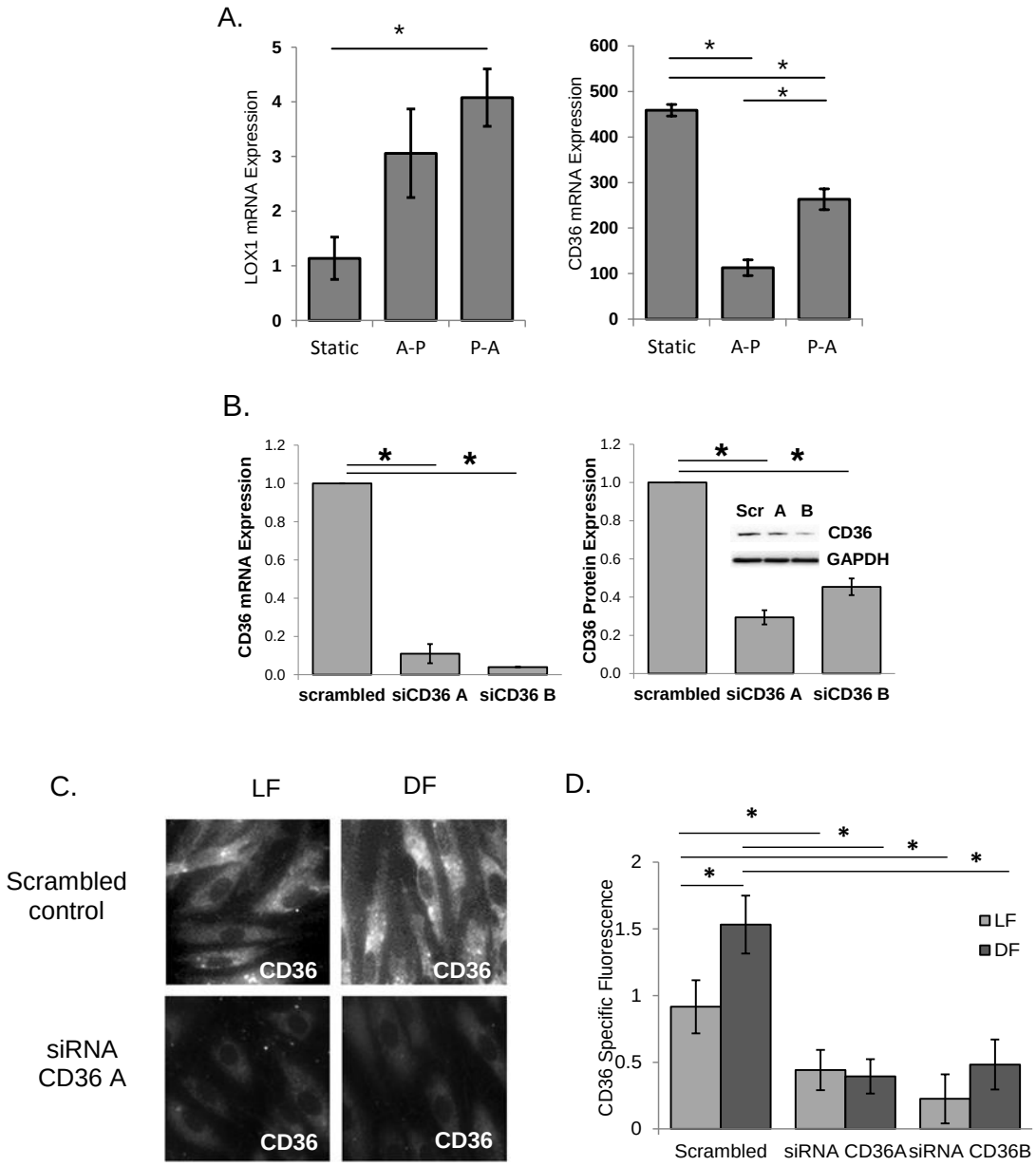

Figure 3.8: Increased CD36 expression under pro-atherogenic disturbed flow compared to athero-protective laminar flow. A. Differential CD36 and LOX1 mRNA expression in HAECs due to athero-protective versus pro-atherogenic waveforms (n = 4-6). **B.** CD36 mRNA (left, n = 3) and protein expression (right, n = 5) of HAECs treated with scrambled control and two different CD36-targetting siRNAs. **C.** Typical images of CD36 specific fluorescence in control (top) and CD36-targeting siRNA (bottom) HAECs from regions of LF (left) versus DF (right). **D.** The average CD36 specific fluorescence from control and two CD36-targeting siRNA treated HAECs from regions of laminar and disturbed flow in the presence of oxLDL (30-50 cells per condition per experiment, n = 3-5). * $p < 0.05$.

DF-induced increase in oxLDL uptake is mediated by CD36

This led us to hypothesize that CD36 may have a role in shear induced oxLDL uptake in endothelial cells. Therefore, we ran shear stress experiments using the step barrier microfluidic chamber to test the role of CD36 in oxLDL uptake. As in the other flow experiments, a medium containing DiI-oxLDL (1 μg /mL) was sheared over a confluent monolayer of siRNA treated HAECs for 48 hours. Cells were then fixed and imaged for oxLDL uptake. As expected, oxLDL uptake into control HAECs was greater under DF conditions as compared to LF. HAECs treated with CD36-targetting siRNAs, though, had reduced oxLDL uptake as compared to controls (Figure 3.9: A, representative fluorescent images; B, their average cellular oxLDL uptake). Additionally, there was no difference in uptake between laminar and disturbed flow conditions in the CD36-targetting siRNA treated ECs. Taken together, the CD36 expression data and these results suggest that CD36 is both highly responsive to pro-atherogenic disturbed flow and critically important in endothelial oxLDL uptake.

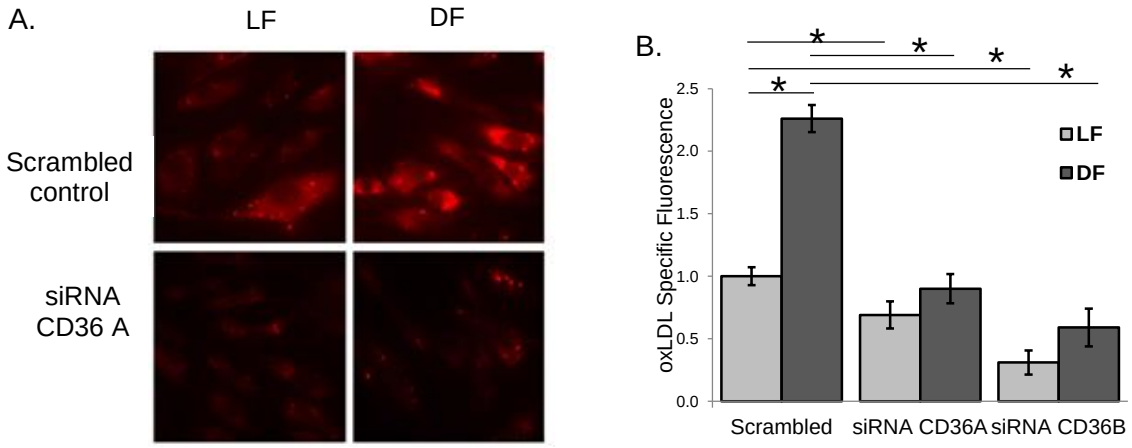

Figure 3.9: OxLDL uptake depends on CD36 scavenger receptor. A. Representative fluorescent images of oxLDL uptake into scrambled control (top) and CD36-targetting siRNA (bottom) treated HAECs under laminar (left) and disturbed (right) flow. **B.** Average oxLDL specific fluorescence in HAECs treated with either scrambled control or CD36-targetting siRNAs under LF and DF (20-40 cells per condition per experiment, 4 independent experiments). * $p < 0.05$.

DF-induced increase in the uptake of oxLDL is not dependent on LOX1

Since LOX1 has been shown to be a major receptor in macrovascular endothelial cells (Lubrano and Balzan, 2014; Pirillo et al., 2013), we wanted to test its role in disturbed flow induced endothelial oxLDL uptake. LOX1 was downregulated using two LOX1-targetting siRNAs compared to control HAECs, which were treated with scrambled siRNA, and were tested using PCR and Western Blotting techniques. These candidate siRNAs (siRNA LOX1 A and B) were selected based on the PCR results showing maximal knockdown from an original pool of four LOX1-targetting siRNAs. There was over 70% reduction in LOX1 mRNA expression and ~70% reduction in LOX1 protein expression in LOX1-targetting siRNA treated ECs as compared to controls (Figure 3.10 A).

Next, we tested the role of LOX1 in DF-induced increased oxLDL uptake in ECs. Our control HAECs showed that there was greater oxLDL uptake under DF as compared to LF conditions as we expected (B, representative fluorescent images; D, average cellular oxLDL uptake). Notably, the LOX1-targetting siRNA treated ECs had the same degree of oxLDL uptake as control ECs and there was increased uptake in cells from the DF regions compared to LF in all siRNA conditions. This indicates that the scavenger receptor CD36, and not LOX1, is required for oxLDL uptake into ECs under flow conditions.

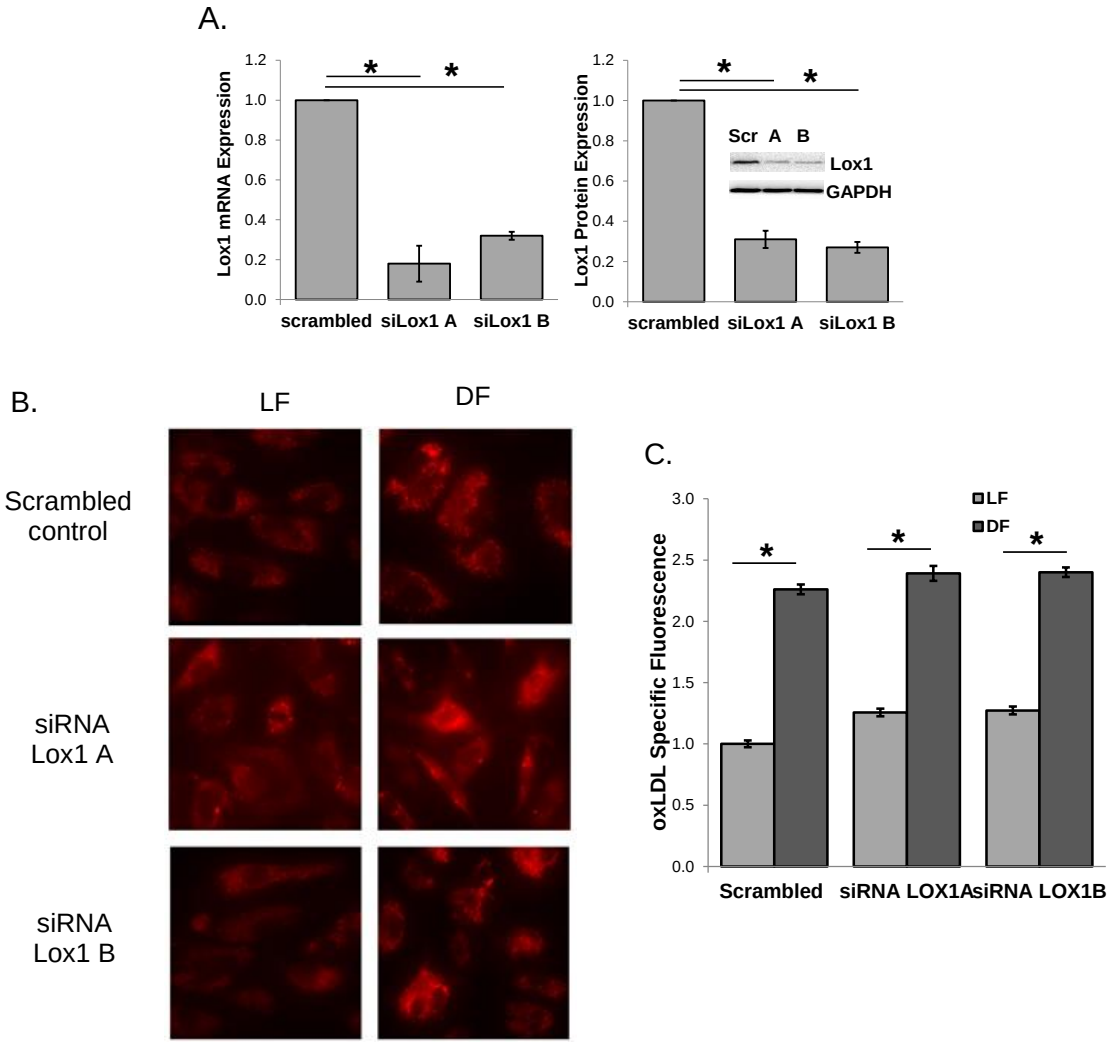

Figure 3.10: OxLDL uptake does not depend on the Lox1 receptor. A. Lox1 mRNA (left, n = 4) and protein expression (right, n = 4) of HAECs treated with scrambled control and two LOX1-targetting siRNAs. **B.** Representative fluorescent images of oxLDL internalization into HAECs treated with either control or two LOX1-targetting siRNAs under laminar and disturbed flow. **C.** Average oxLDL uptake into scrambled control and LOX1-targetting siRNA treated ECs under LF and DF (20-40 cells per condition for each experiment, 4 independent experiments). * $p < 0.05$.

Disturbed flow induced increase in oxLDL uptake is dependent on caveolae

Caveolae are a main mechanism for oxLDL uptake into static cultured endothelial cells (Sun et al., 2010), but the role of caveolae in laminar versus disturbed flow induced oxLDL uptake has not been studied. To this end, we tested the oxLDL uptake following 48 hours of laminar and disturbed flow into WT and Cav1 KO MMVECs. As shown in previous experiments (Figure 3.5 C), there is increased oxLDL uptake under DF conditions as compared to LF in WT ECs (Figure 3.11 A top, representative confocal images; B, average oxLDL specific fluorescence). In cells lacking Cav1, though, oxLDL uptake decreased significantly (~50% reduction) and no difference in uptake is seen in Cav1 KO ECs from the laminar versus disturbed flow regions (A, bottom; B). Additionally, differential uptake in WT versus Cav1 KO ECs was also tested in laminar versus oscillatory flow conditions. As previously shown (Figure 3.6 C, D), there is decreased uptake in WT ECs from the oscillatory flow regions as compared to those from the laminar flow regions (Figure 3.11 C, top; D). Cav1 KO ECs, though, had a dramatic decrease (~70% reduction) in cellular oxLDL uptake as compared to WT controls. Also, there is no observable difference in oxLDL uptake in KO ECs under laminar versus oscillatory flow (Figure 3.11 C, bottom; D). These cells were quantified for alignment to flow. As shown in Figure 3.11 E, there is no discernible alignment to the direction of flow in Cav1 KO cells from either the laminar or the oscillatory flow regions. The results presented here suggest that caveolae is a main endocytotic mechanism for oxLDL internalization into endothelial cells under any shear condition tested, laminar, disturbed and oscillatory flow.

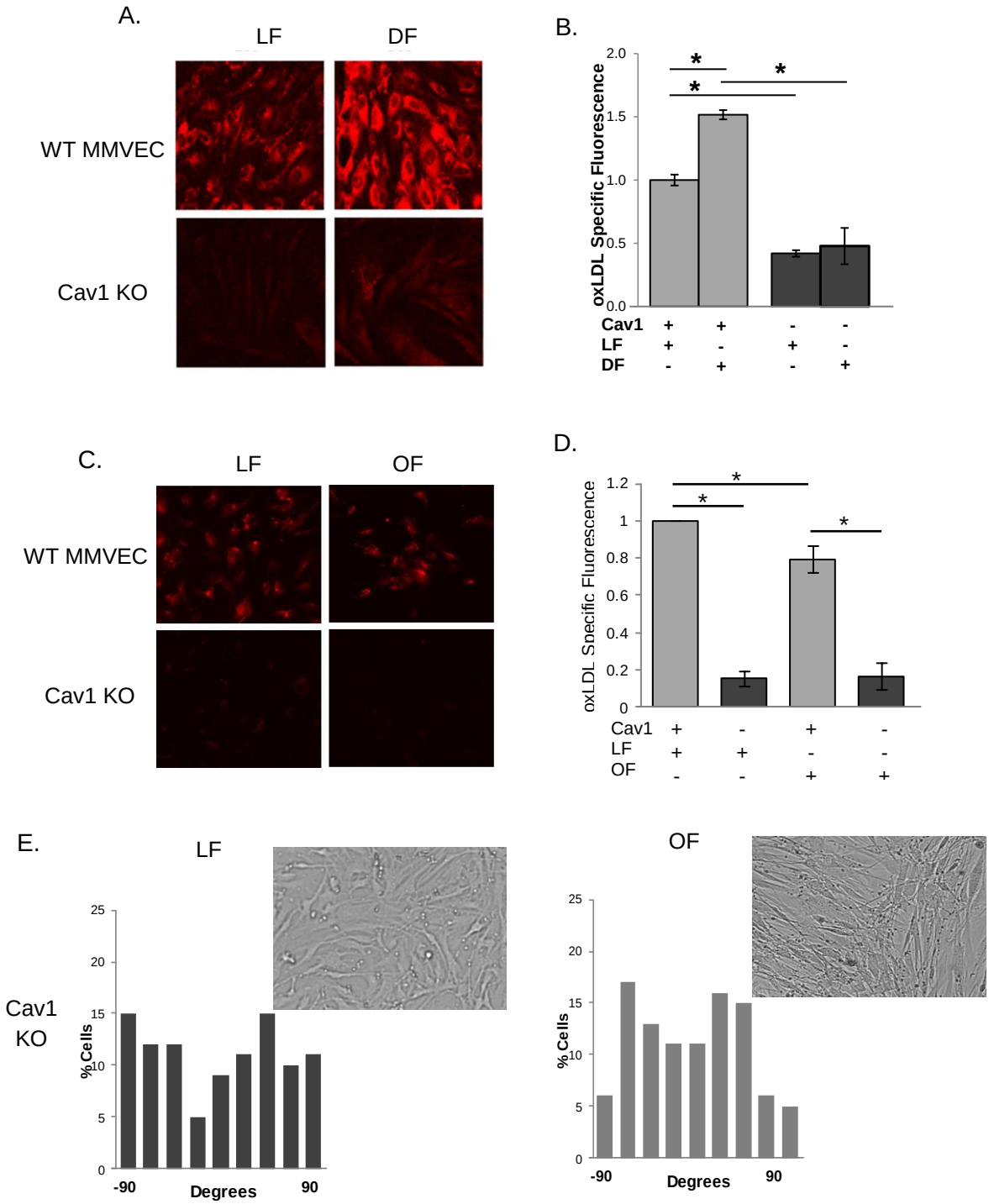

Figure 3.11: OxLDL uptake into ECs depends upon intact caveolae machinery.
A. Representative confocal images of oxLDL uptake into WT MMVECs (top) and Cav1 KO ECs (bottom) from laminar flow (left) and disturbed flow (right) regions of the step barrier microfluidic chamber. **B.** Average cellular oxLDL uptake into WT and Cav1 KO MMVECs in LF versus DF conditions (30-50 cells per condition per experiment, n = 6). **C.** Representative fluorescent images of oxLDL uptake into WT (top) and Cav1 KO MMVECs (bottom) from laminar (left) and oscillatory (right) flow regions. **D.** Average cellular oxLDL uptake into WT and Cav1 KO MMVECs in laminar and oscillatory flow conditions (25-40 cells per condition per experiment, 6 independent experiments). **E.** Cell alignment to the direction of flow in Cav1 KO MMVECs following 48 hours of laminar flow (left) and oscillatory flow (right). 15-30 cells per condition for each experiment, n = 4. The brightfield image insets are representative images of Cav1 KO MMVECs under LF (left) and OF (right). * $p < 0.05$.

CD36 and Cav1 cell membrane expression and co-localization

Since we previously showed that shear induced oxLDL uptake is dependent on both the oxLDL receptor CD36 and caveolae comprised of Cav1 protein, we wanted to determine if CD36 and Cav1 are linked events in oxLDL uptake or function independently. One preliminary step is determining if endothelial CD36 and Cav1 co-localize. In this experiment, we examined co-localization at the basal membrane from images obtained from TIRF (total internal reflection fluorescence) imaging. HAECs were subjected to laminar and disturbed flow conditions in the step barrier microfluidic channel for 48 hours with a medium containing unlabeled oxLDL (1 μg/ml) and were fixed, washed and immunohistochemistry techniques were used to detect membrane and intracellular Cav1 and CD36 expression. TIRF imaging allows the visualization of fluorophores from a very thin section (~100 nm) of a specimen (as compared to ~500-1000 nm of confocal or fluorescent microscopy) by using an angled, induced evanescent wave and the property of different refractive indices of the glass slide, specimen, and aqueous solution. Two types of images are shown: TIRF fluorescent (left column) images of the basal membrane and epifluorescent (right column) images of whole cell Cav1 and CD36 expression. As shown in Figure 3.1 A and B, both Cav1 (rhodamine, top row) and CD36 (green, middle row) are expressed on the membrane (TIRF, left column). A highly expressed Cav1 (top row) and CD36 (middle row) total cellular fluorescent expression (epifluorescence, right column) visually indicated the internalization of both Cav1 and CD36 in ECs exposed to laminar (A) and disturbed (B) flow environments. Co-localization of Cav1 and CD36 at the basal membrane in HAECs was assessed to determine if a difference existed in the co-localization between regions of differential flow, using ImageJ. Our results show that there was no difference between CD36/Cav1 co-localization between the LF versus DF regions in HAECs (Figure 3.13 C), with the co-localization of CD36/Cav1 at the basal membrane around twenty to twenty-five percent.

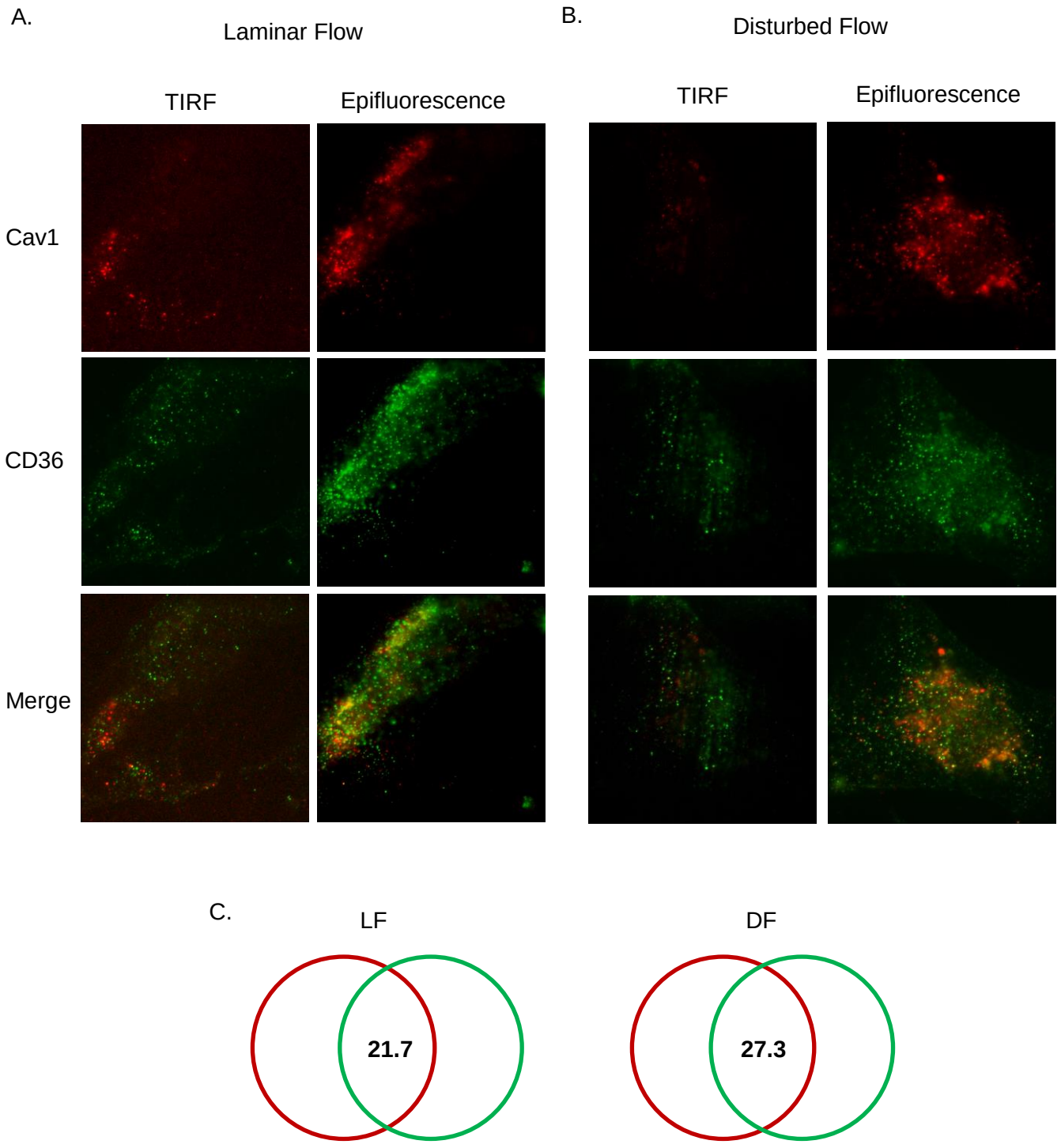

Figure 3.12: Co-localization of Cav1 and CD36 at the cell membrane of sheared HAECs as visualized by TIRF. A and B. Representative TIRF images (left column) and their corresponding epifluorescent confocal images (right column) for Cav1 (rhodamine, top row), CD36 (green, middle row) and the merged (bottom row) images for HAECs exposed to laminar flow **(A)** and disturbed flow **(B)** environments. **C.** Venn diagrams depicting the co-localization of Cav1 and CD36 from LF and DF regions in the basal membrane obtained from the TIRF images. 15-25 cells measured in three experiments.

OxLDL is highly co-localized with Cav1 in sheared ECs

Furthermore, we wanted to quantify the extent of intracellular oxLDL co-localization with caveolae and if differences existed between the laminar and disturbed flow conditions. Using a Nucleofector kit for Nucleofector^{TM} II/2B, HAECs were transfected with a green fluorescent protein-Cav1 tag overexpressing Cav1, seeded into the microfluidic chamber and grown to confluency. Following 48 hours of flow with a medium containing the rhodamine tagged DiI-oxLDL particle, cells were fixed and imaged using a Zeiss LSM 710 confocal microscope with a 63x lens. As expected, there was a high degree of co-localization (> 80%) between oxLDL and Cav-1 under all experimental shear conditions (Figure 3.13). Both oxLDL and caveolin1 appear in rather large punctate aggregations, which we attribute to the possible presence of oxLDL in small caveolar clusters (as shown in Figure 3.1, double arrow) rather than individual caveolae vesicles. Interestingly, the degree of oxLDL/Cav1 co-localization was greater in cells exposed to recirculating DF as compared to LF, as calculated by ImageJ software.

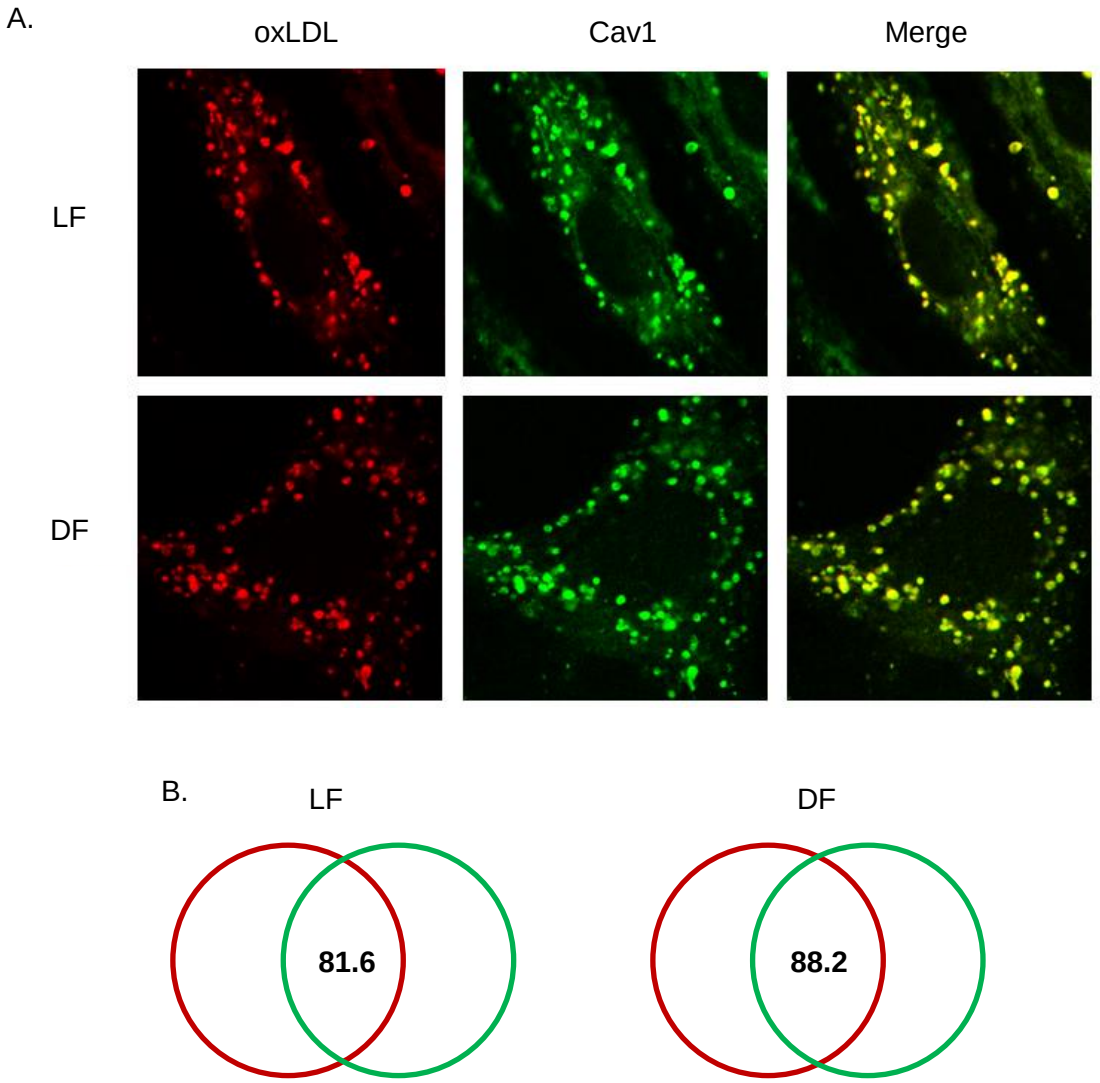

Figure 3.13: Co-localization of oxLDL with Cav1 under different shear conditions. **A.** Representative confocal images of oxLDL (rhodamine) co-localizing with GFP-tagged Cav1 from laminar flow (top) and disturbed flow (bottom) regions. **B.** Venn diagrams depicting the degree of overlap between oxLDL and Cav1 in LF and DF regions. There was statistical significance of $p < 0.05$ in these two flow conditions. 20-30 cells measured in three experiments.

Endocytosis of CD36 in HAECs

To further address the question of whether Cav1 and CD36 are independent or linked events in endocytosis, we examined CD36 endocytosis in control and Cav1 depleted cells. Through a protocol of accelerated immunohistochemistry labeling of CD36 on live cells at 4° C, we visualized CD36 surface staining and endocytosis. The protocol was conducted in the cold to inhibit cellular endocytosis and permit the visualization of endocytotic proteins at the cellular surface. A rhodamine tagged surface staining marker for the plasma membrane was applied to the live cells prior to FITC-CD36 labeling. Their observed co-localization ensured the CD36 is expressed on the cell's membrane (Figure 3.14 A). After CD36 labeling, HAECs were fixed at 4° C for the visualization of CD36 at the membrane (Figure 3.14 B, left) or were warmed in an incubator to permit CD36 endocytosis (Figure 3.14 B, right) prior to their fixation. Confocal z-stack imaging shows the endothelial surface staining and endocytosis of CD36 in the top and right panels of each image.

Furthermore, to determine the impact of Cav1 on CD36 endocytosis, HAECs were treated with either scrambled control siRNA or Cav1-targetting siRNA. Western blot analysis showed that there was a ~70% reduction in Cav1 expression in Cav1-targetting siRNA treated ECs as compared to controls. As shown in Figure 3.14 C, control cells visually showed a greater expression of CD36 and enhanced CD36 internalization (top) as compared to Cav1 depleted ECs (bottom). These results indicate that CD36 enters cells through a caveolae-dependent mechanism.

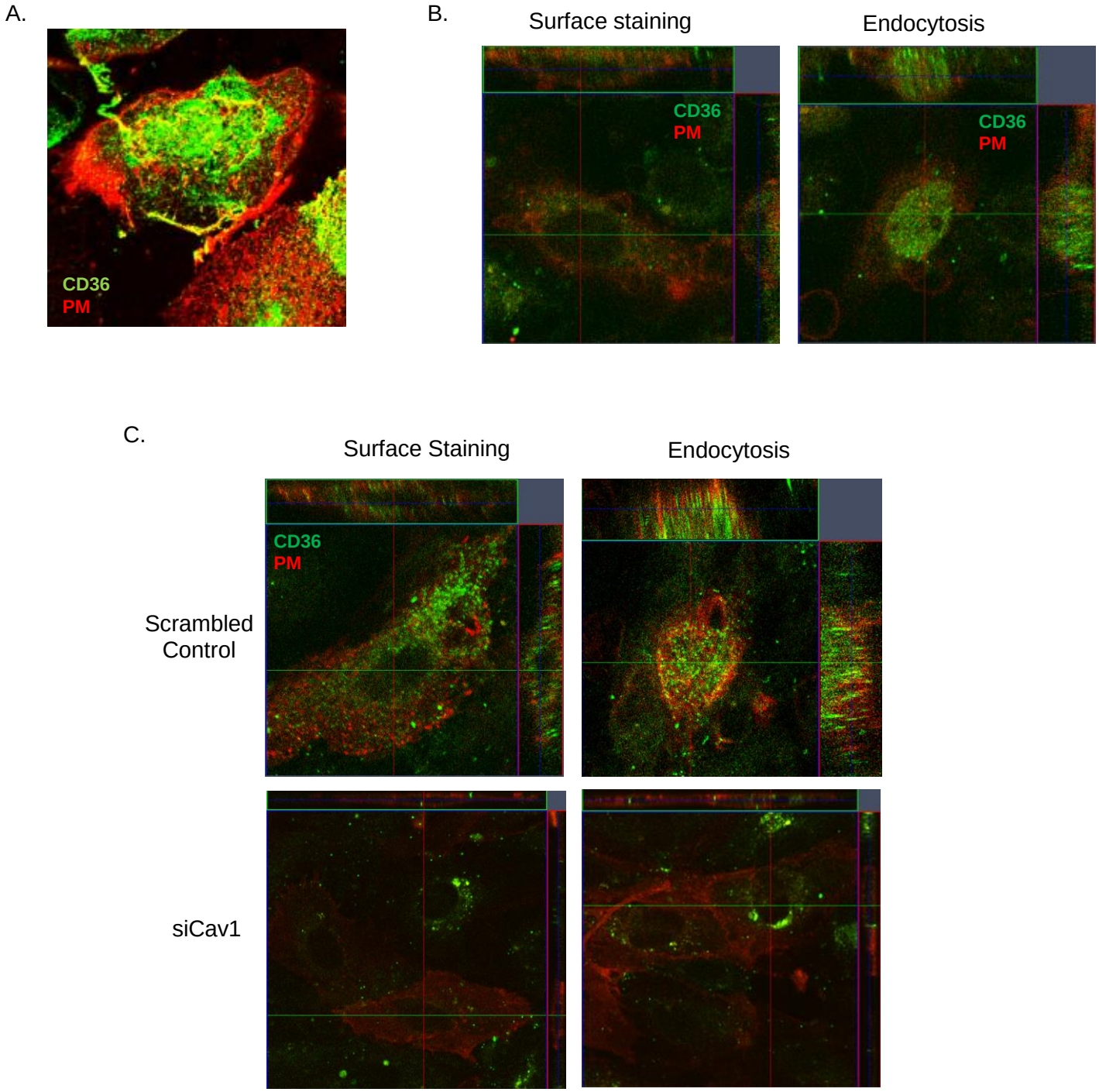

Figure 3.14: Plasma membrane surface expression and endocytosis of CD36 in scrambled control and Cav1 depleted cells. A. Representative confocal image of CD36 expression on the plasma membrane (PM). **B.** CD36 surface expression (left) and endocytosis (right) in HAECs. **C.** CD36 surface expression (left) and endocytosis (right) in control (top) and Cav1 depleted ECs (bottom). 10-20 cells were imaged per experiment, four independent experiments.

The effect of eNOS on oxLDL uptake under laminar and disturbed flow conditions

It is well-known that laminar flow stimulates the production of NO [reviewed by (Chiu and Chien, 2011)], whereas disturbed flow leads to eNOS uncoupling and pro-inflammatory ROS generation (Li et al., 2011). Therefore explore the mechanism of caveolae-mediated oxLDL uptake, we compared the uptake in WT ECs compared to those lacking eNOS. Our preliminary data indicates that eNOS is required for the flow induced increase in oxLDL uptake (Figure 3.15 A). Additionally, cells lacking eNOS have a small but statistically significant decrease (> 30%) in oxLDL uptake compared to WT ECs.

To further study the role of eNOS, we looked at eNOS phosphorylation on Serine 1177 in WT ECs. eNOS phosphorylation (Ser-1177) activates eNOS (Dimmeler et al., 1999) leading to an increase in NO and ROS generation (Chen et al., 2008). Studies from our lab show that an increase in phospho-eNOS are indicative of eNOS hyperactivation and endothelial dysfunction (Bakhshi et al., 2013), but its role in DF induced macromolecular uptake is unknown. We found that that there is, in fact, an increase in eNOS phosphorylation under disturbed flow conditions in the presence of oxLDL (Figure 3.15 B) supporting our data that both eNOS and caveolae are required for the flow induced increase in oxLDL uptake.

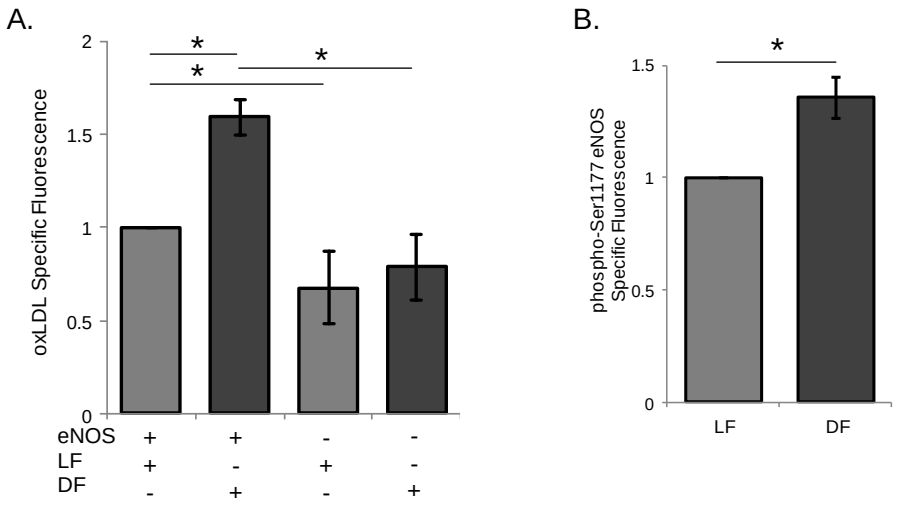

Figure 3.15: OxLDL uptake is dependent upon endothelial nitric oxide synthase (eNOS). A. oxLDL uptake into WT and eNOS deficient (eNOS/Cav1 double knockout-Cav1 YFP) MMVECs under laminar and disturbed flow conditions (20-40 cells per condition per experiment, n=4). **B.** Phospho-serine 1177 eNOS activation in MMVEC from LF and DF regions of the step barrier chamber. * $p < 0.05$.

Disturbed flow has no effect on albumin uptake

Next, we addressed whether DF enhances the caveolae machinery to increase oxLDL internalization, independent of CD36 expression. Studies from our lab and others have shown that caveolae is required for the transport of the major macromolecule, albumin (Shajahan et al., 2004; Vandoorne et al., 2010). Since albumin binds to the gp60 receptor (Ghitescu et al., 1986) and not CD36, we performed experiments with a GFP-labeled albumin (1 μg/mL) containing medium which was sheared over ECs in the step barrier chamber for 48 hours. Following flow cessation, cells were fixed, washed, fluorescently imaged for albumin uptake and average cellular uptake was quantified using ImageJ. Our data shows no difference in albumin uptake into HAECs from laminar or disturbed flow regions (Figure 3.17). This was also found to be the case in human microvascular ECs as well. Therefore, although caveolae plays an important part in oxLDL uptake, these data suggest that disturbed flow does not enhance caveolae machinery in cells. Taken together with our data of enhanced mRNA expression (Figure 3.8 A) and protein expression of CD36 (Figure 3.8 C) under disturbed flow, we suggest that the DF-induced increase in the cellular uptake of oxLDL is mediated by increased expression of the oxLDL receptor and not by enhancing the endocytotic activity of caveolae.

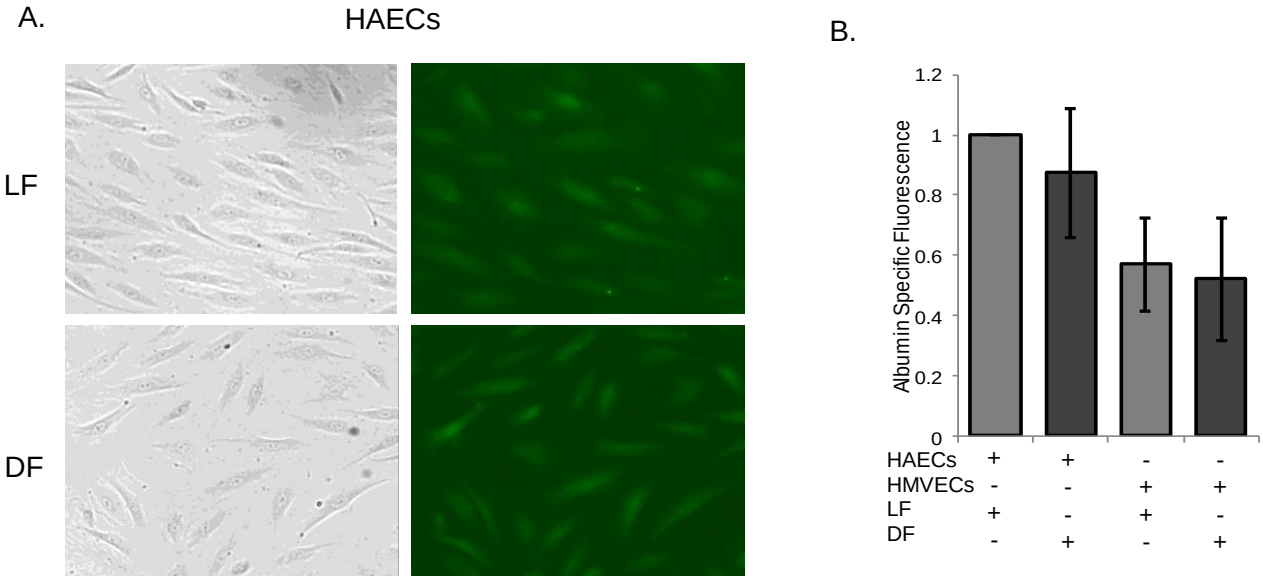

Figure 3.16: Albumin uptake into HAECs and HMVECs is the same under both laminar and disturbed flow conditions. A. Representative brightfield (left) and fluorescent images (right) of albumin uptake into HAECs from laminar (top) and disturbed (bottom) flow regions. **B.** Relative albumin specific fluorescence in HAECs and HMVECs exposed to 48 hours of LF versus DF conditions (20-40 cells per condition per experiment, $n \geq 4$).

3.3 Discussion:

We reproduced physiologically relevant athero-protective and pro-atherogenic flow environments using three different flow systems: a parallel-plate flow apparatus with either (1) unidirectional laminar flow versus high shear stress bi-directional oscillatory flow or (2) a microfluidic flow chamber with a step barrier (DePaola et al., 1999; DePaola et al., 1992) creating LF and lower shear stress recirculating DF within the same chamber, and (3) a cone and plate rheometer which creates shear stress waveforms corresponding to flow profiles based on human arterial geometries previously described (Dai et al., 2004; Wu et al., 2015). These approaches have been used to determine the impact of DF on EC properties, including the activation of several pro-inflammatory pathways, increased EC turnover and enhanced monocyte adhesion (Hahn and Schwartz, 2009; Jiang et al., 2015; Marin et al., 2013; Tarbell et al., 2014). In these studies, we used a fluorescently labeled oxLDL particle. Endothelial cell exposure to oxLDL has been shown to induce cell apoptosis, increase surface adhesion molecule expression which mediates the adhesion of monocytes, stimulate an inflammatory response and disrupt the functioning of the endothelial permeability barrier [reviewed by (Levitan et al., 2010; Pirillo et al., 2013)].

The overall goal of this project was to determine the impact of the synergistic effect of physiological hemodynamic environments and dyslipidemia on endothelial biomechanics. Enhanced aortic stiffness is well known to be associated with the onset and progression of cardiovascular disease [reviewed by (Kohn et al., 2015; Palombo and Kozakova, 2016)]. To address our goal, we first we compared uptake of pro-inflammatory oxLDL in cells exposed to either LF and OF or LF and DF environments, as studies from our lab have shown that oxLDL exposure enhances endothelial stiffness (Oh et al., 2016; Shentu et al., 2012; Shentu et al., 2010). Our data showed that although there is reduced oxLDL uptake into cells from OF

regions compared to LF, there was enhanced uptake into ECs exposed to DF versus LF. We attribute these somewhat contradictory results to the differences between the oscillatory and disturbed flow patterns themselves. Our interpretation of this data is that the lower shear stress values seen in the disturbed flow region after the step barrier facilitate oxLDL uptake. Furthermore, we suggest that since bidirectional flow is a characteristic of both OF and DF, the enhanced oxLDL endocytosis into ECs is primarily attributed to the lower shear stress values rather than bidirectional flow itself. Overall, these sets of experiments showed that the uptake of oxLDL was enhanced in pro-atherogenic disturbed flow as compared to athero-protective laminar flow. At the same time, a similar study recently showed that oxLDL uptake into coronary ECs grown in bifurcated tube sections was greater in the sections exposed to recirculating and laminar flow, as compared to the sections of laminar flow only and the static control sections (Martorell et al., 2014). ECs seeded into whole tubed sections is a more realistic method geometrically, though their approach did not have the advantage of studying defined regions wholly dedicated to disturbed flow versus laminar flow. Atherosclerotic plaques preferentially develop in the *inner* curvatures of the aortic arch and carotid bifurcation, which is subject to low shear stress bi-directional flow and tend to be absence in the high shear stress bi-directional flow regions of the *outer* curvature of the arch and bifurcation [reviewed by (Chiu and Chien, 2011)]. Here we show a distinct difference in the responses of cellular oxLDL uptake based on the shear stress value in bi-directional flow: low (+/- 3 dynes/cm^2) shear stress bi-directional flow results in increased oxLDL uptake whereas high (10 – 20 dynes/cm^2) shear results in decreased oxLDL uptake, as compared to laminar flow control.

Atherosclerosis is a disease of the large arteries and not typically found in the microvasculature. Many of the same inflammatory pathways, though, are activated in both macro- and microvascular ECs, such as localized increase in reactive oxygen species production and enhanced leukocyte recruitment to the endothelial surface (Vitiello et al., 2014). We therefore

wondered if differences in oxLDL uptake would exist between HAECs as compared to HMVECs under laminar and disturbed flow conditions. This was also important to test because one of our mouse models testing the role of caveolae uses microvascular ECs from Cav1 KO mice. Although we did observe a significant increase in oxLDL uptake in the DF regions in HMVECs compared to LF regions, there was significantly less uptake in HMVECs overall (~40% less) as compared to HAECs. These results may contribute to our hypothesis that enhanced oxLDL uptake found in DF regions is a contributing factor in the onset of atherosclerosis.

We further determined that the shear stress induced uptake of oxLDL is mediated by the eNOS/Cav1 endocytotic machinery which has been shown to be a major pathway of macromolecular albumin uptake into endothelial cells (John et al., 2003; Sverdlov et al., 2009). Previous work has shown that oxLDL uptake into static cultured human umbilical vein ECs is caveolae mediated. Our research is consistent with these studies and extended them to include cellular affects due to eNOS and Cav1 in physiologically relevant flow environments. Previous work has shown that Cav1 is a putative mechanosensor in endothelial cells as evidenced by the acute changes in mechanosignalling events upon flow initiation (Rizzo et al., 2003; Yang and Rizzo, 2013). One of these caveolae signaling events is laminar flow induced activation of eNOS leading to the increased production of the essential vasodilator nitric oxide [reviewed by (Chiu and Chien, 2011)]. Our data also shows that Cav1 plays a major role in the differential uptake of oxLDL under flow conditions. The most straightforward interpretation of why Cav1 and eNOS are essential for endothelial oxLDL uptake is that intact eNOS/Cav1 machinery is required for oxLDL endocytosis. However, our results show no difference in albumin uptake under laminar versus disturbed flow. This suggests that although caveolae are required for oxLDL internalization under flow conditions, another molecular system is required to create the phenomena of enhanced oxLDL uptake under disturbed flow conditions.

As far as the mechanism of DF-induced increase in oxLDL uptake into HAECs, our results show that increased uptake is due to increased expression of the CD36 endothelial scavenger receptor whereas another major receptor, LOX1, seems to have no noticeable role. These results were surprising since most studies focus on LOX1 as the primary endothelial oxLDL receptor (Lubrano and Balzan, 2014; Pirillo et al., 2013) whereas CD36 has been primarily studied in monocytes, macrophages and platelets (Silverstein and Febbraio, 2009) with only a couple of research studies showing significant CD36 involvement in endothelial functioning. Specifically, CD36 was shown to have a role in oxLDL-induced EC redistribution of eNOS (Uittenbogaard et al., 2000) and that endothelial CD36 has anti-angiogenic properties (Dawson et al., 1997). Additionally, a recent study from our lab shows that CD36 is required for oxLDL-induced endothelial stiffening (Oh et al., 2016). Here, we show that CD36 expression is significantly higher in HAECs exposed to athero-protective and pro-atherogenic flow conditions than the expression of LOX1, which is suspected to be the reason why the knockdown of LOX1 did not have any effect on oxLDL uptake under flow whereas CD36 significantly reduced flow induced uptake of oxLDL.

Furthermore, our data provide evidence that caveolae endocytosis is a main mechanism in the internalization of oxLDL into endothelial cells and that the DF-induced increase in oxLDL uptake is dependent on the oxLDL receptor CD36. We showed that there is enhanced mRNA and protein expression of CD36 under disturbed flow compared to LF. Additionally, the uptake of albumin, a macromolecule internalized by caveolae, was the same under LF and DF conditions, in both HAECs and HMVECs. Taken together, this data suggests that the DF-induced increase in the cellular uptake of oxLDL is mediated by increased expression of the oxLDL receptor and not by enhancing the endocytotic activity of caveolae.

CHAPTER 4: Role of oxidized lipids in endothelial and sub-endothelial stiffness *in vitro* and *in vivo*

4.1 Introduction:

Increased vascular stiffness in large arteries has been repeatedly shown to be associated with the onset and progression of cardiovascular disease [reviewed by (Kohn et al., 2015; Palombo and Kozakova, 2016)]. Studies show that aortic stiffness has been shown to increase blood pulse wave velocity and aortic pulse pressure which is an important determinant of increased cardiovascular disease events and mortality (Cecelja and Chowienczyk, 2012). However, it is important to note the difference between whole artery stiffness and the stiffness of the endothelial cell monolayer, which on its own can be a major factor in the functioning of the endothelium. For example, research has shown that EC stiffness by itself has a role in increased adhesion, spreading and transendothelial migration of pro-inflammatory leukocytes (Martinelli et al., 2014; Schaefer et al., 2014) which have been shown to be a key initiating factor in the onset of atherosclerosis. A review by Schaefer *et al*. discusses how leukocyte transendothelial migration is activated by increased EC stiffness via enhanced substrate stiffness though the RhoA/ROCK/Myosin light chain (MLC) phosphatase pathway and increased acto-myosin activity [reviewed by (Schaefer and Hordijk, 2015)]. Our group has shown that exposure to oxLDL and certain oxysterols *in vitro* leads to increased endothelial stiffening (Byfield et al., 2006; Shentu et al., 2012), which is abrogated by the loss of CD36 (Oh et al., 2016). The impact of differing shear stress patterns on endothelial stiffening *in vitro*, though, is less clear. Furthermore, very few *ex vivo* biomechanical studies have been conducted on the intact endothelial monolayer of vessels.

Several pro-atherosclerotic and athero-resistant mouse models exist. Much research has shown that the genetic deletion of scavenger receptor CD36 confers protection against the

formation of atherosclerotic lesions (Brown et al., 2015; Febbraio et al., 2000; Guy et al., 2007) though some research indicates increased mean lesion area in the aortic sinus in these mice (Moore et al., 2005). Additionally, studies show that knockout of caveolin1, the main protein in macromolecular transporter caveolae, in mice has an athero-protective effect, even on a pro-atherogenic ApoE KO background (Frank et al., 2004). It is not known, though, whether there are changes in endothelial cell and sub-endothelial matrix stiffening from the intact vessels of these knockout models as compared to wild type. Here we show that stiffness of the endothelial cell monolayer is greater in the aortic arch compared to the descending aorta, an effect that is attributed to the presence of the oxLDL receptor CD36 and the intact caveolae endocytotic machinery.

4.2 Results:

OxLDL-induced stiffness as a function of concentration in HAECs

We conducted two sets of experiments to test oxLDL-induced endothelial stiffening as a function of increasing concentrations. In the first set of experiments, HAECs were seeded onto glass coverslips, grown to semi-confluency and exposed to a physiological range of concentrations (0, 10, 100 and 10,000 ng/mL) of oxLDL for 48 hours followed by elastic modulus measurements using AFM. As shown in Figure 4.1 A and B, our results show that there is a clear increase in endothelial stiffening starting at 100 ng/mL as compared to the 0 and 10 ng/mL oxLDL groups. No further stiffening is observed at 10,000 ng/mL (10 μg/ml) oxLDL.

Since previous studies from our lab show that aortic ECs stiffen in response to 10 μg/mL of oxLDL compared to control cells (Shentu et al., 2012; Shentu et al., 2010) and that a typical range of oxLDL used in *in vitro* experiments can be higher (Zhang et al., 2014), in this second set of experiments we tested endothelial stiffening in HAECs exposed to 0, 10, 50, 100 μg/mL oxLDL for one hour. As shown by the rightward shift in the histogram, our results show increased stiffening in HAECs exposed to 50 μg/mL oxLDL compared to 10 μg/mL or no oxLDL control ECs (Figured 4.1 C D). Increasing the oxLDL concentration to 100 μg/mL did not further stiffen the cells.

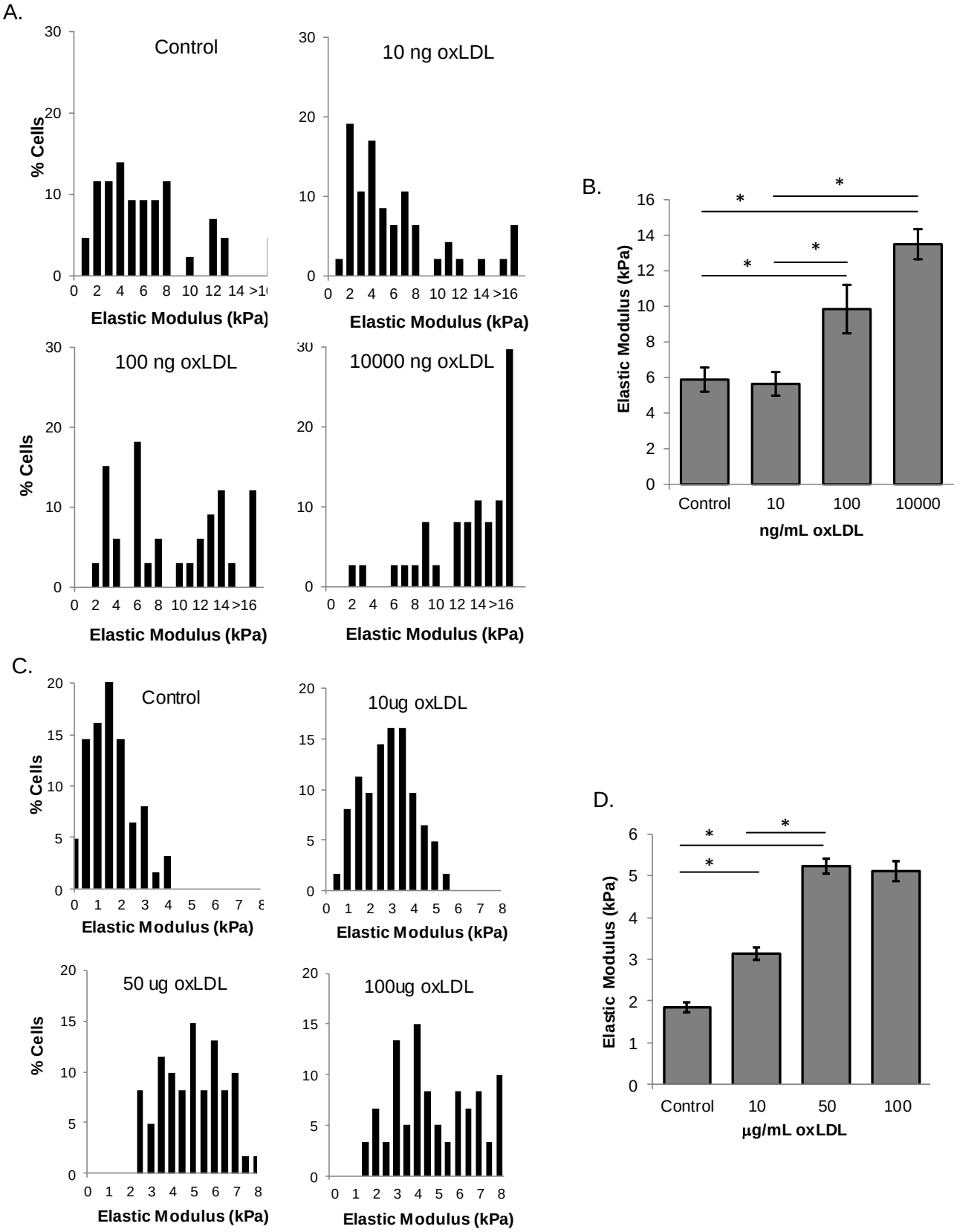

Figure 4.1: Concentration dependence of oxLDL-induced stiffening in HAECs. A. Histograms showing the elastic modulus values of HAECs exposed to varying concentrations of oxLDL for 48 hours. **B.** Average elastic modulus of HAECs treated with 0, 10, 100 or 10,000 ng/mL oxLDL. **C.** Histograms depicting the elastic moduli of HAECs exposed to different concentrations (µg/mL) of oxLDL for one hour. **D.** Average cellular elastic modulus of HAECs treated with 0, 10, 50 or 100 ug/mL oxLDL. 15-25 cells per condition for each experiment, n = 3. * $p < 0.05$. Research from C. and D. was originally published in the Journal of Lipid Research. Oh et al 2016. *Journal of Lipid Research,* 57(5), 791-808.

OxLDL-induced cell stiffness is dependent on Rho kinase

Our lab has previously shown that cellular exposure to oxLDL leads to increased stress fiber formation (Kowalsky et al., 2008), but the mechanism of oxLDL induced stiffening is not well understood. RhoA, a small GTPase, is known to regulate cytoskeleton organization, including acto-myosin contractility, cell adhesion, microtubule dynamics and actin stress fiber formation. A recent study from our group has shown that oxLDL-induced stiffening is RhoA dependent (Oh et al., 2016). Since a major downstream target of RhoA is Rho Kinase (ROCK) (Hall, 2012), we further tested RhoA pathway's involvement in oxLDL-induced cell stiffening by blocking ROCK activity through the application of a known ROCK inhibitor, Y27632. HMVECs were pretreated with 1 μg/mL Y27632 for one hour prior to the addition of oxLDL (50 μg/mL, 1 hour). As shown in Figure 4.2, application of oxLDL stiffened the cells as compared to control cells. Pre-treatment with Y27632 before adding oxLDL did not result in a rightward shift in the elastic modulus histogram, indicating that this treatment abrogated the stiffening affect. Treatment with the ROCK inhibitor alone did not significantly alter endothelial stiffening compared to control or pretreated cells. These results show that oxLDL-induced endothelial stiffening depends on Rho kinase (Oh et al., 2016).

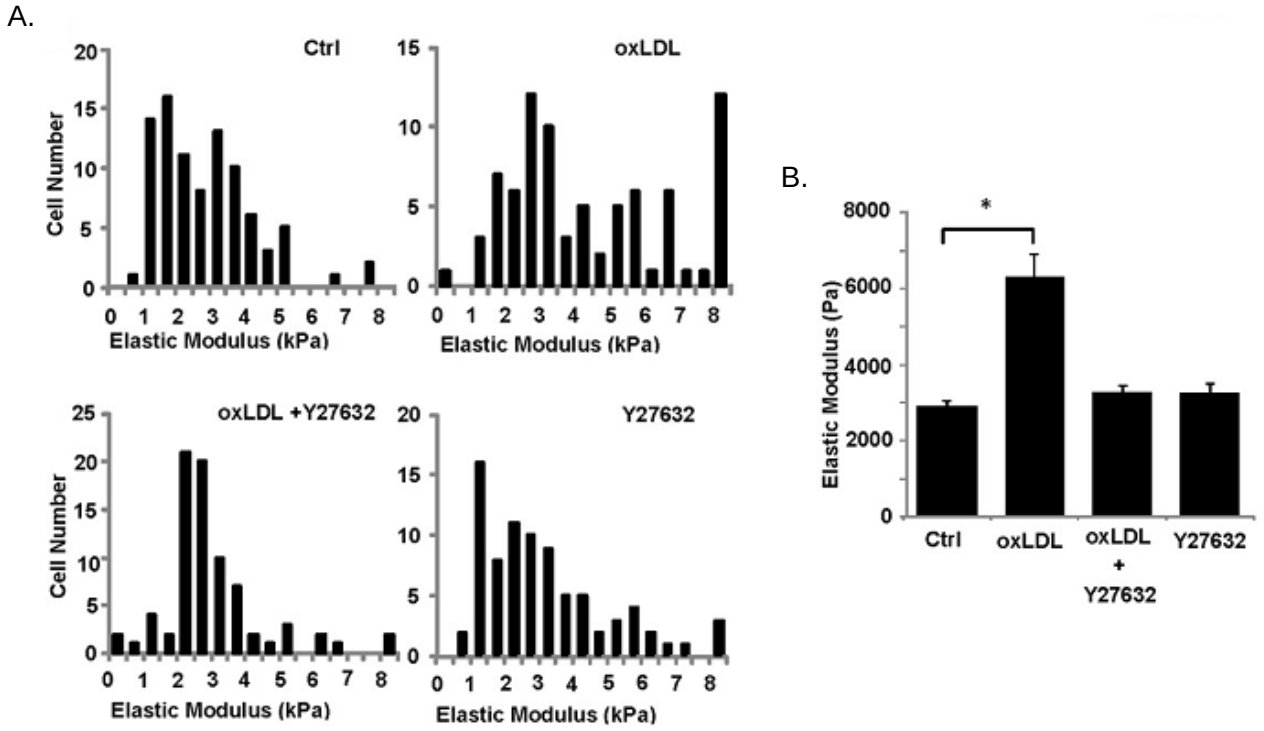

Figure 4.2: OxLDL-induced cell stiffness is through the RhoA kinase (ROCK) pathway. A. Histograms depicting the elastic modulus of ECs exposed to the ROCK inhibitor, Y27632, either with or without oxLDL, or control conditions. **B.** Average cellular elastic modulus of HMVECs. 15-20 cells were examined per condition for each experiment, three independent experiments. * $p < 0.05$. This research was originally published in the Journal of Lipid Research. Oh et al 2016. *Journal of Lipid Research,* 57(5), 791-808.

7-ketocholesterol induces stiffness in HMVECs

Previous studies (Oh et al., 2016; Shentu et al., 2012; Shentu et al., 2010) have shown that 7-ketocholesterol (7KC), a major component of oxLDL, enhances cell stiffening in macrovascular aortic ECs and that 7KC activates the RhoA signaling pathway. We therefore tested if 7KC-induced endothelial stiffening is dependent on the ctivation of the downstream effector Rho kinase. Similar to the previously described experiment, HMVECs were pretreated with the ROCK inhibitor, Y27632 (1 μg/mL, 1 hour), prior to the addition of 7KC (10 μg/mL, 1 hour) and subsequent endothelial stiffening tested using AFM. Similar to what was shown in macrovascular ECs, human microvascular ECs also stiffened in response to 7KC compared to control ECs, as shown by the rightward shift in the elastic modulus histogram (Figure 4.3 A). Pre-treatment with the ROCK inhibitor, though, abrogated this stiffening effect (Figure 4.3 B), indicating that 7KC-induced endothelial stiffening depends upon an intact RhoA/ROCK pathway.

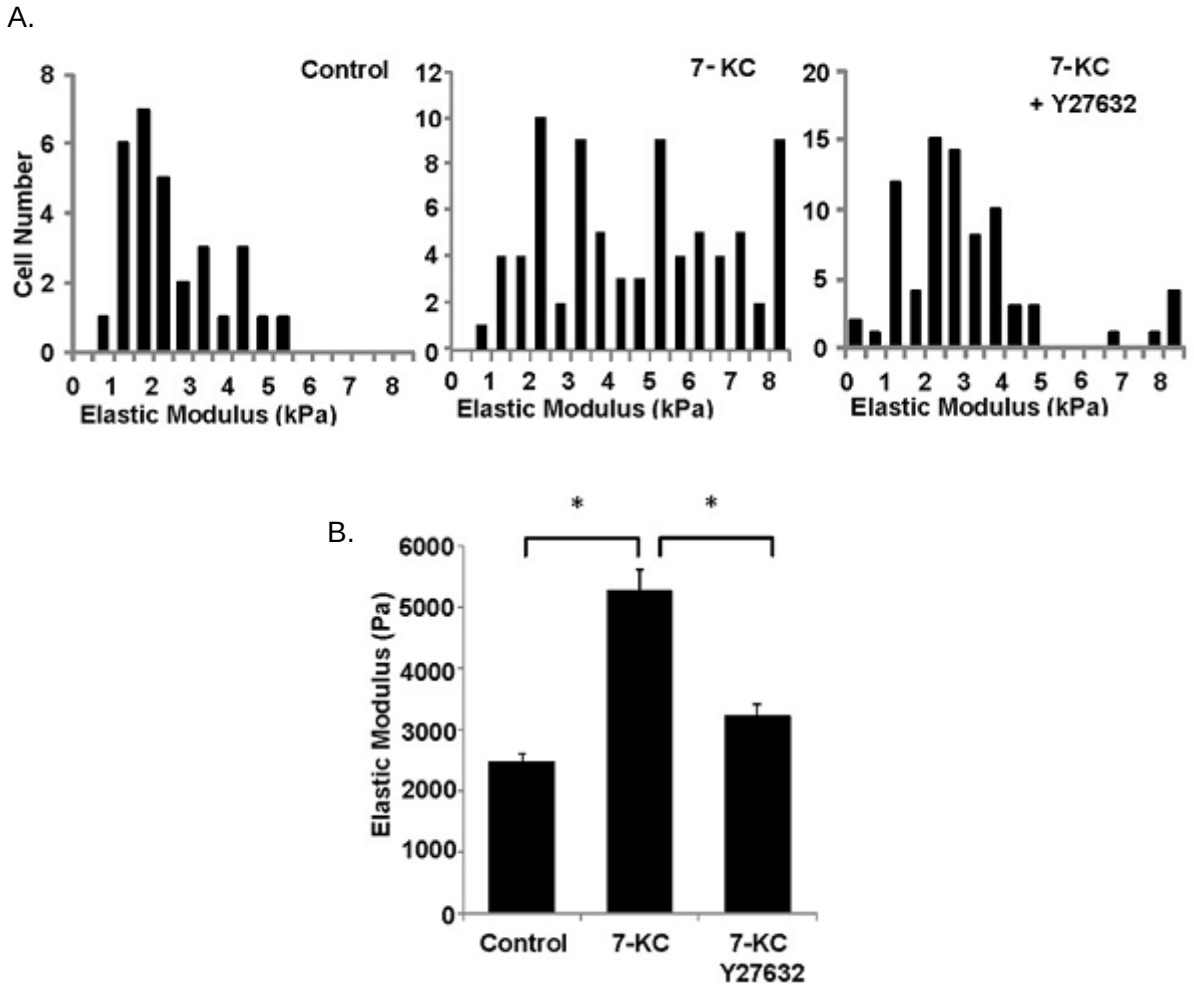

Figure 4.3: 7-Ketocholesterol induced stiffness is abrogated by blocking the ROCK pathway. A. Histograms of the elastic modulus values of HMVECs treated with 7-ketocholesterol, either with or without the ROCK inhibitor Y27632, and control ECs. **B.** Average cellular elastic modulus of HMVECs for the above mentioned conditions (20-25 ECs were tested per condition for each experiment, n = 3). * $p < 0.05$. This research was originally published in the Journal of Lipid Research. Oh et al 2016. *Journal of Lipid Research,* 57(5), 791-808.

OxLDL induced stiffness in HAECs is MLC2 dependent

Myosin light chain phosphatase, MLCP, is a known downstream target of RhoA/ROCK and functions as an acto-myosin relaxant (Kimura et al., 1996). MLCP is an enzyme that dephosphorylates myosin light chain kinase 2 (MLC2). The action of this de-phosphorylation relaxes the contractile state of actin-myosin brought upon by MLC2 (Kimura et al., 1996) ultimately leading to enhanced transendothelial migration of pro-inflammatory leukocytes (Schaefer and Hordijk, 2015). We recently showed that addition of oxLDL to HAECs causes inhibition of MLCP (Oh et al., 2016), which we hypothesize would contribute to endothelial stiffening. To check this hypothesis, we tested if oxLDL-induced endothelial stiffening would be abrogated by the MLCP inhibitor, blebbistatin. As shown in previous experiments, oxLDL exposure (50 μg/mL, 1 hour) caused cell stiffening versus control cells (Figure 4.4 A left and middle, B). Pretreating HAECs with blebbistatin (50 μM, 1 hour) prior to addition of oxLDL abrogated this stiffening effect (Figure 4.4 A right, B). Blebbistatin treatment alone did not significantly alter cell stiffness. Taken together, these data show that oxLDL-induced endothelial stiffening is dependent on an intact RhoA/ROCK/MLCP/MLC2 pathway.

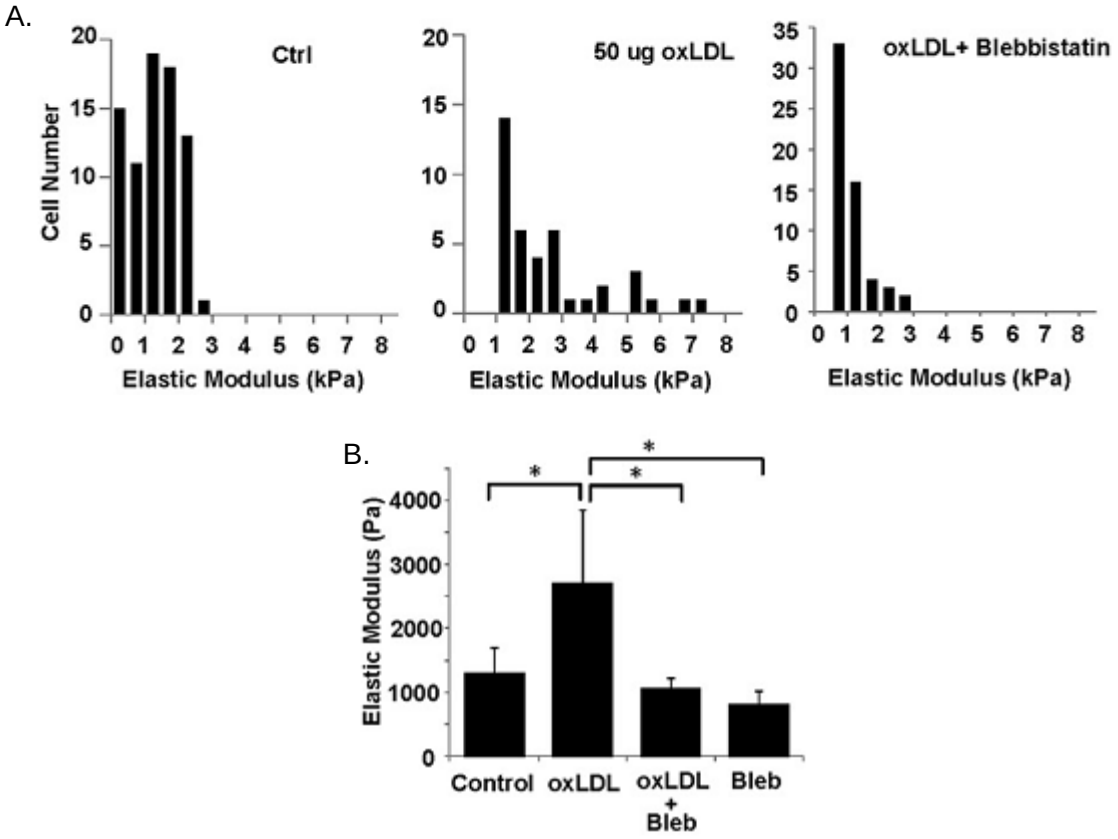

Figure 4.4: Ox-LDL-induced cell stiffness is myosin light chain kinase 2 (MLC2) dependent. **A.** Elastic modulus histograms for oxLDL treated HAECs, with or without blebbistatin (MLCP inhibitor), and control conditions. **B.** Average cellular elastic modulus for these HAECs (20-25 cells per condition for each experiment, n = 3). * $p < 0.05$. This research was originally published in the Journal of Lipid Research. Oh et al 2016. *Journal of Lipid Research,* 57(5), 791-808.

Endothelial membrane changes in lipid ordering due to the incorporation of oxidized phospholipid bi-products, POVPC and PGPC

Oxidized LDL can be separated into several groups of lipids, including phosphatidylcholine (PC), which has been shown to correspond to enhanced cellular stiffness (Shentu et al., 2012). PC is a biologically active compound that can be oxidized. Two components of oxPC, 1-palmitoyl-2-(5-oxovaleroyl)-sn-glycero-3-phosphocholine (POVPC) and 1-palmitoyl-2-glutaroyl-sn-glycero-3-phosphocholine (PGPC), have been shown to enhanced endothelial barrier permeability (Birukova et al., 2013), increase monocyte binding to ECs (Huber et al., 2002) and are increased in the atherosclerotic lesions in rabbits fed a high fat versus regular chow diet (Watson et al., 1997). Our previous studies show that the lipid composition of the cell membrane affects endothelial biomechanical properties (Shentu et al., 2010). We therefore tested if the relative quantity of “ordered” (cholesterol-rich) and “disordered” (cholesterol-poor) membrane domains would change due to the exposure of these two compounds. As described in the methods section, the relative ordering of the domains can be visualized due to the laser’s excitation of the degree of cellular incorporation of Laurden dye, which in turn emits light in two distinct wavelengths, producing two images. As described earlier (Gaus et al., 2003; Shentu et al., 2010), changes in membrane fluidity are estimated by calculating the general polarization ratio from these two images, resulting in a single pseudo-colored image. As shown in the representative images in Figure 4.5 A, lower values (blue and green) correspond to more ordered domains whereas higher values (red and yellow) represent disordered domains. This pseudo-coloring was quantified as described previously (Gaus et al., 2003). In brief, the images’ pixels (blue) each has a general polarization value which can then be separated into 2-Gaussian curves (Figure 4.5 B): a disordered domain (aqua) and an ordered domain (yellow). The generalized polarization values for each cell are determined by the vertex of the Gaussian curves. As shown in Figure 4.5 C, our data showed a statistically significant decrease in both

the ordered and disordered domains in ECs treated with POVPC and PGPC as compared to control ECs (Ayee et al., 2017). Furthermore, we showed that exposure to these biologically active compounds of oxLDL, POVPC and PGPC (10 μg/mL, 30 minutes), increases the elastic modulus values in ECs as compared to non-treated ECs (Ayee et al., 2017).

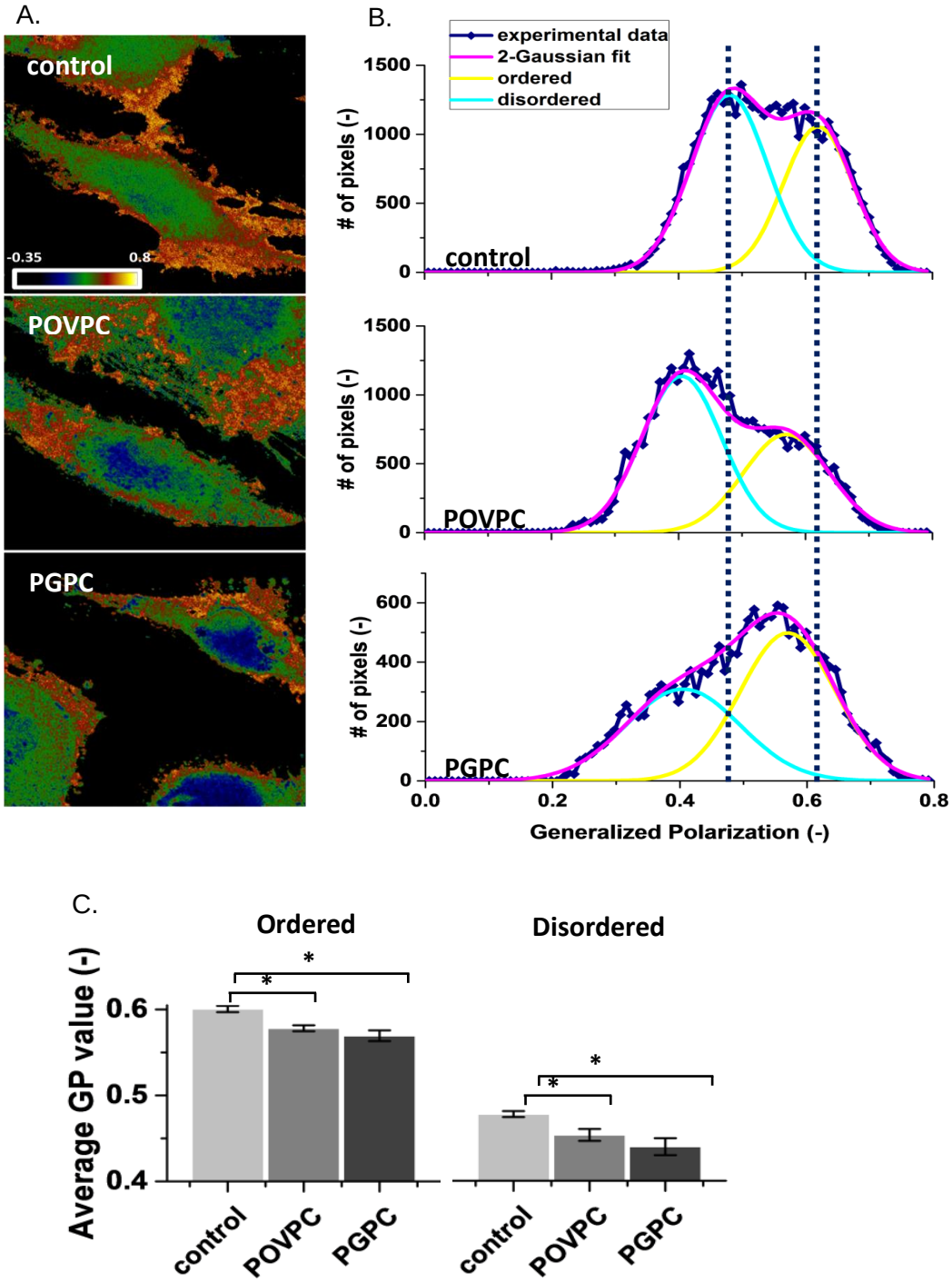

Figure 4.5: Decrease in the lipid membrane order due to incorporation of the biologically active phospholipids POVPC and PGPC. A. Representative pseudo-colored images depicting the relative phospholipid ordering in ECs treated with POVPC and PGPC as compared to control conditions. **B.** Gaussian distribution curves indicating the averaged relative shift in membrane phospholipid ordering in POVPC and PGPG conditions as compared to non-treated control conditions (12-25 cells per experiment, three independent experiments). **C.** Averaged GP values from control, POVPC and PGPC-treated ECs. This research was originally published in Biophysical Journal. Ayee et al 2017. *Biophysical Journal,* 112(2), 325-338.

Differential effects of laminar and disturbed flow on oxLDL-induced endothelial stiffness

Since atherosclerotic plaques preferentially form at disturbed flow regions of the vasculature, it is crucial to study cell stiffness in the presence of athero-protective and pro-atherogenic flow conditions in the absence and presence of oxLDL. Since previous studies showed that oxLDL increases cell stiffness (Byfield et al., 2006; Oh et al., 2016; Shentu et al., 2010) and this present study shows that there is increased uptake of oxLDL into cells exposed to DF as compared to LF, we hypothesized that HAECs exposed to DF would have increased cell stiffness compared to those from LF regions. To test this hypothesis, we first measured the elastic modulus of HAECs exposed to 48 hours of laminar and disturbed flow in the microfluidic step barrier chamber in the presence and absence of oxLDL (10 μg/mL) in the flow medium. Following flow cessation, the stiffness of the cells within the step barrier was tested with AFM. To access these cells, the chamber's upper panel was removed so that the AFM tip could probe the cell's surface. Our data shows that in the absence of oxLDL, there is no difference in cell stiffness between HAECs from the laminar and disturbed flow regions (Figure 4.6 A, top row). The addition of oxLDL to the media, however, increased the elastic moduli of these cells compared to the no oxLDL condition, as shown by the rightward shift in the elastic moduli values in the histograms (Figure 4.6 A, bottom row). Most importantly, HAECs exposed to oxLDL and DF conditions were markedly stiffer than those from LF regions (Figure 4.6 A, bottom row, B), an effect that is attributed to the increased oxLDL uptake into ECs from disturbed flow regions.

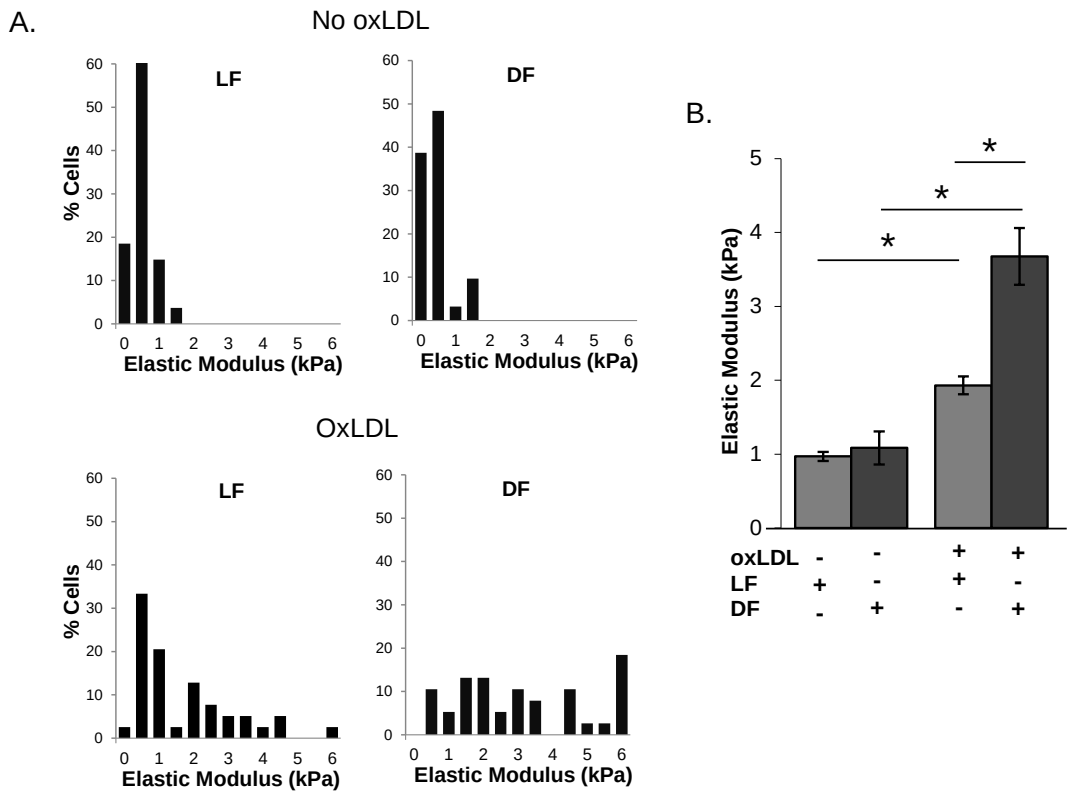

Figure 4.6: Differential effects of laminar and disturbed flow on oxidized LDL-induced stiffness in HAECs. A. Histograms depicting the elastic modulus of ECs from the laminar and disturbed flow regions either in the absence or the presence of oxLDL (30-60 cells per condition, n = 3). **B:** Average elastic modulus of HAECs in the two different flow regions with or without oxLDL in the flow medium. * $p < 0.05$.

We also performed a comparative analysis of oxLDL-induced endothelial stiffening between human macrovascular and microvascular ECs. We continue to see this phenomenon of increased cell stiffening under LF and DF conditions in the presence of oxLDL in HMVECs, but no change in the elastic modulus under LF versus DF in the absence of oxLDL, as we saw in HAECs. In contrast to HAECs, though, there is no differential stiffening affect in response to different flow patterns in the presence of oxLDL. This may be in part due to our previous observation (Figure 3.5) that HAECs had ~50-60% increase in oxLDL uptake under DF versus LF conditions, whereas HMVECs had ~30% increase. Also, the relative oxLDL uptake (Figure 3.5 C) and elastic modulus values (Figure 4.7) in HMVECs are significantly lower than those found in HAECs (Figure 4.6 C).

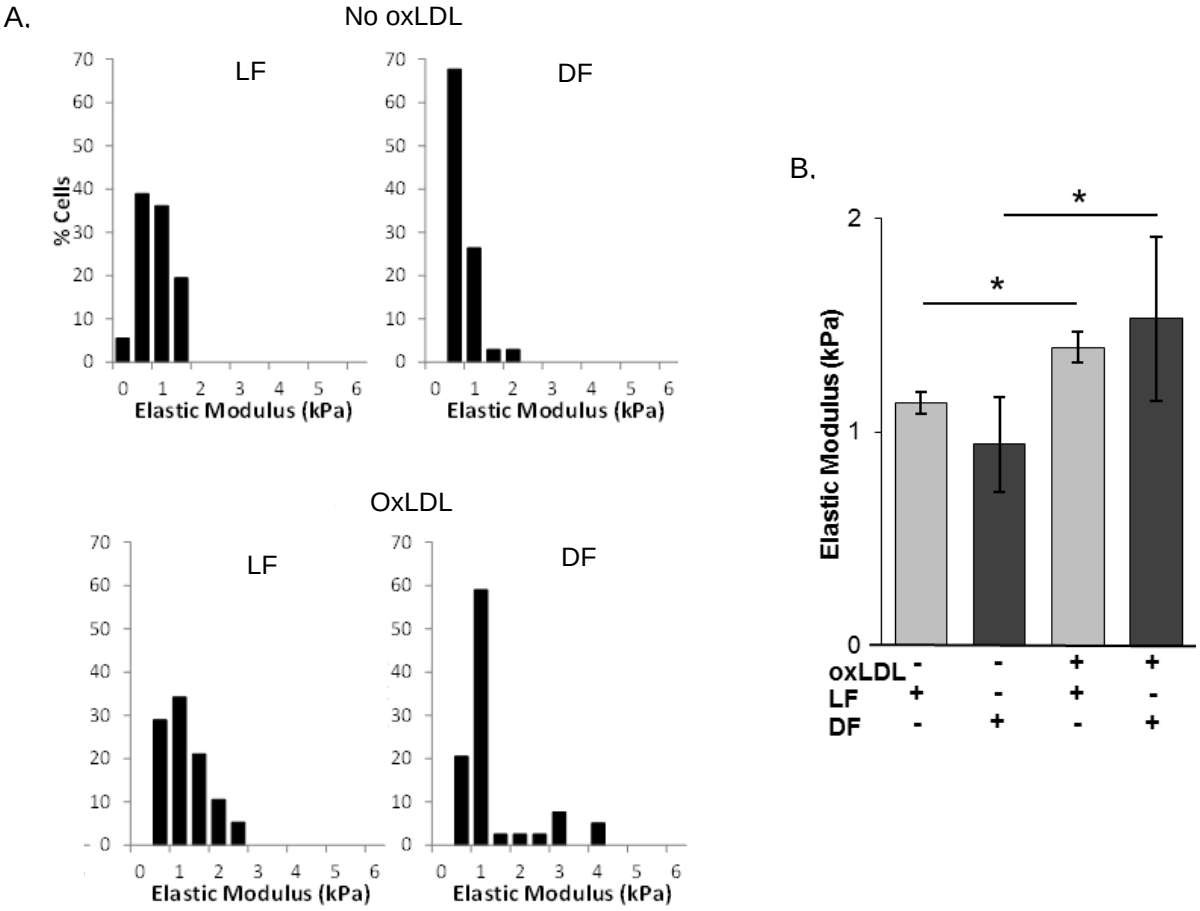

Figure 4.7: Oxidized LDL-induced stiffness in HMVECs under flow. A. Histograms depicting the elastic modulus of HMVECs from the laminar and disturbed flow regions either in the absence or the presence of oxLDL (30-60 cells per condition, n = 3). **B:** Average elastic modulus of HMVECs in the two different flow regions with or without oxLDL in the flow medium. * $p < 0.05$.

Endothelial stiffness under LF versus DF is not affected by the substrate coating in the absence of oxLDL

Growing evidence has shown that substrate stiffness affects cell morphology and cell-cell junctional integrity (Kohn et al., 2015). Research showed that increased sub-endothelial matrix stiffness is correlated with increased age (Huynh et al., 2011) and macro-scale arterial stiffness (Kohn et al., 2016). Additionally, it was shown that large depositions of collagen reside within the mouse descending aorta and that the aortic arch is rich in fibronectin, presumably due to the pro-inflammatory disturbed flow environment (Orr et al., 2005). Recently, evidence suggests that there is increased responsiveness in the endothelial cells in the aortic arch from WT mice, which was attributed to this large fibronectin deposition (Collins et al., 2014).

Since our data shows that there is no change in stiffness *in vitro* in HAECs and HMVECs as the result of laminar versus disturbed flow (Figures 4.6 B and 4.7 B) in the absence of oxLDL in the flow media, we wanted to test whether these results could be due to the gelatin coating on the PDMS microfluidic device. Therefore, we tested cell stiffening of HAECs seeded in the PDMS step barrier device coated with either collagen or fibronectin following 48 hours of flow in the absence of oxLDL. As shown in Figure 4.8, our data shows that although there is increased stiffening in cells with collagen as compared to a fibronectin substrate, there is no significant difference between the laminar versus disturbed flow environment in ECs with the same substrate.

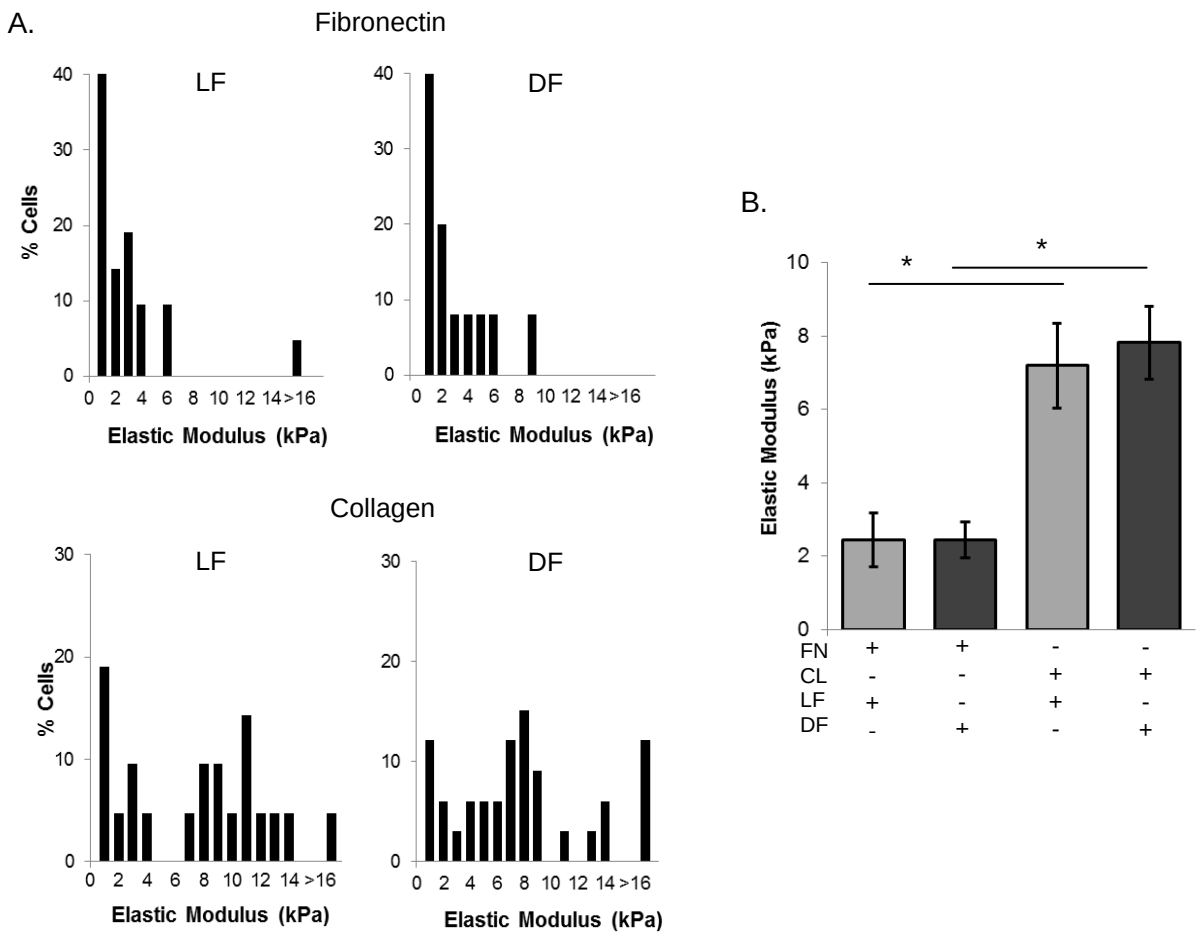

Figure 4.8: Comparative analysis of endothelial stiffness under LF versus DF in ECs seeded on different substrates. A. Histograms depicting the elastic modulus of HAECs grown on fibronectin- (top) and collagen-coated (bottom) PDMS microfluidic devices from the LF (left) and DF regions (right) following 48 hours of flow (20-30 cells per condition, 4 independent experiments). **B:** Average elastic modulus of ECs from the above described conditions. * $p < 0.05$.

The ECs from the DF region of the aortic arch are stiffer than those from the LF region of the descending aorta

The next step in our research was to determine if the oxLDL-induced endothelial stiffening under DF conditions *in vitro* would also correspond to enhanced stiffening in the endothelial monolayer of the athero-prone DF region of the aortic arch as compared to the athero-protected LF region of the descending aorta. To accomplish this task, we used 5-6 month old male WT mice which were maintained on a normal chow diet. The mice were euthanized by CO_2 followed by cervical dislocation. All protocols adhered to the guidelines established by UIC's Institutional Animal Care and Use Committee. Tissue samples were prepared by isolating and gently washing the vessels with PBS. The vessels were opened up longitudinally to permit the AFM tip access to the endothelial monolayer. The samples adhered to the glass coverslip using double sided tape. All samples were measured at multiple (6-10) distinct sites, with several force-distance curves (4 - 8) taken at each site. To ensure the integrity of the endothelium, we first did *en face* staining with the EC junctional marker Pecam1. As expected, the staining showed an intact endothelial monolayer with characteristic EC morphology, elongated cells in the LF region of the DA and a more cobblestone-like cell shape in the DF region of the aortic arch (Figure 4.9 A). Our data shows that there is enhanced cell stiffening in the endothelium from the athero-prone region of the aortic arch (~ 3.9 kPa) as compared the athero-protective region of the descending aorta (~ 2.3 kPa) as shown by the rightward shift in the elastic moduli values in the histogram (Figure 4.9 B, C). These data for the first time provide values of the elastic moduli, a major determinant of cellular biomechanics, of the inner lining of the aortic arch and descending aorta.

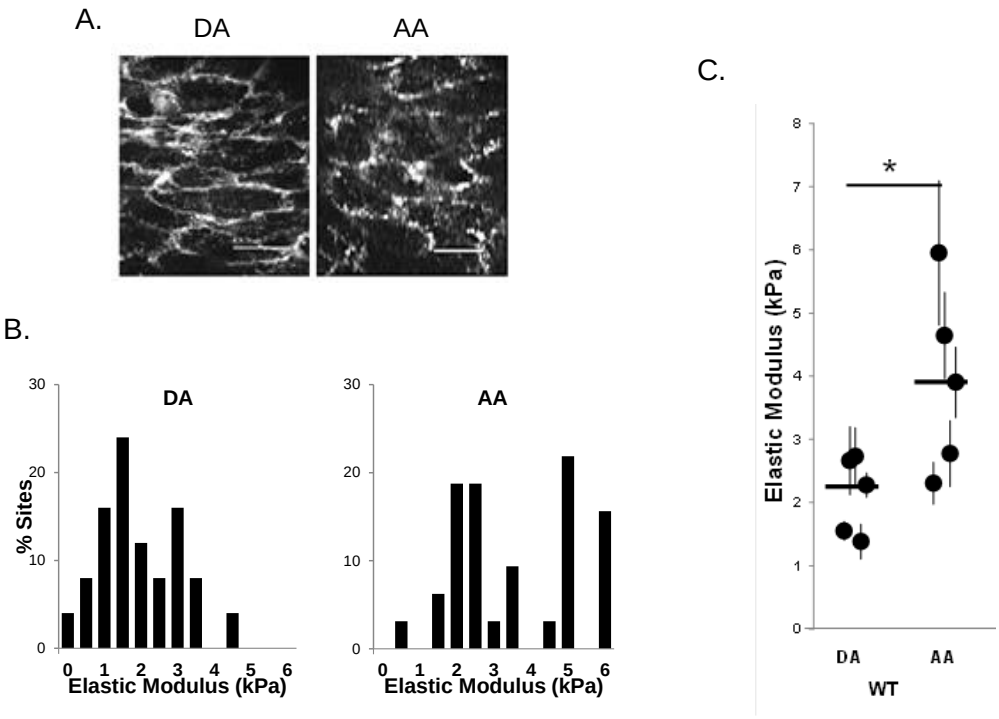

Figure 4.9: ECs from intact aortic arches are stiffer than those from the descending aorta. **A.** Pecam-1 (endothelial cell junctional marker) staining in intact descending aorta (left) and aortic arch (right). **B.** Histograms depicting the elastic modulus of ECs from intact descending aorta (left) and the aortic arch (right) regions (6-10 sites per region per condition, 6-9 force-distance curves per site, n = 5 mice). **C:** Average elastic modulus of ECs from the DA and AA from WT mice. * $p < 0.05$.

Increased oxysterol composition in the aortic arch as compared with the descending aorta

To investigate the differences between the descending aorta and the aortic arch, we isolated whole vessels from WT male mice and had their sterol and oxysterols compositions analyzed using mass spectrometry. Although there was not a statistical significance in the cholesterol composition between the DA and AA, there may be an emerging trend (p=0.25) of increased cholesterol in the aortic arch (Figure 4.10, left). Further testing would be required to confirm the significance of this trend. Two oxPC components, POVPC and PGPC, have been shown to enhanced endothelial barrier permeability (Birukova et al., 2013) and increase monocyte-endothelial binding (Huber et al., 2002). Our data shows that oxPCs (middle) were elevated in the aortic arch as compared to the DA. Cholesterol esters are known to be associated with foam cell formation, the first step in atherosclerosis (Sorci-Thomas and Thomas, 2016). Five cholesterol ester types (right, 14:0, 16:0, 18:1, 18:0 and 20:0) were analyzed from whole vessels. As a group, the composition of cholesterol esters was greater in the aortic arch as compared to the descending aorta in WT mice.

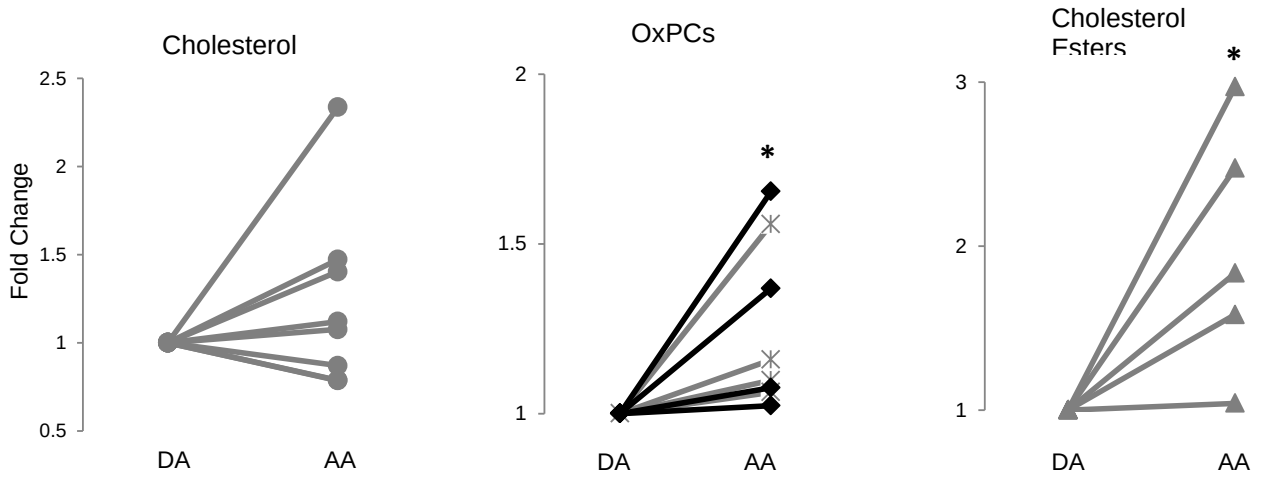

Figure 4.10: The aortic arch has a greater oxidized-PC and cholesterol ester composition than the descending aorta as determined by mass spectrometry. Aortic composition changes in cholesterol (left, n=8 mice, p=0.25), oxidized phosphatidycholines (middle, n=4 mice), POVPC (grey stars) and PGPC (black diamonds) and five cholesterol ester types (right, n=4 mice) from the descending aorta and aortic arch of WT mice. * $p < 0.05$

OxLDL-induced endothelial stiffening under disturbed flow is mediated by CD36

To determine the mechanism of increased oxLDL-induced stiffening under disturbed flow conditions, we first tested the oxLDL receptor, CD36, since we found this to be the primary receptor responsible for oxLDL uptake into ECs under flow conditions. Additionally, a recent study from our lab showed that oxLDL-induced stiffening in static cultured cells is mediated by the oxLDL receptor, CD36 (Oh et al., 2016), but the impact of laminar and disturbed flow is unknown. Our data thus far has shown increased stiffness in both HAECs and HMVECs (Figure 4.6 B, 4.7 B) corresponding to increased oxLDL uptake (Figure 3.5 C). Since our data showed that there was reduced oxLDL uptake in CD36-targetting siRNA treated EC versus scrambled control ECs (Figure 3.9), we therefore tested if there would be a corresponding reduction in stiffening in siRNA treated ECs versus control under shear conditions in the presence of oxLDL. As shown in Figure 4.11, there is a 50% increase in stiffness in control ECs in DF conditions compared to those in LF (2.1 kPa versus 1.45 kPa). In the endothelial cell treatments using two different CD36-targetting siRNAs, there is significantly reduced stiffness (~1.0 kPa) under both laminar and disturbed flow compared to scrambled control ECs. This suggests that CD36 is responsible for the enhanced oxLDL-induced endothelial stiffening under DF conditions.

To ensure that this reduction in stiffness found in CD36-targetting siRNA treated ECs was due to reduced oxLDL uptake and not due to the siRNA treatment itself, we repeated these experiments under control (no oxLDL) conditions. As expected, in the absence of oxLDL, endothelial stiffness in scrambled control cells were significantly less than in the oxLDL exposed scrambled ECs. In fact, our data show that in the absence of oxLDL there is the same low level of stiffness (~ 1.0 kPa) under both laminar and disturbed flow conditions in both scrambled control and CD36-targetting siRNA treated ECs (Figure 4.11). This shows that the loss of the CD36 receptor itself did not reduce cell stiffening.

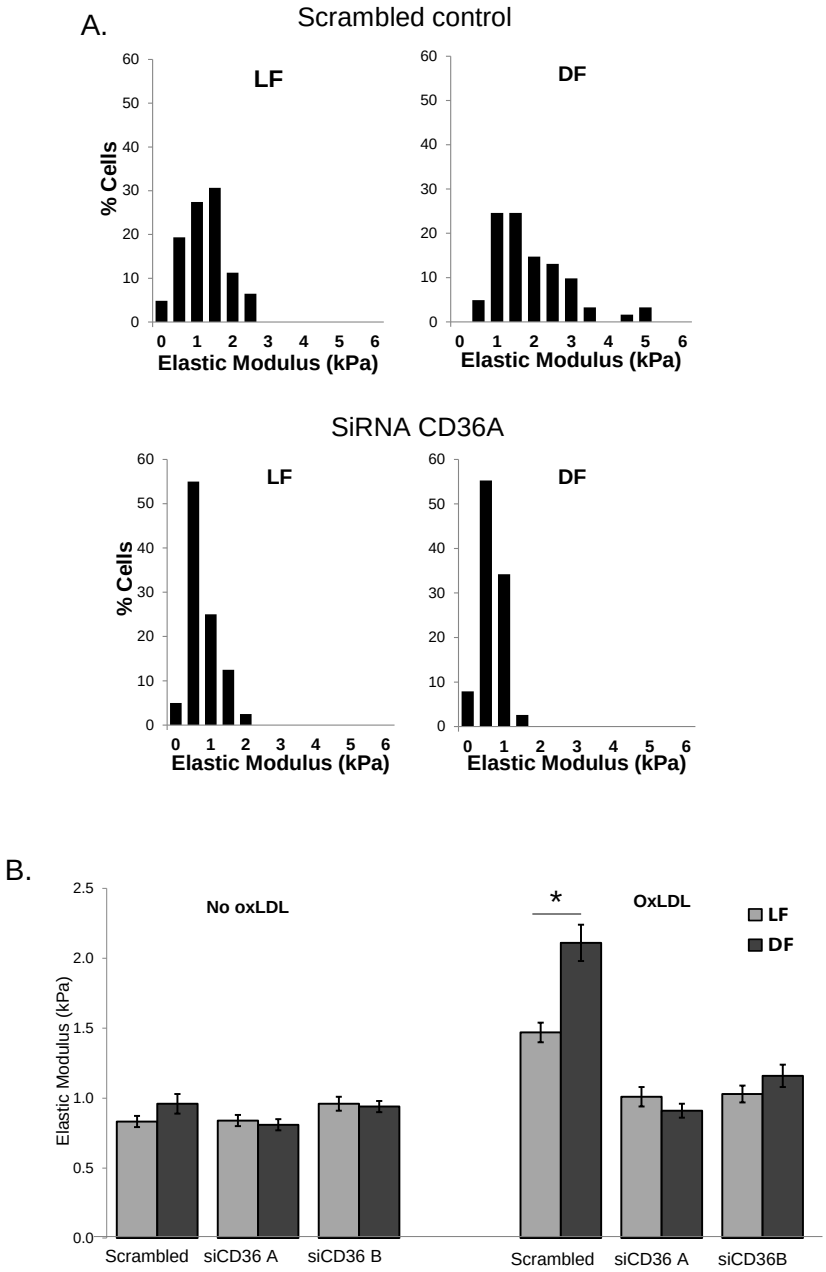

Figure 4.11: OxLDL-induced EC stiffness under LF and DF is CD36 dependent. A. Representative histograms showing the elastic modulus of scrambled control HAECs (top) and CD36-targetting siRNA treated HAECs (bottom) in the presence of oxLDL under laminar (left) or disturbed flow (right) (15-20 cells per condition per experiment, n = 3). **B.** Average elastic modulus of two different CD36-targetted siRNA treated and scrambled control HAECs under laminar or disturbed flow conditions either with or without oxLDL in the flow medium. * $p < 0.05$.

OxLDL uptake and endothelial stiffness is mediated by caveolae

To further determine the signaling pathway of oxLDL internalization under flow, we investigated caveolae-mediated endocytosis, since this is a major pathway for macromolecular internalization into ECs (John et al., 2003; Sverdlov et al., 2009). Mouse microvascular ECs (MMVECs) were isolated from the lungs of WT and Cav1 knockout (Cav1 KO) mice, which have been shown to lack caveolae (Fridolfsson et al., 2014). Since our previous data show that there was reduced oxLDL uptake into Cav1 KO ECs compared to WT ECs, we hypothesized that the reduced oxLDL uptake would correspond to a reduction in stiffening response. To test this hypothesis, we first seeded MMVECs into the step barrier chamber and let them grow to confluency. Like the other shear experiments, the cells were exposed to flow (48 hours) both in the presence and absence of oxLDL (10 μg/mL), followed by elastic modulus quantification using AFM. Similar to HAECs and HMVECs, MMVECs also had enhanced cell stiffening under DF conditions in the presence of oxLDL (Figure 4.12 C, top row, D), but not in its absence (Figure 4.12 A, top row, B). Furthermore, Cav1 KO ECs did not have a stiffening effect either in response to oxLDL exposure or to disturbed flow (A and C, bottom row; B and D). Cav1 KO ECs maintained the same elastic modulus value range both in the presence and absence of oxLDL.

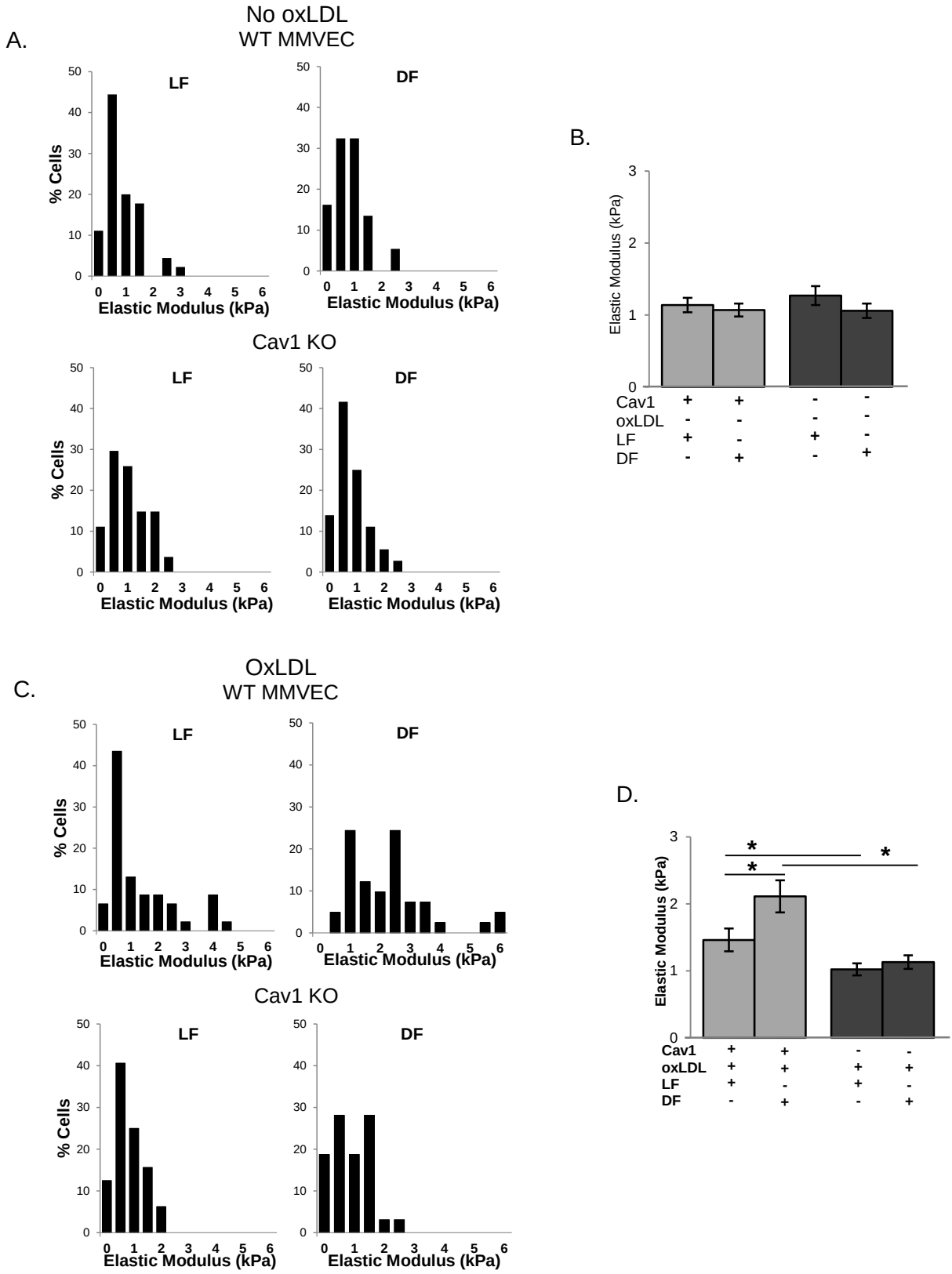

Figure 4.12: OxLDL-induced EC stiffness is mediated by caveolae. A. and C. Histograms showing the elastic modulus of endothelial stiffening in WT MMVEC (top) and Cav1 KO MMVEC (bottom) under laminar (left) and disturbed (right) flow conditions in the absence **(A.)** and presence **(C.)** of oxLDL (15-20 ECs per condition per experiment, n = 3). **B and D.** Average elastic modulus of same cell population without **(B.)** and with oxLDL **(D.)**. * $p < 0.05$.

Endothelial stiffness in the aortic arch critically depends on CD36 and Cav1 expression

In this next portion of our research, we applied the mechanistic insights found from the *in vitro* data showing enhanced oxLDL-induced EC stiffening under DF to determine the mechanism of increased EC stiffening in the athero-prone regions of the aortic arch *in vivo.* This was addressed by using mice globally deficient in CD36 (CD36 KO). As previously described, aortas were harvested from 5-6 month old male WT and CD36 KO mice. Consistent with our previous results, there was enhanced EC stiffening in the aortic arch of the WT mice compared to the descending aorta, as indicated by the rightward shift in the elastic modulus values in the histogram (Figure 4.13 A, top row, B). In contrast, there was no significant difference in the endothelial stiffening from the AA compared to the DA regions in CD36 KO mice (Figure 4.13 A, middle row, B). As compared to WT, the ECs from the AA in the CD36KO had a significantly lower elastic modulus.

Since our previous results show that Cav1 is a main endocytotic pathway for oxLDL uptake *in vitro*, we therefore tested if Cav1 is necessary for the oxLDL-induced endothelial stiffening effect *in vivo*. To address this question, we used a mouse model deficient in caveolin1 protein (Cav1 KO mice). Using age and gender-matched mice, we found no differences in the endothelial cells' elastic modulus values from the disturbed flow region of the arch versus the LF region of the DA (Figure 4.13 A, bottom row, B). There was, though, a significant decrease in the stiffness of the ECs from the AA in the Cav1 KO mice as compared to the comparable cell regions from the WT mice, as indicated by a leftward shift in the elastic modulus values. Taken together, this indicates that the enhanced stiffening effect observed in the aortic arch as compared to the descending aorta critically depends on the expression of CD36 and Cav1.

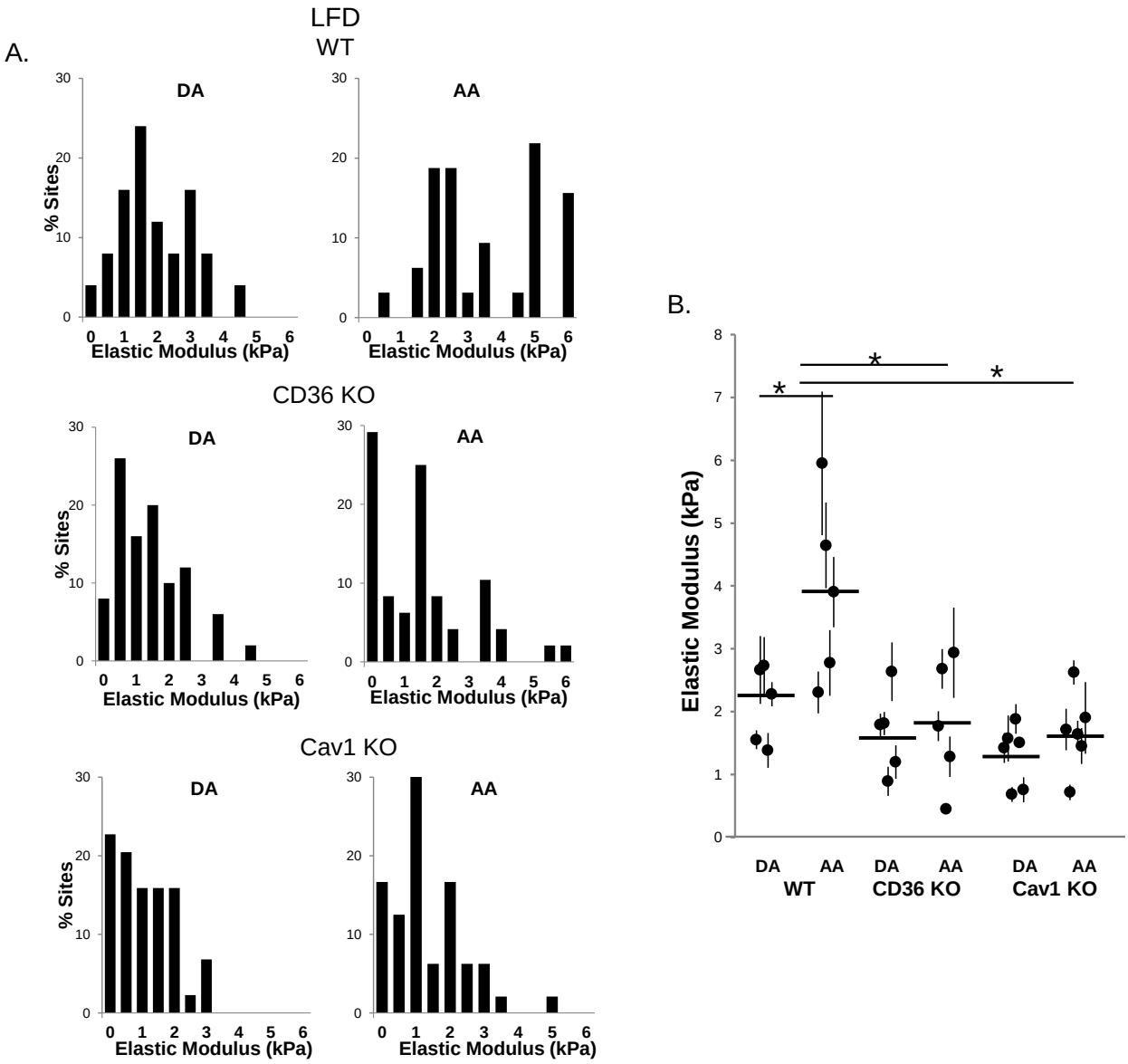

Figure 4.13: EC stiffness in the arch depends upon CD36 and Cav1. A. Histograms of the elastic modulus from endothelial monolayer from the DA (left) and AA (right) regions of WT male mice (top), CD36 KO mice (middle) and Cav1 KO mice (bottom). Measurements were taken at 6-10 sites per sample per experiment, 2-8 force-distance curves per site. n = 5. **B.** Average elastic modulus for the DA and AA from WT, CD36 KO and Cav1 KO mice. * $p < 0.05$.

Endothelial CD36 is required for stiffness in the aortic arch.

Most studies focus on LOX1 as the primary endothelial oxLDL receptor (Lubrano and Balzan, 2014; Pirillo et al., 2013) with only a couple of research studies showing significant CD36 involvement in endothelial functioning (Dawson et al., 1997; Oh et al., 2016; Uittenbogaard et al., 2000). To test whether our results showing that endothelial stiffening in the aortic arch depends upon CD36, we irradiated recipient CD36 KO and WT control mice and did a bone marrow transfer (BMT) from donor WT mice tagged with Ly5.1 (fluorescence). Since CD36 is highly expressed in monocytes circulating in the blood and in monocyte-derived macrophages in the sub-endothelial wall [reviewed by (Libby et al., 2011)], this experiment tests whether the loss of stiffening in the AA of CD36 KO mice compared to WT mice is an endothelial phenomenon and not a 'trans' effect of CD36 loss on circulating cells. One month post-BMT, blood was collected from each mouse for flow cytometry analysis to detect the degree of incorporation of the WT Ly5.1 tagged donor into the WT and CD36 KO mice. Figure 4.14 A shows representative flow cytometry quartile graphs. Host WT mice showed ~95% incorporation of the donor and CD36 KO mice showed ~97% successful incorporation of the WT donor bone marrow.

Two months post-BMT, endothelial stiffening from the DA and AA of the WT and CD36 KO mice was assessed by AFM. Our data show increased EC stiffening in the AA of the WT mice compared to the DA, an effect which is not observed in CD36 KO mice (Figure 4.14 B and C). Additionally, there was a statistically significant lower elastic modulus values in the arches of the CD36 KO mice as compared to those from mice. Our results show that endothelial CD36 is required for the observed stiffening effect in the aortic arch.

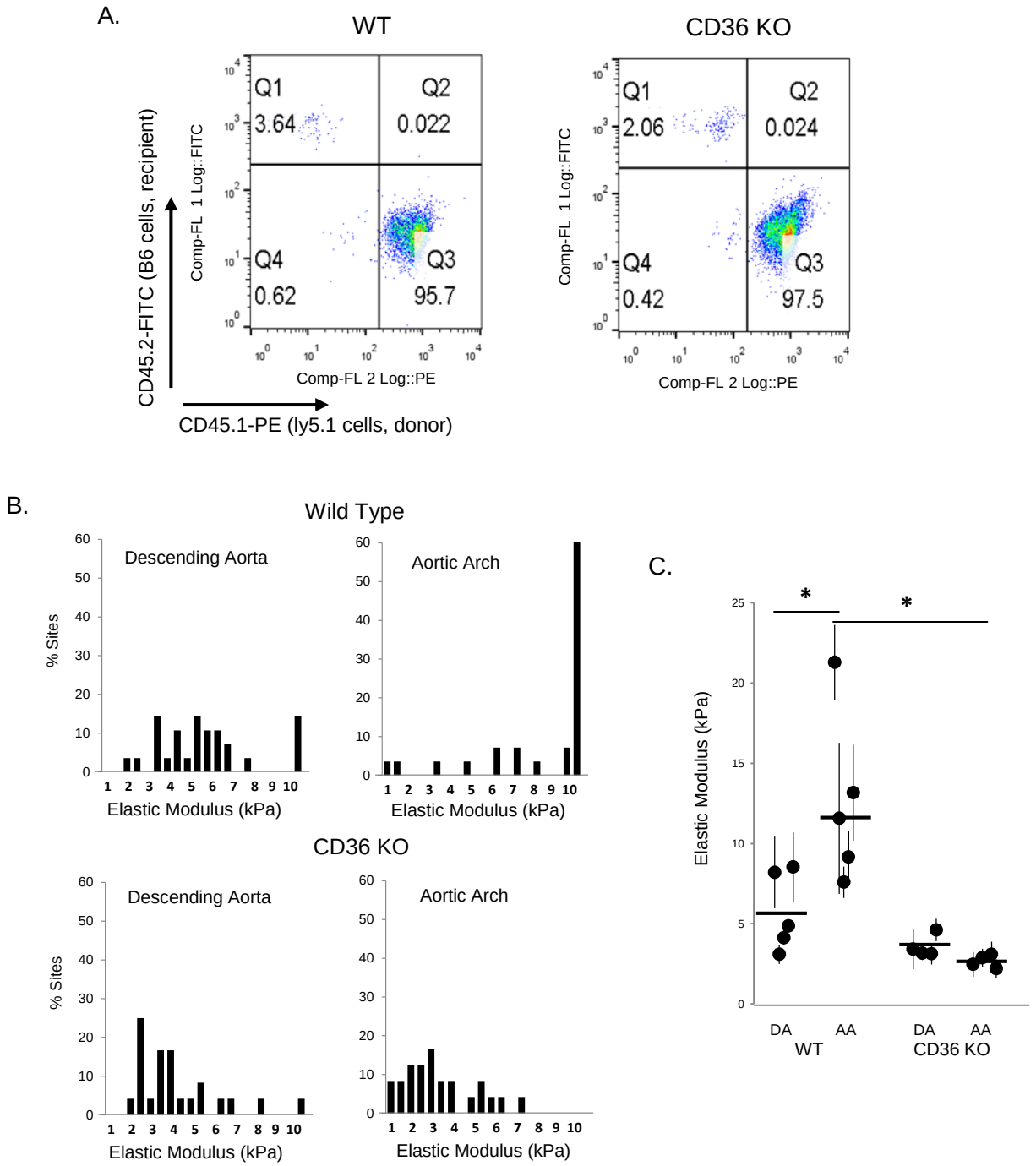

Figure 4.14: Endothelial CD36 is required for stiffening in the aortic arch. A: Representative plots depicting bone marrow transfer (BMT) of Ly5.1 tagged WT macrophages into WT host (95.7% transfer, left) and CD36 KO host mice (97.5% transfer, right). **B:** Histograms of the elastic modulus for the DA and AA regions from WT and CD36KO BMT mice. **C:** Average elastic modulus for the DA and AA from WT and CD36 KO mice two months following irradiation and bone marrow transplantation of Ly5.1 tagged WT macrophages (6-8 sites [50-70 measurements] per sample, n=4-5 mice per condition. * $p < 0.05$.

Comparative analysis of intact endothelial and sub-endothelial denuded monolayers in the aortas of WT mice

To further understand the biomechanical properties of the athero-prone aortic arch as compared to the athero-protective descending aorta, we measured the elastic modulus of the intact endothelial and denuded layer that lies below the endothelium. This was an important next step in our research since it is well known that atherosclerosis is characterized by plaque depositions in the intima and medial layers (below the endothelium) of large vessels primarily in the regions where blood flow patterns are disturbed. Additionally, a growing amount of evidence has shown that the biomechanical properties of endothelial cells are altered based on the substrate they are grown on (Kohn et al., 2015). To test the elastic modulus of the sub-endothelial monolayer, we used a denuding technique previously described (Peloquin et al., 2011). Briefly, a cotton-tipped applicator saturated with buffering solution was gently brushed over the EC monolayer 10-15 times and then gently washed in solution. Figure 4.15 A shows a representative image of the EC monolayer (left) and sub-endothelial denuded layer (right) stained with FITC-PECAM1. The FITC-stained EC junctions are clearly shown in the EC layer (left) with little to no staining after denudation (right).

Using atomic force microscopy, the elastic modulus in the intact endothelial (left) and denuded layers (right) in both the DA (top) and the AA (bottom) was determined (Figure 4.15 B, C). As previously shown, there is a greater elastic modulus in the ECs from the aortic arch as compared to the DA. Stiffening in arch versus DA is not limited to intact monolayer, but is also seen in the denuded layer. In the DA, the elastic modulus of the cells from the denuded layer was nearly 50% reduced as compared to the EC values (1.28 kPa versus 2.28 kPa). In the AA, though, the elastic modulus of the denuded layer was 25% greater than that of the endothelial layer, but was not statistically significant ($p = 0.20$).

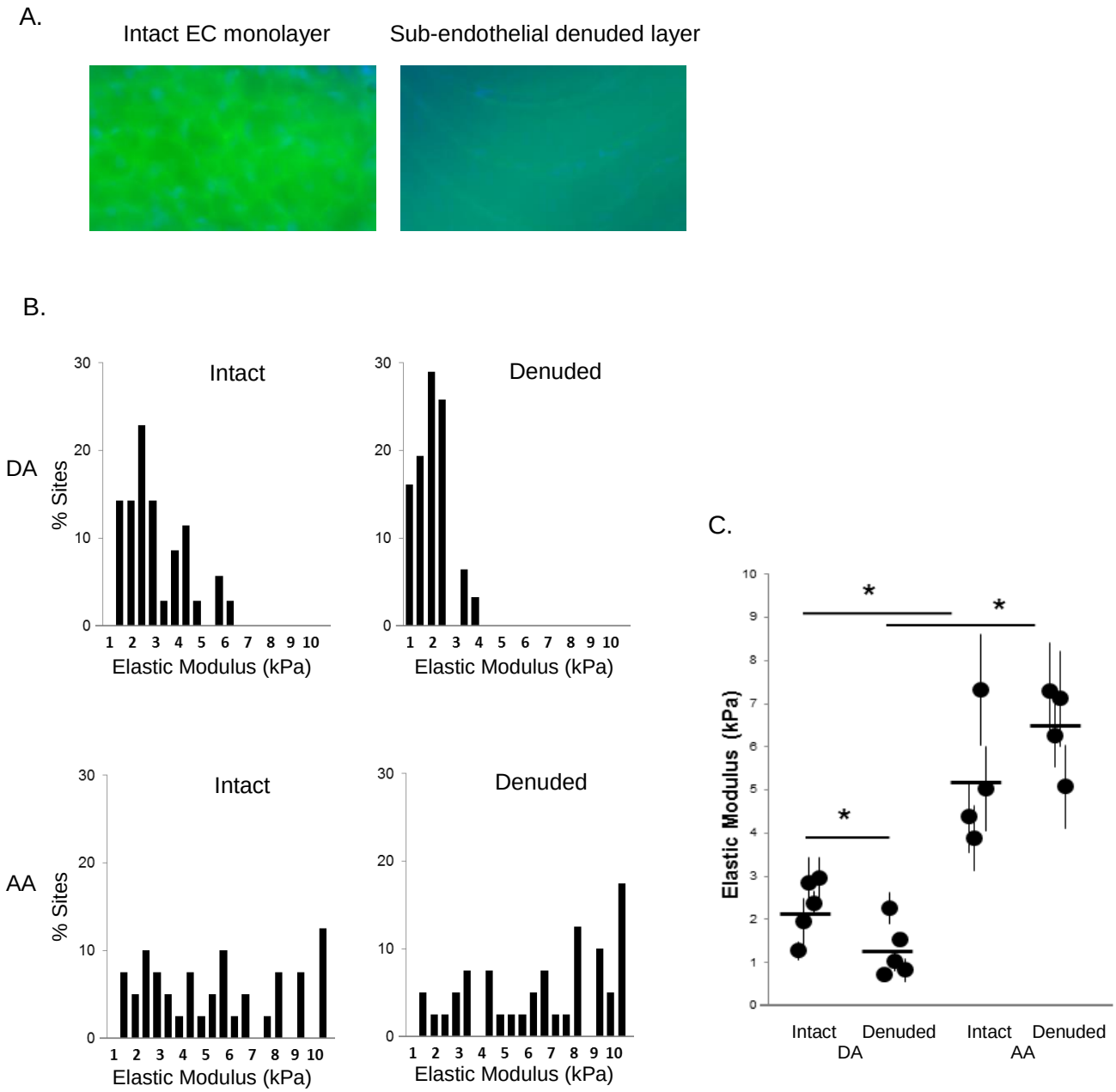

Figure 4.15: Comparison of intact endothelial and sub-endothelial denuded aortas in WT mice. A. Histograms of the elastic modulus from the intact endothelial (top) and denuded monolayers (bottom) from the DA (left) and AA (right) regions of 5-6 month old WT male mice. Measurements were taken at 6-10 sites per sample per experiment, 2-8 force-distance curves per site. n $\geq$ 4. **B.** Average elastic modulus for the endothelial and denuded cell layers from the DA and AA from WT mice. * $p < 0.05$.

Comparative analysis of intact endothelial and sub-endothelial denuded monolayers in the aortas of CD36 KO mice

In order to better understand the CD36-dependent increased endothelial stiffening in the aortic arch, we did a comparative analysis of intact and denuded cell monolayers' biomechanical properties in 5-6 month old CD36 KO male mice. Consistent with previous data (Figure 4.13 B), the ECs from the DA and AA in Figure 4.16 have a similar elastic modulus (1-2 kPa). The endothelial cell layer was immediately denuded following the ECs measurements to reveal the sub-endothelial denuded layer. In both the DA and AA, the cells from the denuded layer were significantly stiffer than their endothelial counterparts (Figure 4.16), with a nearly three times greater elastic modulus in the denuded monolayer as compared to the ECs. Like the endothelium, there is no difference in stiffness between the cells from the descending aorta versus the aortic arch of the denuded layer. This data shows that the decrease in stiffness observed in the endothelium of CD36 KO mice is not due to the loss of CD36 in the aortic denuded monolayers. Additionally, since the arch of WT mice have the same elastic modulus for both the ECs and their denuded layers (Figure 4.14) but the CD36KO ECs and denuded cells have different modulus values, this suggests that stiffness of the endothelial cells does not necessarily reflect the stiffness of the monolayer below.

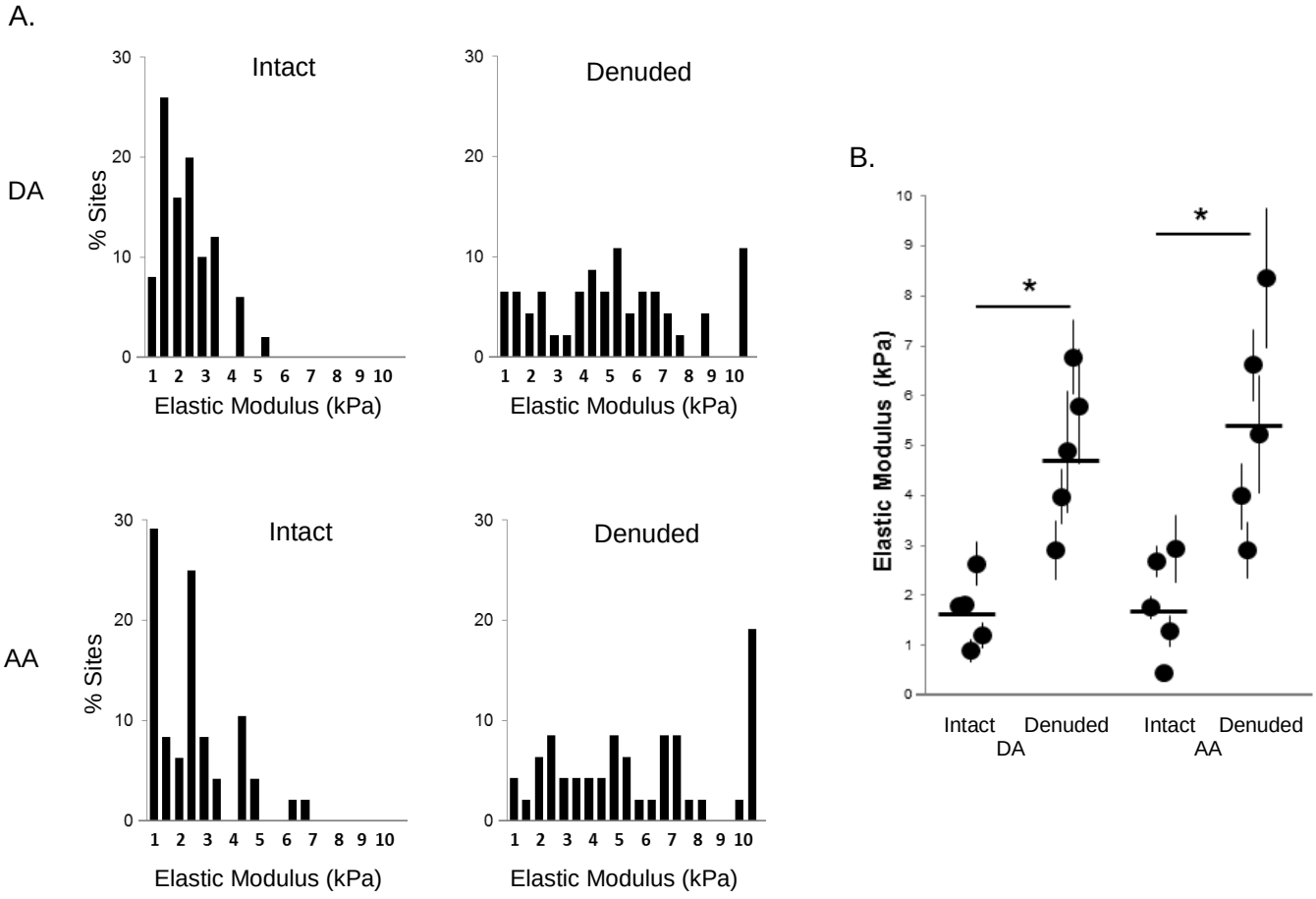

Figure 4.16: Comparison of intact endothelial and sub-endothelial denuded aorta in CD36 KO mice. A. Histograms of the elastic modulus from endothelial (top) and denuded monolayer (bottom) from the DA (left) and AA (right) regions of 5-6 month old male CD36 KO mice. Measurements were taken at 6-10 sites per sample per experiment, 2-8 force-distance curves per site. n = 5. **B.** Average elastic modulus for the intact endothelial and sub-endothelial denuded layers from the DA and AA of CD36 KO mice. * $p < 0.05$.

4.3 Discussion:

It is becoming more widely recognized that biomechanics is a driving force in cell development, phenotype and morphogenesis. Mechanical forces, both acting on and created by cells, alter chemical signaling cues and affect gene expression. It has been suggested that increased control over mechano-chemical forces may aid in the reversal of developmental defects and in combatting certain diseases, such as cancer [reviewed by (Mammoto and Ingber, 2010)]. This work focused on the biomechanical changes in endothelial cells resulting from vascular hemodynamics, genetic deficiencies, the direct application of oxLDL and the activation/suppression of the RhoA/ROCK/MLCP signaling pathway.

To determine the signaling pathways involved in oxLDL-mediated EC stiffness, as described above, previous studies from our group and others show the involvement of the RhoA/ROCK/MLCP pathway leading to changes in acto-myosin stress fiber formation (Kole et al., 2004; Kowalsky et al., 2008; Ryoo et al., 2011; Sugimoto et al., 2009). Earlier studies from our lab have shown that short-term oxLDL exposure (1-6 hours, 10-50 μg/mL) results in increased cell stiffness and contractility in ECs from large arteries (Byfield et al., 2006; Shentu et al., 2012; Shentu et al., 2010). Here we show that the oxLDL-induced increase in EC stiffness from both large vessels and small vasculature is dependent on the RhoA/ROCK pathway (Oh et al., 2016) and intact CD36/caveolae endocytotic machinery.

Previous studies from our group have linked the disruption of lipid packing order in endothelial cells to increased cell stiffening: specifically, that increased cell stiffening in Ecs often corresponds to a decrease in the surface area in the “ordered” and “disordered” packing regions (Shentu et al., 2010). Here we show that exposing ECs to the biologically active and highly reactive oxidative components of minimally oxidized LDL [reviewed by (Levitan et al., 2010)], specifically POVPC and PGPC, decreases the amount of both ordered and disordered lipid packing domains, an observation that also corresponds to an increase in elastic modulus values

as compared to control ECs (Ayee et al., 2017). Further studies are needed to investigate the effect of endothelial stiffening based on flow patterns in the RhoA pathway and from oxPC exposure.

Since a main external stimulus on ECs is blood pumping through the systemic vasculature, we focused the main portion of our work to include the biomechanical changes on cells due to hemodynamic shear stresses found in the athero-prone regions of the aortic arch and the athero-protective regions of the descending aorta. Very few studies have been conducted on biomechanical changes due altered shear patterns. One *in vitro* study showed increased cell stiffness due to the application of uni-directional laminar flow compared to static conditions (Sato and Ohashi, 2005). An *ex vivo* study by Collins *et al.* showed increased responsiveness to mechanical load in the endothelial monolayer of the aortic arch region as compared to the descending aortic region in WT mice (Collins et al., 2014). This increased responsiveness was suggested to correspond to the fibronectin-rich sub-endothelial layer in the aortic arch as compared to the collagen-rich layer in the descending aorta. Consistent with our results, another study showed that the endothelial cells from intact rabbit vessels are stiffer in the disturbed flow, pro-atherogenic regions of the medial common iliac artery (CIA) as compared to the high shear stress, athero-protective region of the lateral CIA (Hayashi and Higaki, 2016; Miyazaki and Hayashi, 1999). Our work is the first study to investigate the impact of oxLDL uptake under athero-protective and pro-atherogenic flow environments leading to altered endothelial biomechanical properties. Specifically, pro-atherogenic disturbed flow by itself did not change EC stiffness in the absence of oxLDL, suggesting that the stiffening effect is the result of enhanced oxLDL internalization and not the disturbed flow patterns themselves. Furthermore, we show that the down-regulation of the oxLDL scavenger receptor CD36 using a siRNA approach significantly reduced endothelial cell stiffness in the presence of oxLDL under both laminar and disturbed flow conditions, an effect that can be attributed to increased oxLDL

uptake into control ECs. Additional studies using ECs from mice globally deficient in Cav1 determined that oxLDL-induced EC stiffening is mediated by caveolae. Importantly, we also show that loss of CD36 and Cav1 *in vitro* does not alter EC elastic modulus values. These studies were extended to determine if these results corresponded to biomechanical changes *in vivo*. Here we show for the first time that the stiffening effect observed in the pro-atherogenic DF region of the aortic arch is critically dependent on the oxLDL receptor CD36 and intact caveolae endocytotic machinery.

CHAPTER 5: Impact on dyslipidemia and age on endothelial and sub-endothelial stiffness in mouse aortas

5.1 Introduction:

It is well known that while disturbed flow itself causes EC dysfunction and an athero-prone inflammatory phenotype, an additional crucial factor in atherogenesis is plasma dyslipidemia [reviewed by (Kruth, 2001; Libby et al., 2011)]. Previous studies from our lab have shown that ECs freshly isolated from the aortas of high cholesterol, high fat diet fed pigs are stiffer than ECs harvested from the aortas of LFD fed pigs (Byfield et al., 2006), indicating that diet induced dyslipidemia leads to increased EC stiffening in the porcine model of atherosclerosis. Another study has shown heterogeneity in stiffness within different portions of atherosclerotic plaques, with the hypocellular fibrous caps (60 kPa) of 6-7 month old female hyperlipidemic ApoE KO mice on a HFD stiffer than the cellular fibrotic (10 kPa) and lipid rich regions (6 kPa) (Tracqui et al., 2011). These stiffness measurements of the plaques were performed on aortic ring sections from the aortic arch using AFM. In the present studies, two mouse models of plasma dyslipidemia were implemented. (1) A high fat atherogenic diet was used in WT, CD36 KO and Cav1 KO mice and has been shown to induce EC dysfunction in WT mice, as well as enhance the progression of obesity and atherosclerosis. This diet is considered to have a translational impact compared to human obesity (Collins et al., 2004; Park et al., 2012). (2) Another dyslipidemic model uses ApoE KO mice which lack apolipoprotein E, a glycoprotein essential for the transport and metabolic clearance of lipids in blood plasma, resulting in plasma dyslipidemia and the development of atherosclerotic lesions (Nakashima et al., 1994; Zhang et al., 1992). ApoE KO mice were fed a second high fat, high cholesterol diet, which has been shown to induce atherosclerotic lesion formation in mice (Paigen et al., 1985). Although the effect of high fat diets and the dyslipidemic condition in the ApoE KO mouse are well studied, little is known

regarding the synergetic interactions between dyslipidemia and disturbed flow on endothelial biomechanical properties.

Another objective was to study the effect of aging on the stiffness of the intact endothelial and denuded monolayers. A study by Reinheart-King's group (Huynh et al., 2011) has shown that sub-endothelial matrix (SEM) stiffening in the descending aortas of WT mice increases with age (10 weeks vs 21-25 months old) as well as a corresponding increase in cell-cell junctional width and enhanced monolayer barrier permeability. They showed inhibiting the Rho-kinase pathway in older mice, through the use of Y-27632, tighten the junctional width to the same levels that were seen in younger mice, but did not decrease the sub-endothelial stiffening in the older mice. Age induced stiffness in the SEM (Kohn et al., 2015) has been shown to be reversible by exercise (Kohn et al., 2016). Studies described in previous chapters show increased endothelial cell stiffening as the result of disturbed flow induced oxLDL uptake *in vitro* and increased EC stiffening in the pro-atherogenic region of the aortic arch compared to the athero-resistant region of the descending aorta on a low fat diet. This stiffening was shown to be dependent on the oxLDL receptor CD36 and intact caveolae machinery. The research described in this chapter include the comparison of EC stiffness from intact aortas between several different mouse models of atherosclerosis on LFD versus HFD, including the dyslipidemic mouse model of global apolipoprotein deficiency, as well as a comparison between the stiffness of cells from intact endothelial and denuded monolayers in the descending aorta and aortic arch in aging mice.

5.2 Results:

High fat, high cholesterol diet induces increased EC stiffening: an enhanced effect in the pro-atherogenic regions of the aorta

To test the impact of a high fat/cholesterol diet (HFD) on EC stiffening *in vivo*, we used a mouse model of diet-induced EC dysfunction (Collins et al., 2004) which is recognized to be an initiating factor in atherogenesis [reviewed by (Libby et al., 2011)]. Two to three month old C57BL/6 (WT) male mice were fed a HFD for a month. There was a significant increase in body weight, total cholesterol, LDL and oxLDL plasma levels (Figure 5.1 A) as compared to mice fed a regular chow, low fat diet (LFD). Mass spectrometry analysis (Figure 5.1 B) revealed that there was a significant increase in pro-inflammatory cholesterol esters in tissues of the arch of LFD fed WT mice as compared to the DA. Additionally, a HFD further increased the composition of cholesterol esters in the DA and AA, with the cholesterol ester composition significantly enhanced in the AA.

Endothelial stiffening was tested using AFM on the endothelial cell monolayer from the intact arteries from the LF region of the descending aorta as compared to the pro-atherogenic DF region of the aortic arch. As previously shown (Figure 4.9), the elastic modulus values of the ECs in the LFD fed WT mice are greater in the aortic arch as compared to the descending aorta as shown by the rightward shift in the histogram (Figure 5.1 C, top row). Introduction of a high fat diet resulted in increased stiffening of the endothelial monolayer in both the DA and AA, with the stiffening effect significantly enhanced in the aortic arch region (Figure 5.1 C, bottom row, D). These experiments with the LFD and HFD fed mice were conducted in parallel.

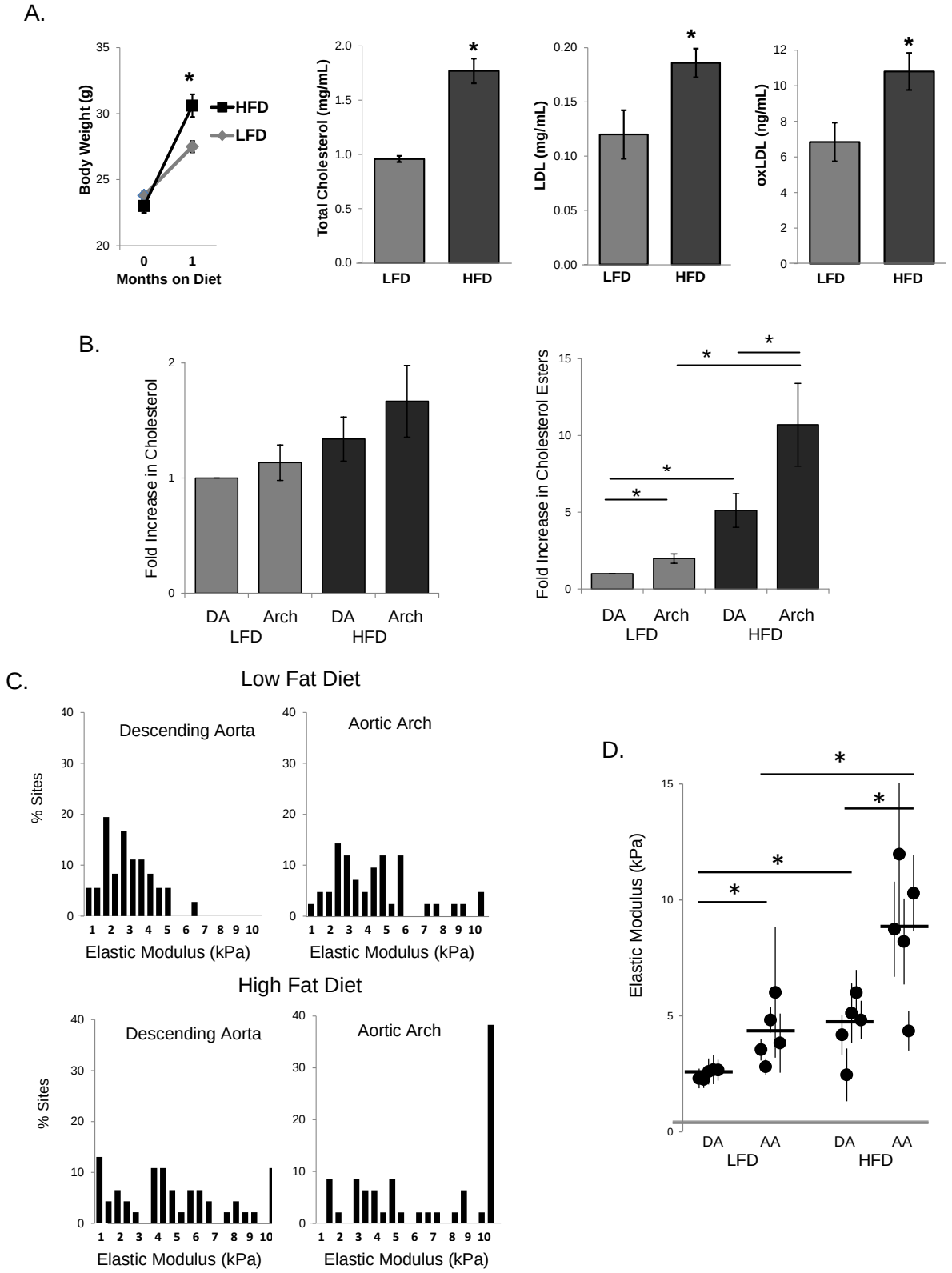

Figure 5.1: High fat/cholesterol diet induced endothelial stiffness in WT mice. A. Average body weight, total cholesterol, LDL and oxLDL measurements in WT mice fed a LFD or HFD for one month (n $\geq$ 7). **B.** Cholesterol (left) and cholesterol esters (right) in the aortic tissues in 3-4 month old WT mice fed either a LFD (n=4) or HFD (n=4) for one month, as analyzed by mass spectrometry. **C.** Histograms depicting the elastic modulus values from the LFD (top) and HFD (bottom) from the DA (left) and AA (right) regions of 3-4 month old WT male mice. Measurements were taken at 6-10 distinct sites per sample per experiment, 2-8 force-distance curves per site. n = 5. **D.** Average elastic modulus for the ECs from LFD and HFD fed mice in different aortic regions. * $p < 0.05$.

Endothelial stiffness in the DA and AA in HFD fed mice critically depends upon CD36

In this next set of experiments, a group of 2-3 month old male CD36 knockout mice were maintained on either a HFD or LFD for a month for the purpose of testing the elastic modulus of the endothelial monolayers in the DA compared to the AA and measuring the plasma oxLDL concentration levels between the two groups. As shown in Figure 5.2 A, there was a significant increase in the average body weight and oxLDL levels in HFD fed compared to the LFD fed CD36 KO mice. Interestingly, the range of the oxLDL levels in the CD36 KO mice were similar to what we observed in the WT mice (Figure 5.1, right). Our data also showed that in contrast to WT and similar to the 5-6 month old CD36 KO mice (Figure 4.13), there was no difference in the endothelial stiffness between the descending aorta and the aortic arch in the 3-4 month old CD36 KO mice fed a LFD (Figure 5.2 B, top row). Furthermore, in contrast to the WT mice, a HFD did not affect the elastic modulus values in the ECs from the intact vessels from both the DA and AA in CD36 KO mice (Figure 5.2 B, bottom row, C). It is significant to note that the elastic modulus values in the DA and AA regions of the CD36 KO mice were similar to the descending aorta in the age matched WT mice fed a low fat, regular chow diet.

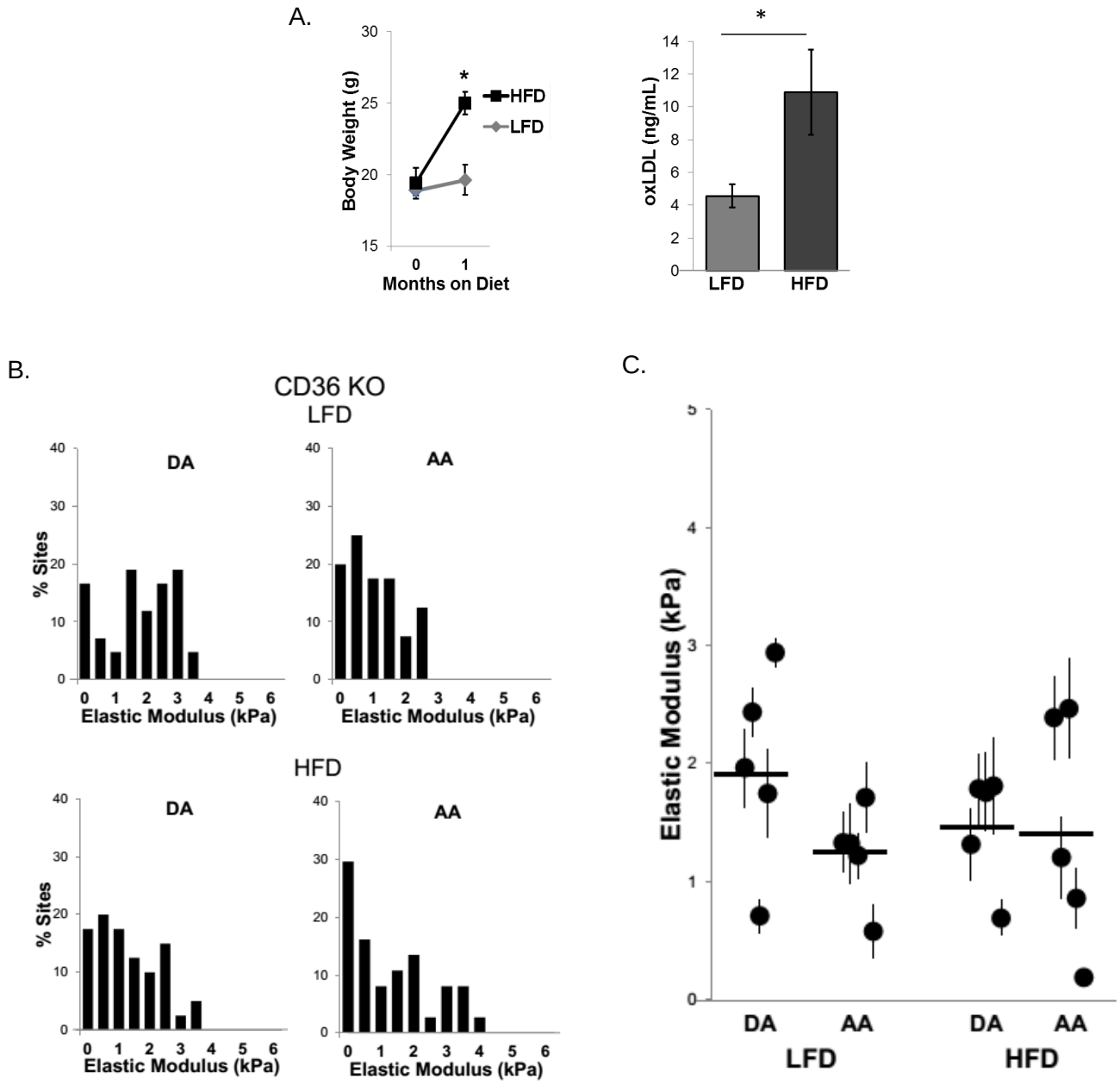

Figure 5.2: EC stiffness in the aortic arch depends on the expression of scavenger receptor CD36. **A.** Body weight changes and oxLDL plasma measurements from CD36 KO mice fed a LFD or HFD for one month ($n \geq 5$). **B.** Histograms depicting the elastic modulus values from the LFD (top) and HFD (bottom) fed CD36 KO male mice from the DA (left) and AA (right) regions. Measurements were taken at 6-10 sites per sample per experiment, 2-8 force-distance curves per site. n = 5. **C.** Average endothelial elastic modulus values from the DA and AA of LFD and HFD fed mice. * $p < 0.05$

Endothelial stiffness in in the DA and AA of HFD fed mice critically depends upon Cav1

To further explore the roles of caveolae and a HFD on endothelial stiffening, we measured the plasma oxLDL levels and endothelial stiffness in mice globally deficient in the caveolin1 gene. These 2-3 month old mice were either fed a LFD or HFD for one month. Similar to the results from both the WT and CD36 KO mice, there was a statistically significant increase in the average body weights and oxLDL levels in the Cav1 KO mice fed a HFD as compared to those on a LFD (Figure 5.3 A). Furthermore, similar to our data in CD36 knockout mice, caveolin1 deficiency abrogated the EC stiffening in both the athero-prone AA region on a LFD (Figure 5.3 B, top row, C) and the increased endothelial stiffening in response to a HFD (B, bottom row, C). Interestingly, although there are similar levels of increased plasma oxLDL and total body weight measurements in HFD versus LFD fed WT, CD36 KO and Cav1 KO mice, there is only an increase in endothelial stiffening in WT mice, highlighting the importance of CD36 and Cav1 in biomechanical changes in the vascular endothelium.

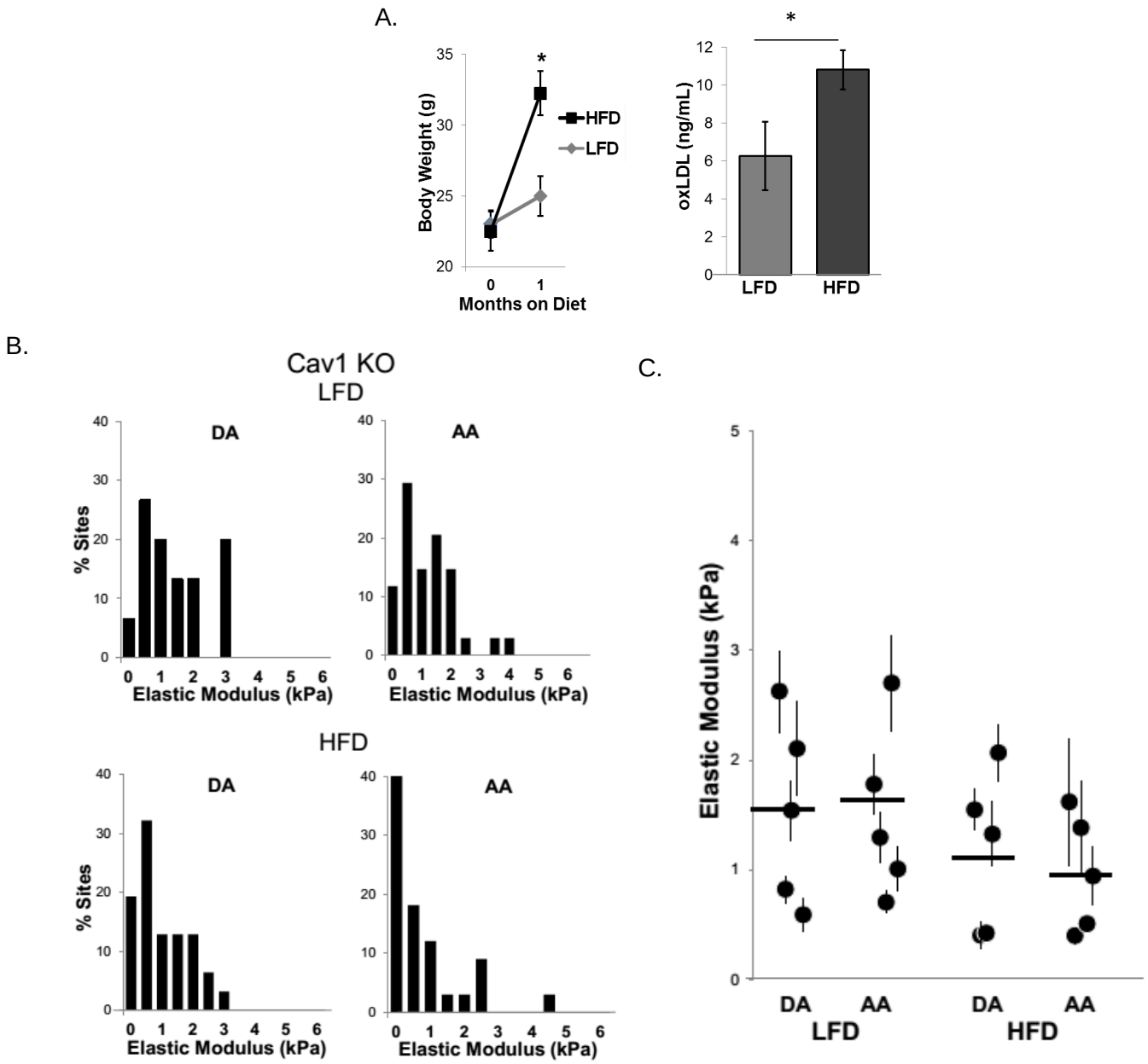

Figure 5.3: Endothelial cell stiffness in the aortic arch depends on Cav1 expression. **A.** Body weight changes and oxLDL plasma measurements of Cav1 KO mice fed a LFD or HFD for one month ($n \geq 5$). **B.** Histograms depicting the elastic modulus values from the LFD (top) and HFD (bottom) from the DA (left) and AA (right) regions of Cav1 KO mice. Measurements were taken at 6-10 sites per sample per experiment, 2-8 force-distance curves per site. n = 5. **C.** Average elastic modulus values of the endothelium from the DA and AA regions in LFD and HFD fed Cav1 KO mice. * $p < 0.05$.

Endothelial stiffness in the aortic arch of ApoE KO mice

Since ApoE KO mice are a known and well-studied model of atherosclerosis due in part to their plasma dyslipidemia, we therefore tested EC stiffening in the DA versus the AA in male ApoE KO mice fed either a low fat or high fat diet for 3-4 months beginning at two months old, as well as 5-6 month old LFD fed WT controls. Consistent with previous studies (Nakashima et al., 1994), our data shows that there is an increase in total plasma cholesterol from ApoE KO mice on a LFD compared to WT mice and that there is a further increase when ApoE KO mice are fed a high fat, high cholesterol diet (Figure 5.4 A). As previously shown, there is endothelial stiffening in the aortic arch of WT mice as compared to the descending aorta (Figure 5.4 B top, C). Next, we measured the elastic moduli of the intact endothelial cell monolayers of the LF region of the descending aorta compared to the DF region of the aortic arch in 5-6 month old ApoE KO male mice fed a LFD. Similar to WT mice, our results show that ApoE KO mice have increased endothelial stiffening in the aortic arch versus the descending aorta (B, middle; C). Our data show that there is a softening effect in the aortas of ApoE KO mice fed a LFD as compared to WT controls. A high fat diet, though, did not increase endothelial stiffness in the aortic arch like ApoE KO mice fed a LFD. We attribute this lack of stiffening to the particular diet that was used in this study, which made many of the ApoE KO mice sick after the 3-4 months of HFD feeding.

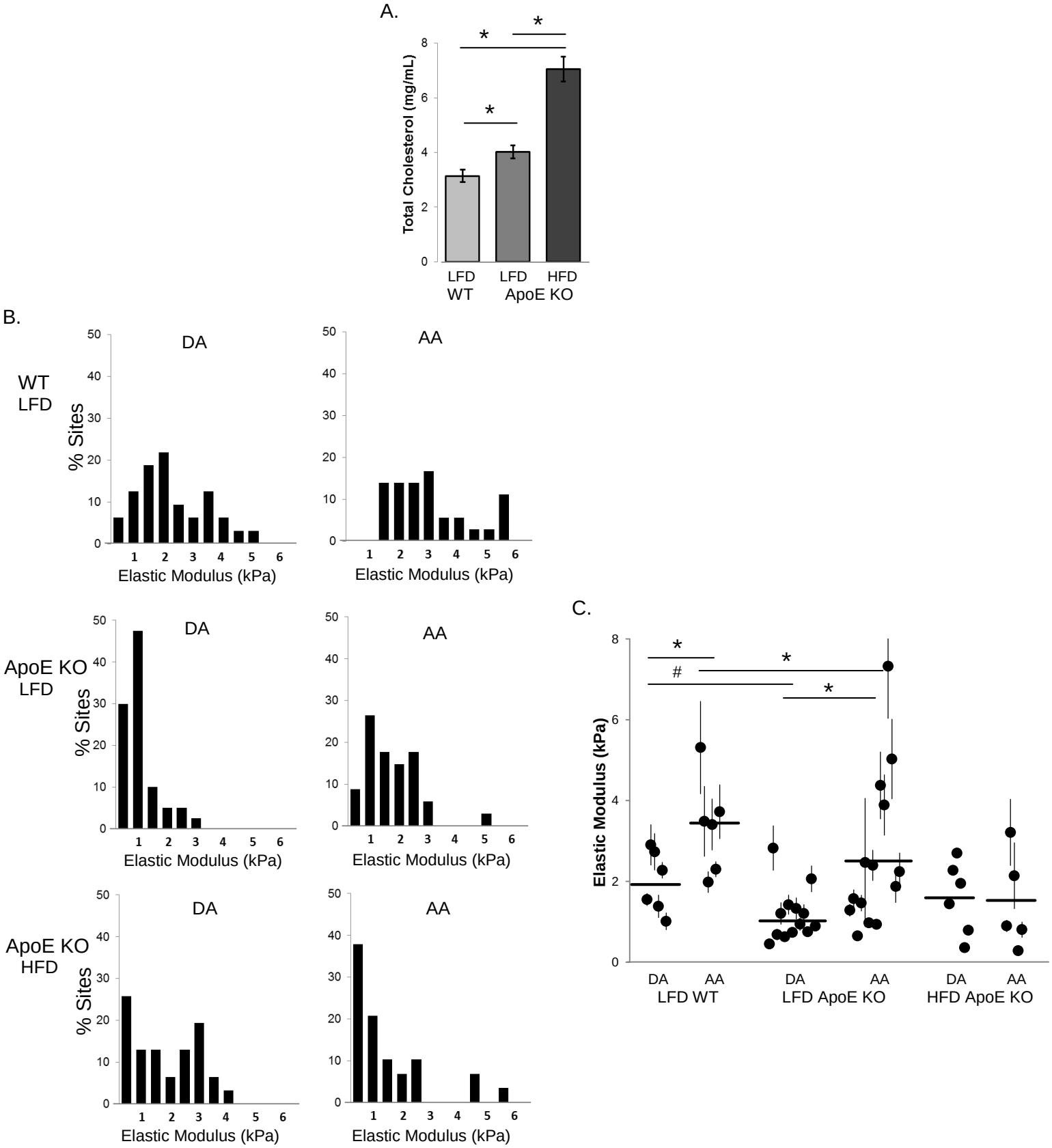

Figure 5.4: Endothelial stiffening in the aortic arch of ApoE KO mice. **A.** Total cholesterol measurements from 5-6 month old ApoE KO male mice on LFD versus HFD with LFD fed WT controls. n = 5–7. **B.** Histograms depicting the elastic modulus values from the descending aorta (left) and aortic arch (right) regions in LFD fed WT (top), LFD fed ApoE KO (middle) and HFD fed ApoE KO (bottom) mice. Measurements were taken at 4-6 sites per sample per experiment, 2-8 force-distance curves per site (n = 5-9). **C.** Average elastic modulus values of the ECs from the DA and AA regions in LFD fed WT and ApoE KO mice and HFD fed ApoE KO mice. * $p < 0.05$ and # $p=0.054$

The effect of aging on the stiffness of intact endothelial and denuded monolayers in WT mice

In the next set of experiments we looked at how aging (2-8 month old 'younger' group versus 12-24 month 'older' group) impacted endothelial stiffness in the intact endothelial and denuded layers from the descending aorta and aortic arch of WT mice. First, the elastic modulus of the intact endothelial monolayer was measured in the DA and AA, followed by the gentle removal of the ECs using a cotton tipped applicator as previously described (Peloquin et al., 2011) and subsequent stiffness measurements all recorded in the same day using AFM. As shown in Figure 5.5, these preliminary studies showed that there is an increase in endothelial stiffness (left) in the DA (top, R^2 = 0.7781) and AA (bottom, R^2 = 0.7262) in WT mice as they age, an effect that may be more pronounced in the DF region of the aortic arch. Measurements from the denuded monolayers (right) of the DA (top, R^2 = 0.7442) and AA (bottom, R^2 = 0.6946) suggest that there is also an increase in stiffness with age though more testing will need to be done to confirm these preliminary observations.

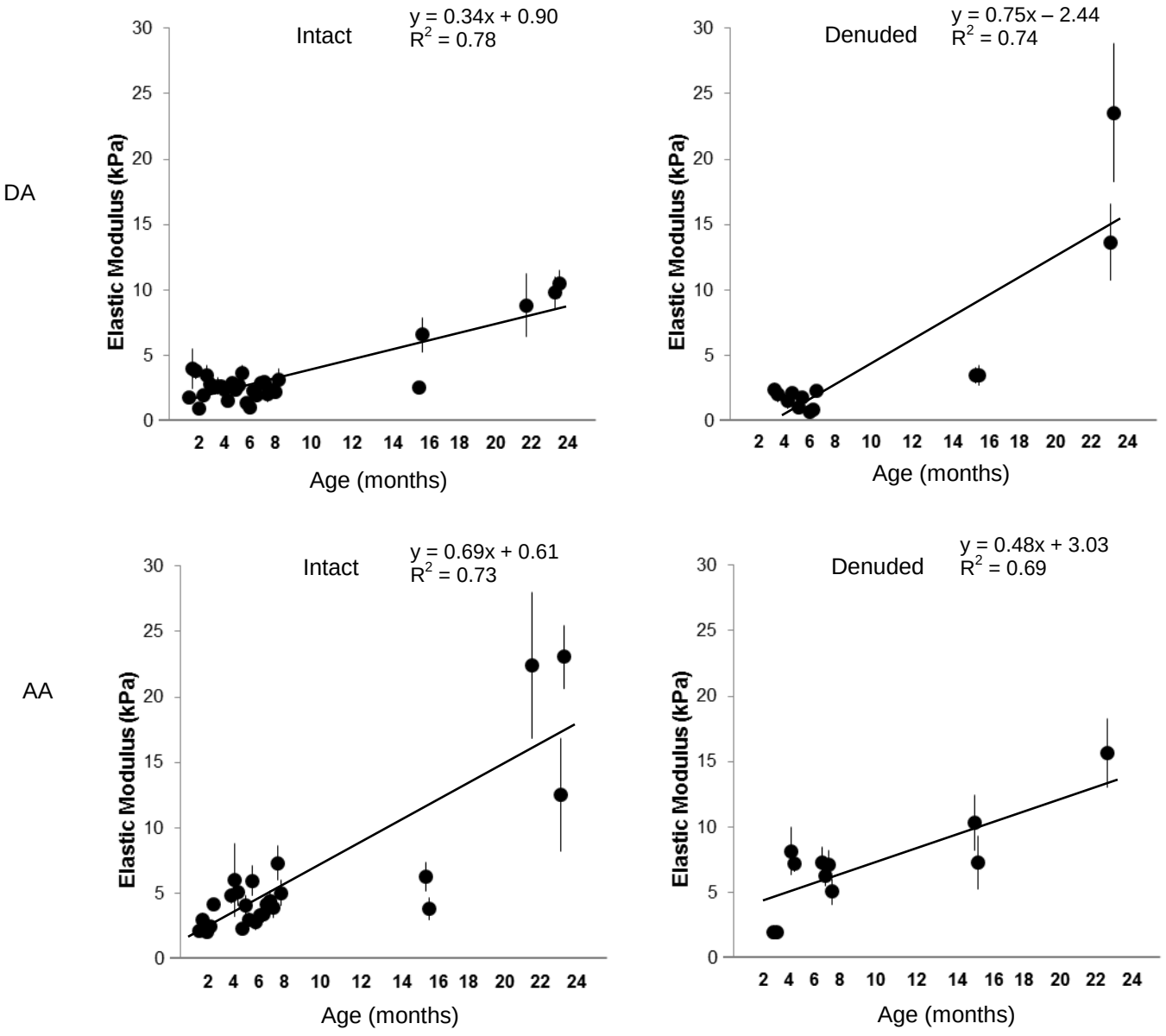

Figure 5.5: Age comparison of the cell stiffness from the intact endothelial and denuded sub-endothelial layer from the DA and AA in WT mice. Average elastic modulus for the intact endothelial (left) and denuded monolayers (right) from the DA (top) and AA (bottom) in WT mice from 2-24 months of age. Measurements were taken at 6-10 sites per sample per experiment, 2-8 force-distance curves per site. Intact DA (top left): n > 10 'younger' mice and n=5 'older' mice; Denuded DA (top right): n > 6 'younger' mice and n=4 'older' mice; Intact AA (bottom left): n > 10 'younger' mice and n=5 'older' mice; Denuded AA (bottom right): n=8 'younger' mice and n=3 'older' mice.

The effect of aging on the stiffness of intact endothelial and denuded monolayers in ApoE KO mice

We next compared the stiffness of the intact endothelial layer compared to the sub-endothelial denuded layer in the DA and AA in 'younger' versus 'older' ApoE KO male mice fed a LFD. Our preliminary data suggests that EC stiffness (Figure 5.6, left) continues to be relative low (~2-5 kPa range) in both the DA and AA in both younger and aged populations. Notably, in the intact DA, there was a moderate decrease in the stiffness from 2 to 8 months of age, followed by a slight increase from 12 to 24 months of age. In the intact arch, there was no significant trend (R^2=0.04) in the younger group, yet the older group showed a trend (R^2=0.76) of slight increase (0.26) in stiffness with age. On the other hand, the elastic modulus of the denuded layer in ApoE KO mice (right) appears to be greater than that of the intact EC layer and particularly greater in the denuded aortic arch (right, bottom, R^2 = 0.67). More experiments will need to be performed in order to confirm these preliminary results.

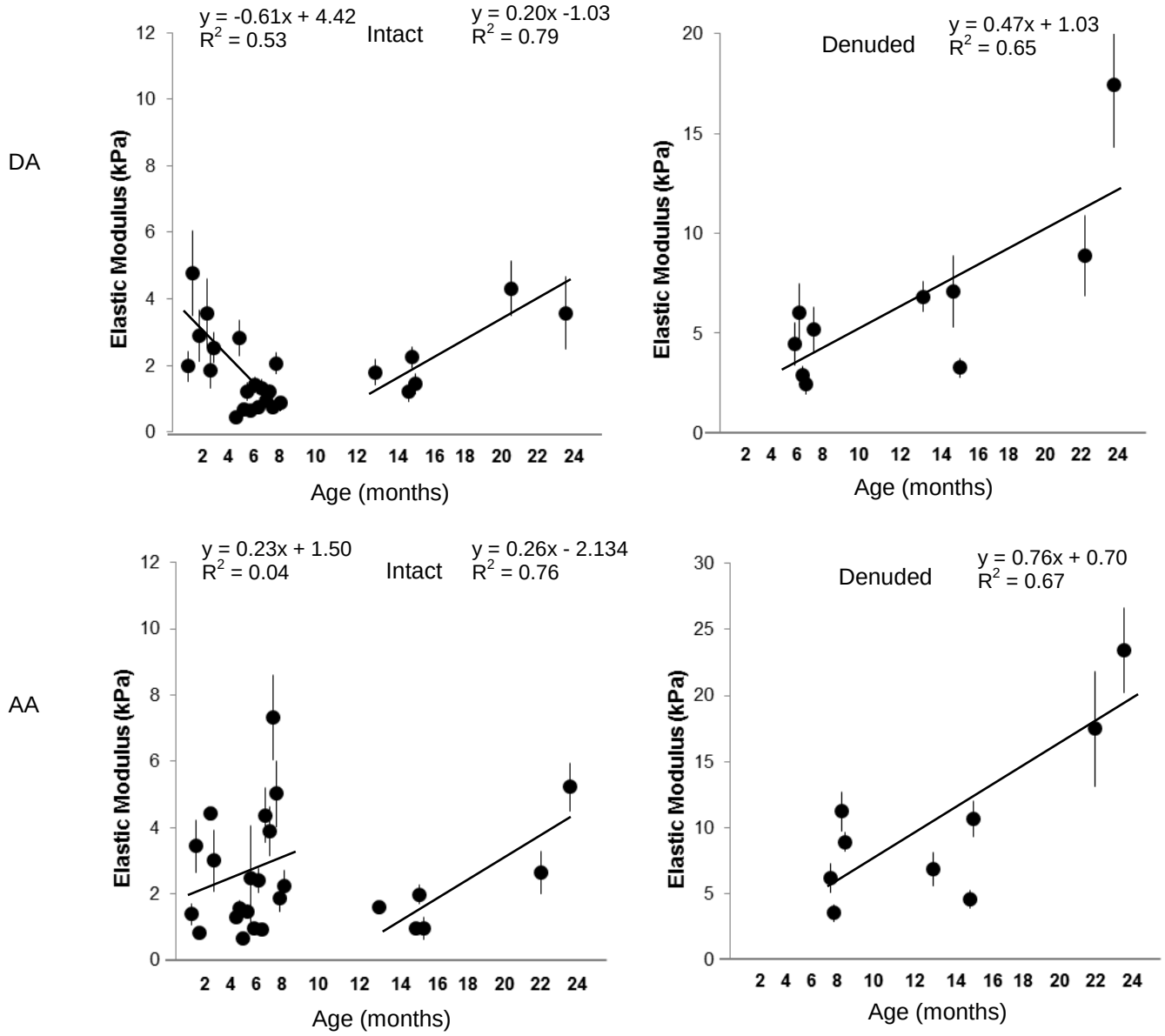

Figure 5.6: Age comparison of the cell stiffness from the intact endothelial and denuded sub-endothelial layer from the DA and AA in ApoE KO mice. Average elastic modulus for the endothelial (left) and denuded (right) monolayers from the DA (top) and AA (bottom) in ApoE KO mice from 2-24 months of age. Measurements were taken at 4-10 sites per sample per experiment, 2-8 force-distance curves per site. Intact DA (top left): n > 10 'younger' mice and n=6 'older' mice; Denuded DA (top right): n=5 'younger' mice and n=5 'older' mice; Intact AA (bottom left): n > 10 'younger' mice and n=6 'older' mice; Denuded AA (bottom right): n=4 'younger' mice and n=5 'older' mice.

5.3 Discussion:

The mouse model of diet-induced obesity in WT, CD36 KO and Cav1 KO mice used in this study has been widely implemented to investigate EC dysfunction and cardiovascular disease. This high fat, atherogenic diet has been previously shown to induce endothelial dysfunction in WT mice, especially those with a C57BL/6 background (Collins et al., 2004; Park et al., 2012). Importantly, endothelial dysfunction, atherosclerosis and the progression of obesity in this model is considered to have translational impact in human obesity (Collins et al., 2004; Paigen, 1995). As is found in humans, central adiposity is markedly increased in C57BL/6 mice on a high fat diet and is accompanied by gradual EC dysfunction (Park et al., 2012; Rebuffe-Scrive et al., 1993). Therefore, we used this translational high fat, atherogenic diet in C57BL/6 male mice to determine the effects of diet-induced dyslipidemia on pro-atherogenic EC dysfunction. Consistent with previous studies, our data shows an increase in total body weight and in blood plasma levels of LDL and oxLDL after one month on this HFD. Our results also demonstrated that short-term plasma dyslipidemia is sufficient to bring about a significant increase in EC elastic modulus from the intact aortas in WT mice. Furthermore, our data showed that there is considerable heterogeneity in EC stiffness between the pro-atherogenic regions of the aortic arch and the athero-protective regions of the descending aorta, with a significant increase in EC stiffness in the arch region. This effect is markedly exacerbated by this short-term HFD, an effect we show to be highly dependent on the oxLDL receptor CD36 and the endocytotic caveolae machinery.

A separate study of the effect of plasma dyslipidemia on endothelial vascular stiffness was conducted using ApoE KO mice. Many studies [reviewed by (Meyrelles et al., 2011)] have provided evidence of endothelial dysfunction in the vasculature of ApoE KO mice, such as impaired endothelial nitric oxide-mediated dilation due to a reduction in NO bioavailability, in addition to the spontaneous plaque development and elevated levels of total plasma cholesterol

and pro-atherogenic LDL in ApoE KO mice compared to WT mice [reviewed by (Meyrelles et al., 2011)]. Some studies have shown that ApoE KO mice fed a regular low fat diet developed lesions at a young age: 8-10 week olds developed foam cell formation and 15-20 week olds developed fibrous plaques (Plump, 1992; Nakashima, 1994), though other studies show that lesion formation increases sharply after 20 weeks (Itabe, 2011). Although it is well known that these mice will spontaneously develop atherosclerotic plaques preferentially at sites of disturbed flow such as the aortic arch [reviewed by (Meyrelles et al., 2011)], the effect of their plasma dyslipidemia and pro-atherogenic disturbed flow on endothelial cell biomechanical properties such as stiffness is less defined. Similar to WT mice, there was an increase in endothelial elastic modulus in the aortic arch in ApoE KO mice compared to the descending aorta. Interestingly, our results show that the elastic modulus values of the ECs from the DA and AA in ApoE KO mice are softer than those from age and gender matched WT mice. Our preliminary explanation for this softening is due to the increased uptake of LDL into ECs rather than oxLDL. The deletion of apolipoprotein E hinders lipoprotein clearance from the blood, which significantly elevates LDL plasma levels, especially when on a HFD. Preliminary unpublished studies from our lab (PhD thesis of M-J Oh) have shown that pathological levels of LDL soften endothelial cells compared to control and oxLDL-treated ECs. Additional studies will need to be conducted to support these preliminary hypotheses.

The application of a high fat diet has been shown to facilitate the adhesion of mononuclear cells to the endothelial surface and subsequent lesion formation in ApoE KO mice compared to those on a LFD (Nakashima et al., 1994). The combined effect of HFD feeding and plasma dyslipidemia on endothelial stiffening in the athero-protective compared to the pro-atherogenic regions has not been well studied. Implementing a high fat diet feeding in ApoE KO mice did not alter endothelial stiffening in either the DA or the AA. We attribute the lack of stiffening in the aortic arch on the fact that many of the mice become sick towards the end of the HFD

feeding period. This particular high fat diet had 1.25% cholesterol, which is far greater than the subsequent HFD (0.2% cholesterol) used in the studies with WT, CD36 KO and Cav1 KO mice. Additional studies quantified the elastic modulus of intact endothelial and sub-endothelial denuded monolayers from the DA and AA in WT mice from 2 months to 24 months old. Under all conditions, there was a significant increase in elastic modulus values as the mice age (all $R^2 > 0.67$). This effect was more pronounced in the ECs from the arch as compared to the descending aorta. On the other hand, the denuded layer in the DA had a more pronounced increase in stiffness over time as compared to the denuded layer in the AA. These results show that there maybe two different processes of cell stiffening in the intact versus the denuded layers, as evidenced by a greater slope in the AA (0.69) versus the DA (0.34) in the intact layer yet in the intact layer the slope is greater in the DA (0.75) over time versus the AA (0.48). This suggests that the stiffness in one layer may not necessarily affect the stiffness in the other layer.

Although many studies have quantified oxLDL levels in atherosclerotic plaques (Ehara et al., 2001; Yla-Herttuala et al., 1989), relatively few studies have focused on determining the level of oxLDL in the blood. The correct level of oxLDL in the blood plasma remains controversial. As reported in a review by Itabe *et al.* (Itabe and Ueda, 2007), there are many different techniques and epitopes on oxLDL to probe for and therefore a high degree of variability in the results among the different techniques [reviewed by (Fraley and Tsimikas, 2006)]. Therefore, the best way to interpret oxLDL concentration results may be to compare within each experiment. One consistency among the results is that humans have 10-100Xs higher concentration of plasma oxLDL than mice. This may be due to the maturation age differences or that mice have ~2x greater protective HDL level as compared to humans (Xiangdong et al., 2011). Holvoet *et al.* showed the levels of circulating oxLDL in humans were 31.1 μg/mL in patients with coronary artery disease whereas healthy controls had a 55% reduction in circulating oxLDL (13.3 μg/mL)

(Holvoet et al., 2001). Additionally, several studies have shown that oxLDL plasma levels are elevated in patients with carotid arteriosclerosis, transplant-associated atherosclerosis, and diabetes [reviewed by (Itabe and Ueda, 2007)]. In our study, we showed that the oxLDL levels in WT, CD36 KO and Cav1 KO mice are essentially the same. The studies described above, though, describe enhanced oxLDL levels in patients' versus healthy controls, yet our data shows that there is roughly the same oxLDL levels in WT mice as in CD36KO and Cav1 KO mice and that all three of these mice have an increase in their plasma oxLDL levels when fed a HFD. These results show that even when challenged with oxLDL/increased oxLDL levels, the loss of CD36 and Cav1 are important in abrogating cell stiffness.

Here we have shown several different mouse models of atherosclerosis, including both short-term and long-term high fat diet feedings, use of mice lacking the apolipoprotein E gene leading to chronic dyslipidemia, and the effect aging has on cellular biomechanical changes. Our data provides strong evidence that diet induced dyslipidemia induces EC stiffening in the aortic arch, which is critically dependent upon the expression of the scavenger receptor CD36 and on an intact caveolae endocytotic pathway.

CHAPTER 6: Conclusion

This work focuses on the biomechanical changes in endothelial cells resulting from dyslipidemia and vascular hemodynamics. Endothelial dysfunction is a known initiating factor in the onset of atherosclerosis. These studies provide insights into the mechanisms of pro-inflammatory oxLDL uptake into endothelial cells exposed to different flow environments and oxLDL-induced stiffening *in vitro* as well as *ex vivo* biomechanical changes including those resulting from dyslipidemia.

To mimic physiological vascular shear stress, we have used two complementary flow systems, a fabricated microfluidic chamber with a step barrier and a cone and plate rheometer, which both showed that oxLDL uptake into endothelial cells *in vitro* is enhanced under pro-atherogenic disturbed flow conditions as compared to athero-protective laminar flow. Enhanced oxLDL uptake was dependent on an intact caveolin1/eNOS complex and the endothelial oxLDL receptor CD36, but not LOX1.

Furthermore, this increase in oxLDL uptake resulted in cellular stiffening *in vitro* and *ex vivo* measurements show enhanced stiffness in the DF regions of the aortic arch compared to the LF regions of the descending aorta. Further exploration of this DF-induced stiffening effect was tested using knockdown *in vitro* techniques and *ex vivo* analysis of murine models of global knockout of the oxLDL receptor CD36 and knockout of the caveolin1 protein. Our results showed that oxLDL-induced stiffening *in vitro* is mediated by Cav1 and CD36, which is further supported by *ex vivo* data that the increased stiffness observed in the DF region of the aortic arch compared to the LF region of the descending aorta is critically dependent on the expression of CD36 and Cav1. This observation persisted even when challenged with a high fat diet. Moreover, we show that there is stiffening in the endothelial monolayer in the aortic arch of a known model of atherosclerosis, the dyslipidemic ApoE KO mouse. Further exploration of this phenomenon is required.

In summary, the results provided in this thesis demonstrate that plasma dyslipidemia results in endothelial stiffening at the pro-atherogenic region of the aortic arch, and provide evidence that this effect is mediated by increased uptake of oxLDL, the oxLDL receptor CD36 and endocytotic caveolae. Finally, we propose that increased endothelial uptake of oxLDL and endothelial stiffening in pro-atherogenic aortic regions are important factors in the local disruption of the endothelial barrier and the onset of the inflammatory response.

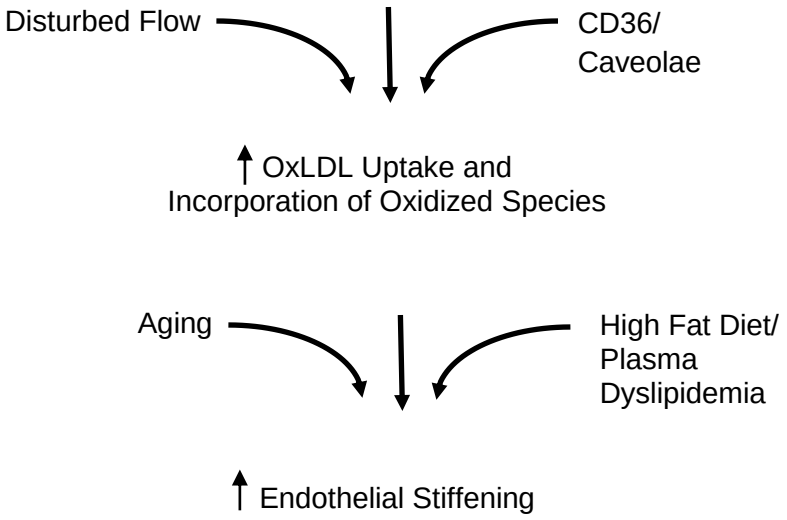

Figure 6.1: Summary schematic of the impact of hemodynamic environment and plasma dyslipidemia have on endothelial biomechanics.

REFERENCES

Ayee, M.A., LeMaster, E., Shentu, T.P., Singh, D.K., Barbera, N., Soni, D., Tiruppathi, C., Subbaiah, P.V., Berdyshev, E., Bronova, I., Cho, M., Akpa, B.S., Levitan, I., 2017. Molecular-Scale Biophysical Modulation of an Endothelial Membrane by Oxidized Phospholipids. Biophysical journal 112, 325-338.

Bakhshi, F.R., Mao, M., Shajahan, A.N., Piegeler, T., Chen, Z., Chernaya, O., Sharma, T., Elliott, W.M., Szulcek, R., Bogaard, H.J., Comhair, S., Erzurum, S., van Nieuw Amerongen, G.P., Bonini, M.G., Minshall, R.D., 2013. Nitrosation-dependent caveolin 1 phosphorylation, ubiquitination, and degradation and its association with idiopathic pulmonary arterial hypertension. Pulmonary circulation 3, 816-830.

Birukov, K.G., 2006. Oxidized lipids: the two faces of vascular inflammation. Current atherosclerosis reports 8, 223-231.

Birukova, A.A., Starosta, V., Tian, X., Higginbotham, K., Koroniak, L., Berliner, J.A., Birukov, K.G., 2013. Fragmented oxidation products define barrier disruptive endothelial cell response to OxPAPC. Translational research : the journal of laboratory and clinical medicine 161, 495-504.

Brown, P.M., Kennedy, D.J., Morton, R.E., Febbraio, M., 2015. CD36/SR-B2-TLR2 Dependent Pathways Enhance Porphyromonas gingivalis Mediated Atherosclerosis in the Ldlr KO Mouse Model. PloS one 10, e0125126.

Byfield, F.J., Aranda-Espinoza, H., Romanenko, V.G., Rothblat, G.H., Levitan, I., 2004. Cholesterol depletion increases membrane stiffness of aortic endothelial cells. Biophysical journal 87, 3336-3343.

Byfield, F.J., Reen, R.K., Shentu, T.P., Levitan, I., Gooch, K.J., 2009. Endothelial actin and cell stiffness is modulated by substrate stiffness in 2D and 3D. Journal of biomechanics 42, 1114-1119.

Byfield, F.J., Tikku, S., Rothblat, G.H., Gooch, K.J., Levitan, I., 2006. OxLDL increases endothelial stiffness, force generation, and network formation. Journal of lipid research 47, 715-723.

Cecelja, M., Chowienczyk, P., 2012. Role of arterial stiffness in cardiovascular disease. JRSM cardiovascular disease 1.

Chen, C.A., Druhan, L.J., Varadharaj, S., Chen, Y.R., Zweier, J.L., 2008. Phosphorylation of endothelial nitric-oxide synthase regulates superoxide generation from the enzyme. The Journal of biological chemistry 283, 27038-27047.

Chiu, J.J., Chien, S., 2011. Effects of disturbed flow on vascular endothelium: pathophysiological basis and clinical perspectives. Physiological reviews 91, 327-387.

Collins, C., Guilluy, C., Welch, C., O'Brien, E.T., Hahn, K., Superfine, R., Burridge, K., Tzima, E., 2012. Localized tensional forces on PECAM-1 elicit a global mechanotransduction response via the integrin-RhoA pathway. Current biology : CB 22, 2087-2094.

Collins, C., Osborne, L.D., Guilluy, C., Chen, Z., O'Brien, E.T., 3rd, Reader, J.S., Burridge, K., Superfine, R., Tzima, E., 2014. Haemodynamic and extracellular matrix cues regulate the mechanical phenotype and stiffness of aortic endothelial cells. Nature communications 5, 3984.

Collins, R.F., Touret, N., Kuwata, H., Tandon, N.N., Grinstein, S., Trimble, W.S., 2009. Uptake of Oxidized Low Density Lipoprotein by CD36 Occurs by an Actin-dependent Pathway Distinct from Macropinocytosis. The Journal of biological chemistry 284, 30288-30297.

Collins, S., Martin, T.L., Surwit, R.S., Robidoux, J., 2004. Genetic vulnerability to diet-induced obesity in the C57BL/6J mouse: physiological and molecular characteristics. Physiology & behavior 81, 243-248.

Cominacini, L., Rigoni, A., Pasini, A.F., Garbin, U., Davoli, A., Campagnola, M., Pastorino, A.M., Lo Cascio, V., Sawamura, T., 2001. The binding of oxidized low density lipoprotein (ox-LDL) to ox-LDL receptor-1 reduces the intracellular concentration of nitric oxide in endothelial cells through an increased production of superoxide. The Journal of biological chemistry 276, 13750-13755.

Dai, G., Kaazempur-Mofrad, M.R., Natarajan, S., Zhang, Y., Vaughn, S., Blackman, B.R., Kamm, R.D., Garcia-Cardena, G., Gimbrone, M.A., Jr., 2004. Distinct endothelial phenotypes evoked by arterial waveforms derived from atherosclerosis-susceptible and -resistant regions of human vasculature. Proceedings of the National Academy of Sciences of the United States of America 101, 14871-14876.

Daiber, A., Steven, S., Weber, A., Shuvaev, V.V., Muzykantov, V.R., Laher, I., Li, H., Lamas, S., Munzel, T., 2016. Targeting vascular (endothelial) dysfunction. British journal of pharmacology.

Dawson, D.W., Pearce, S.F., Zhong, R., Silverstein, R.L., Frazier, W.A., Bouck, N.P., 1997. CD36 mediates the In vitro inhibitory effects of thrombospondin-1 on endothelial cells. The Journal of cell biology 138, 707-717.

DePaola, N., Davies, P.F., Pritchard, W.F., Jr., Florez, L., Harbeck, N., Polacek, D.C., 1999. Spatial and temporal regulation of gap junction connexin43 in vascular endothelial cells exposed to controlled disturbed flows in vitro. Proceedings of the National Academy of Sciences of the United States of America 96, 3154-3159.

DePaola, N., Gimbrone, M.A., Jr., Davies, P.F., Dewey, C.F., Jr., 1992. Vascular endothelium responds to fluid shear stress gradients. Arteriosclerosis and thrombosis : a journal of vascular biology / American Heart Association 12, 1254-1257.

Dimmeler, S., Fleming, I., Fisslthaler, B., Hermann, C., Busse, R., Zeiher, A.M., 1999. Activation of nitric oxide synthase in endothelial cells by Akt-dependent phosphorylation. Nature 399, 601-605.

Ehara, S., Ueda, M., Naruko, T., Haze, K., Itoh, A., Otsuka, M., Komatsu, R., Matsuo, T., Itabe, H., Takano, T., Tsukamoto, Y., Yoshiyama, M., Takeuchi, K., Yoshikawa, J., Becker, A.E., 2001. Elevated levels of oxidized low density lipoprotein show a positive relationship with the severity of acute coronary syndromes. Circulation 103, 1955-1960.

Essler, M., Retzer, M., Bauer, M., Heemskerk, J.W., Aepfelbacher, M., Siess, W., 1999. Mildly oxidized low density lipoprotein induces contraction of human endothelial cells through activation of Rho/Rho kinase and inhibition of myosin light chain phosphatase. The Journal of biological chemistry 274, 30361-30364.

Febbraio, M., Hajjar, D.P., Silverstein, R.L., 2001. CD36: a class B scavenger receptor involved in angiogenesis, atherosclerosis, inflammation, and lipid metabolism. The Journal of clinical investigation 108, 785-791.

Febbraio, M., Podrez, E.A., Smith, J.D., Hajjar, D.P., Hazen, S.L., Hoff, H.F., Sharma, K., Silverstein, R.L., 2000. Targeted disruption of the class B scavenger receptor CD36 protects against atherosclerotic lesion development in mice. Journal of Clinical Investigation 105, 1049-1056.

Fraley, A.E., Tsimikas, S., 2006. Clinical applications of circulating oxidized low-density lipoprotein biomarkers in cardiovascular disease. Current opinion in lipidology 17, 502-509.

Frank, P.G., Lee, H., Park, D.S., Tandon, N.N., Scherer, P.E., Lisanti, M.P., 2004. Genetic ablation of caveolin-1 confers protection against atherosclerosis. Arteriosclerosis, thrombosis, and vascular biology 24, 98-105.

Fridolfsson, H.N., Roth, D.M., Insel, P.A., Patel, H.H., 2014. Regulation of intracellular signaling and function by caveolin. FASEB journal : official publication of the Federation of American Societies for Experimental Biology 28, 3823-3831.

Gaus, K., Gratton, E., Kable, E.P., Jones, A.S., Gelissen, I., Kritharides, L., Jessup, W., 2003. Visualizing lipid structure and raft domains in living cells with two-photon microscopy. Proceedings of the National Academy of Sciences of the United States of America 100, 15554-15559.

Ghitescu, L., Fixman, A., Simionescu, M., Simionescu, N., 1986. Specific binding sites for albumin restricted to plasmalemmal vesicles of continuous capillary endothelium: receptor-mediated transcytosis. The Journal of cell biology 102, 1304-1311.

Goldstein, J.L., Brown, M.S., 2009. The LDL receptor. Arteriosclerosis, thrombosis, and vascular biology 29, 431-438.

Goyal, T., Mitra, S., Khaidakov, M., Wang, X., Singla, S., Ding, Z., Liu, S., Mehta, J.L., 2012. Current Concepts of the Role of Oxidized LDL Receptors in Atherosclerosis. Current atherosclerosis reports.

Guy, E., Kuchibhotla, S., Silverstein, R., Febbraio, M., 2007. Continued inhibition of atherosclerotic lesion development in long term Western diet fed CD36o /apoEo mice. Atherosclerosis 192, 123-130.

Hahn, C., Schwartz, M.A., 2009. Mechanotransduction in vascular physiology and atherogenesis. Nature reviews. Molecular cell biology 10, 53-62.

Hall, A., 2012. Rho family GTPases. Biochemical Society transactions 40, 1378-1382.

Hayashi, K., Higaki, M., 2016. Stiffness of Intact Endothelial Cells from Fresh Aortic Bifurcations of Atherosclerotic Rabbits - Atomic Force Microscopic Study. Journal of cellular physiology.

Holdsworth, D.W., Norley, C.J., Frayne, R., Steinman, D.A., Rutt, B.K., 1999. Characterization of common carotid artery blood-flow waveforms in normal human subjects. Physiol Meas 20, 219-240.

Holvoet, P., Mertens, A., Verhamme, P., Bogaerts, K., Beyens, G., Verhaeghe, R., Collen, D., Muls, E., Van de Werf, F., 2001. Circulating oxidized LDL is a useful marker for identifying patients with coronary artery disease. Arteriosclerosis, thrombosis, and vascular biology 21, 844-848.

Huber, J., Vales, A., Mitulovic, G., Blumer, M., Schmid, R., Witztum, J.L., Binder, B.R., Leitinger, N., 2002. Oxidized membrane vesicles and blebs from apoptotic cells contain biologically active oxidized phospholipids that induce monocyte-endothelial interactions. Arteriosclerosis, thrombosis, and vascular biology 22, 101-107.

Huynh, J., Nishimura, N., Rana, K., Peloquin, J.M., Califano, J.P., Montague, C.R., King, M.R., Schaffer, C.B., Reinhart-King, C.A., 2011. Age-related intimal stiffening enhances endothelial permeability and leukocyte transmigration. Science translational medicine 3, 112ra122.

Ikonen, E., 2008. Cellular cholesterol trafficking and compartmentalization. Nature reviews. Molecular cell biology 9, 125-138.

Itabe, H., Obama, T., Kato, R., 2011. The Dynamics of Oxidized LDL during Atherogenesis. Journal of lipids 2011, 418313.

Itabe, H., Ueda, M., 2007. Measurement of plasma oxidized low-density lipoprotein and its clinical implications. Journal of atherosclerosis and thrombosis 14, 1-11.

Jiang, Y.Z., Manduchi, E., Jimenez, J.M., Davies, P.F., 2015. Endothelial epigenetics in biomechanical stress: disturbed flow-mediated epigenomic plasticity in vivo and in vitro. Arteriosclerosis, thrombosis, and vascular biology 35, 1317-1326.

John, T.A., Vogel, S.M., Tiruppathi, C., Malik, A.B., Minshall, R.D., 2003. Quantitative analysis of albumin uptake and transport in the rat microvessel endothelial monolayer. American journal of physiology. Lung cellular and molecular physiology 284, L187-196.

Katsumi, A., Orr, A.W., Tzima, E., Schwartz, M.A., 2004. Integrins in mechanotransduction. The Journal of biological chemistry 279, 12001-12004.

Khalil, I.A., Kogure, K., Akita, H., Harashima, H., 2006. Uptake pathways and subsequent intracellular trafficking in nonviral gene delivery. Pharmacological reviews 58, 32-45.

Kimura, K., Ito, M., Amano, M., Chihara, K., Fukata, Y., Nakafuku, M., Yamamori, B., Feng, J., Nakano, T., Okawa, K., Iwamatsu, A., Kaibuchi, K., 1996. Regulation of myosin phosphatase by Rho and Rho-associated kinase (Rho-kinase). Science 273, 245-248.

Kiss, A.L., 2012. Caveolae and the regulation of endocytosis. Advances in experimental medicine and biology 729, 14-28.

Kohn, J.C., Chen, A., Cheng, S., Kowal, D.R., King, M.R., Reinhart-King, C.A., 2016. Mechanical heterogeneities in the subendothelial matrix develop with age and decrease with exercise. Journal of biomechanics 49, 1447-1453.

Kohn, J.C., Lampi, M.C., Reinhart-King, C.A., 2015. Age-related vascular stiffening: causes and consequences. Frontiers in genetics 6, 112.

Kole, T.P., Tseng, Y., Huang, L., Katz, J.L., Wirtz, D., 2004. Rho kinase regulates the intracellular micromechanical response of adherent cells to rho activation. Molecular biology of the cell 15, 3475-3484.

Kowalsky, G.B., Byfield, F.J., Levitan, I., 2008. oxLDL facilitates flow-induced realignment of aortic endothelial cells. American journal of physiology. Cell physiology 295, C332-340.

Kruth, H.S., 2001. Lipoprotein cholesterol and atherosclerosis. Current molecular medicine 1, 633-653.

Ku, D.N., Giddens, D.P., Zarins, C.K., Glagov, S., 1985. Pulsatile flow and atherosclerosis in the human carotid bifurcation. Positive correlation between plaque location and low oscillating shear stress. Arteriosclerosis (Dallas, Tex.) 5, 293-302.

Kuliczkowska-Plaksej, J., Bednarek-Tupikowska, G., Plaksej, R., Filus, A., 2006. [Scavenger receptor CD36: its expression, regulation, and role in the pathogenesis of atherosclerosis. Part I]. Postepy higieny i medycyny doswiadczalnej (Online) 60, 142-151.

Kumano-Kuramochi, M., Xie, Q., Kajiwara, S., Komba, S., Minowa, T., Machida, S., 2013. Lectin-like oxidized LDL receptor-1 is palmitoylated and internalizes ligands via caveolae/raft-dependent endocytosis. Biochemical and biophysical research communications 434, 594-599.

Levitan, I., Volkov, S., Subbaiah, P.V., 2010. Oxidized LDL: diversity, patterns of recognition, and pathophysiology. Antioxidants & redox signaling 13, 39-75.

Li, L., Chen, W., Rezvan, A., Jo, H., Harrison, D.G., 2011. Tetrahydrobiopterin deficiency and nitric oxide synthase uncoupling contribute to atherosclerosis induced by disturbed flow. Arteriosclerosis, thrombosis, and vascular biology 31, 1547-1554.

Libby, P., Ridker, P.M., Hansson, G.K., 2011. Progress and challenges in translating the biology of atherosclerosis. Nature 473, 317-325.

Lisanti, M.P., Scherer, P.E., Vidugiriene, J., Tang, Z., Hermanowski-Vosatka, A., Tu, Y.H., Cook, R.F., Sargiacomo, M., 1994. Characterization of caveolin-rich membrane domains isolated from an endothelial-rich source: implications for human disease. The Journal of cell biology 126, 111-126.

Lubrano, V., Balzan, S., 2014. LOX-1 and ROS, inseparable factors in the process of endothelial damage. Free radical research 48, 841-848.

Maiolino, G., Rossitto, G., Caielli, P., Bisogni, V., Rossi, G.P., Calo, L.A., 2013. The role of oxidized low-density lipoproteins in atherosclerosis: the myths and the facts. Mediators of inflammation 2013, 714653.

Mammoto, T., Ingber, D.E., 2010. Mechanical control of tissue and organ development. Development (Cambridge, England) 137, 1407-1420.

Marin, T., Gongol, B., Chen, Z., Woo, B., Subramaniam, S., Chien, S., Shyy, J.Y., 2013. Mechanosensitive microRNAs-role in endothelial responses to shear stress and redox state. Free radical biology & medicine 64, 61-68.

Martinelli, R., Zeiger, A.S., Whitfield, M., Sciuto, T.E., Dvorak, A., Van Vliet, K.J., Greenwood, J., Carman, C.V., 2014. Probing the biomechanical contribution of the endothelium to lymphocyte migration: diapedesis by the path of least resistance. Journal of cell science 127, 3720-3734.

Martorell, J., Santoma, P., Kolandaivelu, K., Kolachalama, V.B., Melgar-Lesmes, P., Molins, J.J., Garcia, L., Edelman, E.R., Balcells, M., 2014. Extent of flow recirculation governs expression of atherosclerotic and thrombotic biomarkers in arterial bifurcations. Cardiovasc Res 103, 37-46.

Matsumoto, T., Abe, H., Ohashi, T., Kato, Y., Sato, M., 2002. Local elastic modulus of atherosclerotic lesions of rabbit thoracic aortas measured by pipette aspiration method. Physiological Measurement 23, 635.

May, J.M., Qu, Z.C., 2010. Ascorbic acid prevents increased endothelial permeability caused by oxidized low density lipoprotein. Free radical research 44, 1359-1368.

Meyrelles, S.S., Peotta, V.A., Pereira, T.M., Vasquez, E.C., 2011. Endothelial dysfunction in the apolipoprotein E-deficient mouse: insights into the influence of diet, gender and aging. Lipids in health and disease 10, 211.

Miyazaki, H., Hayashi, K., 1999. Atomic force microscopic measurement of the mechanical properties of intact endothelial cells in fresh arteries. Medical & biological engineering & computing 37, 530-536.

Moore, K.J., Kunjathoor, V.V., Koehn, S.L., Manning, J.J., Tseng, A.A., Silver, J.M., McKee, M., Freeman, M.W., 2005. Loss of receptor-mediated lipid uptake via scavenger receptor A or CD36 pathways does not ameliorate atherosclerosis in hyperlipidemic mice. The Journal of clinical investigation 115, 2192-2201.

Nakashima, Y., Plump, A.S., Raines, E.W., Breslow, J.L., Ross, R., 1994. ApoE-deficient mice develop lesions of all phases of atherosclerosis throughout the arterial tree. Arteriosclerosis and thrombosis : a journal of vascular biology / American Heart Association 14, 133-140.

Oh, M.J., Zhang, C., LeMaster, E., Adamos, C., Berdyshev, E., Bogachkov, Y., Kohler, E.E., Baruah, J., Fang, Y., Schraufnagel, D.E., Wary, K.K., Levitan, I., 2016. Oxidized-LDL Signals through Rho-GTPase to Induce Endothelial Cell Stiffening and Promote Capillary Formation. Journal of lipid research.

Olesen, S.P., Clapham, D.E., Davies, P.F., 1988. Haemodynamic shear stress activates a K+ current in vascular endothelial cells. Nature 331, 168-170.

Orr, A.W., Sanders, J.M., Bevard, M., Coleman, E., Sarembock, I.J., Schwartz, M.A., 2005. The subendothelial extracellular matrix modulates NF-kappaB activation by flow: a potential role in atherosclerosis. The Journal of cell biology 169, 191-202.

Paigen, B., 1995. Genetics of responsiveness to high-fat and high-cholesterol diets in the mouse. The American journal of clinical nutrition 62, 458s-462s.

Paigen, B., Morrow, A., Brandon, C., Mitchell, D., Holmes, P., 1985. Variation in susceptibility to atherosclerosis among inbred strains of mice. Atherosclerosis 57, 65-73.

Palombo, C., Kozakova, M., 2016. Arterial stiffness, atherosclerosis and cardiovascular risk: Pathophysiologic mechanisms and emerging clinical indications. Vascular pharmacology 77, 1-7.

Park, Y., Booth, F.W., Lee, S., Laye, M.J., Zhang, C., 2012. Physical activity opposes coronary vascular dysfunction induced during high fat feeding in mice. The Journal of physiology 590, 4255-4268.

Park, Y.M., 2014. CD36, a scavenger receptor implicated in atherosclerosis. Experimental & molecular medicine 46, e99.

Parton, R. G. and K. Simons , 2007. The multiple faces of caveolae. Nat Rev Mol Cell Biol 8(3): 185-194.

Pavlides, S., Gutierrez-Pajares, J.L., Danilo, C., Lisanti, M.P., Frank, P.G., 2012. Atherosclerosis, caveolae and caveolin-1. Advances in experimental medicine and biology 729, 127-144.

Peloquin, J., Huynh, J., Williams, R.M., Reinhart-King, C.A., 2011. Indentation measurements of the subendothelial matrix in bovine carotid arteries. Journal of biomechanics 44, 815-821.

Pirillo, A., Norata, G.D., Catapano, A.L., 2013. LOX-1, OxLDL, and atherosclerosis. Mediators of inflammation 2013, 152786.

Plump, A. S., J. D. Smith, T. Hayek, K. Aalto-Setälä, A. Walsh, J. G. Verstuyft, E. M. Rubin and J. L. Breslow., 1992. Severe hypercholesterolemia and atherosclerosis in apolipoprotein E-deficient mice created by homologous recombination in ES cells. Cell 71, 343-353.

Rangaswamy, S., Penn, M.S., Saidel, G.M., Chisolm, G.M., 1997. Exogenous oxidized low-density lipoprotein injures and alters the barrier function of endothelium in rats in vivo. Circulation research 80, 37-44.

Rebuffe-Scrive, M., Surwit, R., Feinglos, M., Kuhn, C., Rodin, J., 1993. Regional fat distribution and metabolism in a new mouse model (C57BL/6J) of non-insulin-dependent diabetes mellitus. Metabolism: clinical and experimental 42, 1405-1409.

Rizzo, V., Morton, C., DePaola, N., Schnitzer, J.E., Davies, P.F., 2003. Recruitment of endothelial caveolae into mechanotransduction pathways by flow conditioning in vitro. American journal of physiology. Heart and circulatory physiology 285, H1720-1729.

Ryoo, S., Bhunia, A., Chang, F., Shoukas, A., Berkowitz, D.E., Romer, L.H., 2011. OxLDL-dependent activation of arginase II is dependent on the LOX-1 receptor and downstream RhoA signaling. Atherosclerosis 214, 279-287.

Sato, M., Ohashi, T., 2005. Biorheological views of endothelial cell responses to mechanical stimuli. Biorheology 42, 421-441.

Schaefer, A., Hordijk, P.L., 2015. Cell-stiffness-induced mechanosignaling - a key driver of leukocyte transendothelial migration. Journal of cell science 128, 2221-2230.

Schaefer, A., Te Riet, J., Ritz, K., Hoogenboezem, M., Anthony, E.C., Mul, F.P., de Vries, C.J., Daemen, M.J., Figdor, C.G., van Buul, J.D., Hordijk, P.L., 2014. Actin-binding proteins differentially regulate endothelial cell stiffness, ICAM-1 function and neutrophil transmigration. Journal of cell science 127, 4470-4482.

Shajahan, A.N., Timblin, B.K., Sandoval, R., Tiruppathi, C., Malik, A.B., Minshall, R.D., 2004. Role of Src-induced dynamin-2 phosphorylation in caveolae-mediated endocytosis in endothelial cells. The Journal of biological chemistry 279, 20392-20400.

Shentu, T.P., Singh, D.K., Oh, M.J., Sun, S., Sadaat, L., Makino, A., Mazzone, T., Subbaiah, P.V., Cho, M., Levitan, I., 2012. The role of oxysterols in control of endothelial stiffness. Journal of lipid research 53, 1348-1358.

Shentu, T.P., Titushkin, I., Singh, D.K., Gooch, K.J., Subbaiah, P.V., Cho, M., Levitan, I., 2010. oxLDL-induced decrease in lipid order of membrane domains is inversely correlated with endothelial stiffness and network formation. American journal of physiology. Cell physiology 299, C218-229.

Silverstein, R.L., Febbraio, M., 2009. CD36, a scavenger receptor involved in immunity, metabolism, angiogenesis, and behavior. Science signaling 2, re3.

Sorci-Thomas, M.G., Thomas, M.J., 2016. Microdomains, Inflammation, and Atherosclerosis. Circulation research 118, 679-691.

Sugimoto, K., Ishibashi, T., Sawamura, T., Inoue, N., Kamioka, M., Uekita, H., Ohkawara, H., Sakamoto, T., Sakamoto, N., Okamoto, Y., Takuwa, Y., Kakino, A., Fujita, Y., Tanaka, T., Teramoto, T., Maruyama, Y., Takeishi, Y., 2009. LOX-1-MT1-MMP axis is crucial for RhoA and Rac1 activation induced by oxidized low-density lipoprotein in endothelial cells. Cardiovasc Res 84, 127-136.

Sun, B., Boyanovsky, B.B., Connelly, M.A., Shridas, P., van der Westhuyzen, D.R., Webb, N.R., 2007. Distinct mechanisms for OxLDL uptake and cellular trafficking by class B scavenger receptors CD36 and SR-BI. Journal of lipid research 48, 2560-2570.

Sun, S.W., Zu, X.Y., Tuo, Q.H., Chen, L.X., Lei, X.Y., Li, K., Tang, C.K., Liao, D.F., 2010. Caveolae and caveolin-1 mediate endocytosis and transcytosis of oxidized low density lipoprotein in endothelial cells. Acta pharmacologica Sinica 31, 1336-1342.

Sverdlov, M., Shajahan, A.N., Minshall, R.D., 2007. Tyrosine phosphorylation-dependence of caveolae-mediated endocytosis. Journal of cellular and molecular medicine 11, 1239-1250.

Sverdlov, M., Shinin, V., Place, A.T., Castellon, M., Minshall, R.D., 2009. Filamin A regulates caveolae internalization and trafficking in endothelial cells. Molecular biology of the cell 20, 4531-4540.

Tarbell, J.M., Pahakis, M.Y., 2006. Mechanotransduction and the glycocalyx. Journal of internal medicine 259, 339-350.

Tarbell, J.M., Shi, Z.D., Dunn, J., Jo, H., 2014. Fluid Mechanics, Arterial Disease, and Gene Expression. Annual review of fluid mechanics 46, 591-614.

Tracqui, P., Broisat, A., Toczek, J., Mesnier, N., Ohayon, J., Riou, L., 2011. Mapping elasticity moduli of atherosclerotic plaque in situ via atomic force microscopy. Journal of structural biology 174, 115-123.

Tzima, E., Irani-Tehrani, M., Kiosses, W.B., Dejana, E., Schultz, D.A., Engelhardt, B., Cao, G., DeLisser, H., Schwartz, M.A., 2005. A mechanosensory complex that mediates the endothelial cell response to fluid shear stress. Nature 437, 426-431.

Uittenbogaard, A., Shaul, P.W., Yuhanna, I.S., Blair, A., Smart, E.J., 2000. High density lipoprotein prevents oxidized low density lipoprotein-induced inhibition of endothelial nitric-oxide synthase localization and activation in caveolae. The Journal of biological chemistry 275, 11278-11283.

van Tits, L., de Graaf, J., Hak-Lemmers, H., Bredie, S., Demacker, P., Holvoet, P., Stalenhoef, A., 2003. Increased Levels of Low-Density Lipoprotein Oxidation in Patients with Familial Hypercholesterolemia and in End-Stage Renal Disease Patients on Hemodialysis. Lab Invest 83, 13-21.

VanderLaan, P.A., Reardon, C.A., Getz, G.S., 2004. Site specificity of atherosclerosis: site-selective responses to atherosclerotic modulators. Arteriosclerosis, thrombosis, and vascular biology 24, 12-22.

Vandoorne, K., Addadi, Y., Neeman, M., 2010. Visualizing vascular permeability and lymphatic drainage using labeled serum albumin. Angiogenesis 13, 75-85.

Vitiello, L., Spoletini, I., Gorini, S., Pontecorvo, L., Ferrari, D., Ferraro, E., Stabile, E., Caprio, M., la Sala, A., 2014. Microvascular inflammation in atherosclerosis. IJC Metabolic & Endocrine 3, 1-7.

Watson, A.D., Leitinger, N., Navab, M., Faull, K.F., Horkko, S., Witztum, J.L., Palinski, W., Schwenke, D., Salomon, R.G., Sha, W., Subbanagounder, G., Fogelman, A.M., Berliner, J.A., 1997. Structural identification by mass spectrometry of oxidized phospholipids in minimally oxidized low density lipoprotein that induce monocyte/endothelial interactions and evidence for their presence in vivo. The Journal of biological chemistry 272, 13597-13607.

Wu, C., Huang, R.T., Kuo, C.H., Kumar, S., Kim, C.W., Lin, Y.C., Chen, Y.J., Birukova, A., Birukov, K.G., Dulin, N.O., Civelek, M., Lusis, A.J., Loyer, X., Tedgui, A., Dai, G., Jo, H., Fang, Y., 2015. Mechanosensitive PPAP2B Regulates Endothelial Responses to Atherorelevant Hemodynamic Forces. Circulation research 117, e41-53.

Xiangdong, L., Yuanwu, L., Hua, Z., Liming, R., Qiuyan, L., Ning, L., 2011. Animal models for the atherosclerosis research: a review. Protein & cell 2, 189-201.

Yang, B., Rizzo, V., 2013. Shear Stress Activates eNOS at the Endothelial Apical Surface Through 1 Containing Integrins and Caveolae. Cellular and molecular bioengineering 6, 346-354.

Yla-Herttuala, S., Palinski, W., Rosenfeld, M.E., Parthasarathy, S., Carew, T.E., Butler, S., Witztum, J.L., Steinberg, D., 1989. Evidence for the presence of oxidatively modified low density lipoprotein in atherosclerotic lesions of rabbit and man. The Journal of clinical investigation 84, 1086-1095.

Yoshimoto, R., Fujita, Y., Kakino, A., Iwamoto, S., Takaya, T., Sawamura, T., 2011. The discovery of LOX-1, its ligands and clinical significance. Cardiovascular drugs and therapy 25, 379-391.

Youngblom, E., Pariani, M., Knowles, J.W., 1993. Familial Hypercholesterolemia, in: Pagon, R.A., Adam, M.P., Ardinger, H.H., Wallace, S.E., Amemiya, A., Bean, L.J.H., Bird, T.D., Ledbetter, N., Mefford, H.C., Smith, R.J.H., Stephens, K. (Eds.), GeneReviews(R). University of Washington, Seattle

University of Washington, Seattle. GeneReviews is a registered trademark of the University of Washington, Seattle. All rights reserved., Seattle (WA).

Zeng, Y., Tao, N., Chung, K.N., Heuser, J.E., Lublin, D.M., 2003. Endocytosis of oxidized low density lipoprotein through scavenger receptor CD36 utilizes a lipid raft pathway that does not require caveolin-1. The Journal of biological chemistry 278, 45931-45936.

Zhang, Q., Liu, J., Liu, J., Huang, W., Tian, L., Quan, J., Wang, Y., Niu, R., 2014. oxLDL induces injury and defenestration of human liver sinusoidal endothelial cells via LOX1. Journal of molecular endocrinology 53, 281-293.

Zhang, S., Reddick, R., Piedrahita, J., Maeda, N., 1992. Spontaneous hypercholesterolemia and arterial lesions in mice lacking apolipoprotein E. Science 258, 468-471.

Elizabeth LeMaster

Education:

University of Illinois at Chicago – Ph.D. in Cell and Tissue Bioengineering, GPA: 3.48/4.0, 2017

University of Illinois at Chicago – B.S. Bioengineering, Concentration Area: Bioinformatics Spring 2009, GPA: 3.27/4.0

Illinois State University – B.S. Special Education, Fall 2002, GPA: 3.72/4.0, Cum Laude, Presidential Scholar: Full academic scholarship

Research Experience:

Research Assistant in Multi-disciplinary Project (BioE, Pharmacology, Dept. of Medicine), 2010-current

- Determined the impact of shear stress patterns, CD36 receptor and caveolin-1 protein on oxidized LDL uptake into endothelial cells (ECs) *in vitro*
- Designed microfluidic chamber based on fluid dynamics simulations to better mimic *in vivo* shear stress conditions at vascular bifurcations
- Optimized *ex vivo* stiffness measurement of ECs from intact vessels using atomic force microscopy
- *In silico* modeling of vesicles to investigate the mechanism of caveolae formation

Research Assistant at UIC's Molecular Systems Computational Bioengineering Lab, 2009-2010

- Data mined biological databases and characterized protein kinase ATP binding sites for the potential functional classification of proteins
- Applied thermodynamics and protein evolution theories to explain why some allosteric proteins require a large conformational change to function
- Developed Matlab program to characterized functional residues in allosteric proteins

Research Assistant at UIC's Physiologic Imaging and Modeling Lab, 2008-2009

- Characterized biomechanical properties of the upper spinal canal using cerebrospinal fluid pulse wave velocity (PWV)
- Created Matlab program to calculate PWV using axial MR images

Publications:

E. LeMaster, et al.: 'Pro-atherogenic Disturbed Flow Increases Endothelial Stiffness via Enhanced CD36/Cav1-mediated oxLDL Uptake. (Re-submitted to *ATVB*).

Ayee MAA, E. LeMaster, et al.: 'Molecular-Scale Biophysical Modulation of an Endothelial Membrane by Oxidized Phospholipids. *Biophysical Journal*. 2017; 112:325-338.

Oh MJ, Zhang C, E. LeMaster, et al.: 'Oxidized-LDL Signals through Rho-GTPase to Induce Endothelial Cell Stiffening and Promote Capillary Formation. *Journal of Lipid Research*. 2016.

Invited Conference Oral Presentations:

E. LeMaster, et al.: 'Enhanced oxLDL Uptake Results in Increased Endothelial Stiffness in Disturbed Flow Regions.' North American Vascular Biology Organization, Cape Cod, MA, 2015.

E. LeMaster, et al.: 'Disturbed Shear Stress Facilitates Caveolae-Mediated oxLDL Uptake Leading to Increased Endothelial Stiffening.' American Heart Association Conference, Chicago, 2014.

Selected Poster Presentations:

E. LeMaster, et al.: 'Pro-atherogenic Disturbed Flow Increases Endothelial Stiffness via Enhanced CD36/Cav1-mediated oxLDL Uptake.' Experimental Biology Conference, Chicago, IL, 2017.

E. LeMaster, et al.: 'Enhanced oxLDL Uptake Results in Increased Endothelial Stiffness in Disturbed Flow Areas,' UIC Department of Medicine Forum, 2016.

E. LeMaster, et al.: 'Disturbed Shear Stress Promotes Caveolae-Mediated oxLDL Uptake Leading to Increased Endothelial Stiffness.' Experimental Biology Conference, Boston, MA, 2015.

E. LeMaster, et al.: 'Disturbed Flow Increases Caveolae-Mediated oxLDL Uptake into Endothelial Cells,' Experimental Biology Conference, Boston, MA, 2013.

E. LeMaster, et al.: 'Mechanism of oxLDL Uptake into Endothelial Cells: Role of Caveolin-1 and Shear Stress,' UIC Department of Medicine Forum and Department of Pharmacology Retreat, 2012.

E. LeMaster, et al.: 'On the Mechanism of Shear Stress-Induced Increase in Oxidized LDL Uptake', UIC Department of Pharmacology Retreat, 2011.

E. LeMaster, et al.: 'Designing a Biofilm-Resistant Catheter and a Bioreactor for *in vitro* Analysis', UIC College of Engineering Senior Design Expo, 2009.

E. LeMaster, et al.: 'Approaches for the Estimation of Pulse Wave Velocity in the Spinal Canal', Journal of Undergraduate Research, 2009, 2.

E. LeMaster, et al.: 'MRI Measurement of CSF Pulse Wave Velocity in the Cervical Spine: A Potential New Marker for the Diagnosis of Chiari Malformation,' Student Research Forum, 2008.

Awards/Honors:

- American Heart Association Pre-doctoral Grant, 2014-2016
- Scientific Excellence Award, Scholarly Activities Day, 2014
- Honorable Mention at UIC's College of Medicine Research Forum, 2012
- Pre-doctoral Training Grant (NIH NHLBI T32, Professor Dudely, PI), 2010-2011
- First Place, 2008 UIC Undergraduate Research Forum, Biological Science Category
- NSF-DoD Grant: Research Experiences for Undergraduates (REU) Program, 2008
- Golden Key International Honor Society
- Barth Engineering Scholarship

Leadership Experiences:

Mentor for Bioengineering Senior Design Students, 2011-2012

- Students won first place in Medical Application category for the design, fabrication and testing of novel flow slides for the application of atherosclerosis research

High School Teacher at Plainfield South High School, 2003-2005

- Developed math and science curriculum for students with learning and behavioral disabilities
- Trained and supervised classroom assistants

Chicago Lutheran Representative, South Africa, 2003

- Constructed an AIDS hospice, clinic, and education center in South Africa

Novice Educator at University of Brighton, England, 2000

- Developed leadership skills to enhance the efficiency of a school system

Hindawi

Mediators of Inflammation

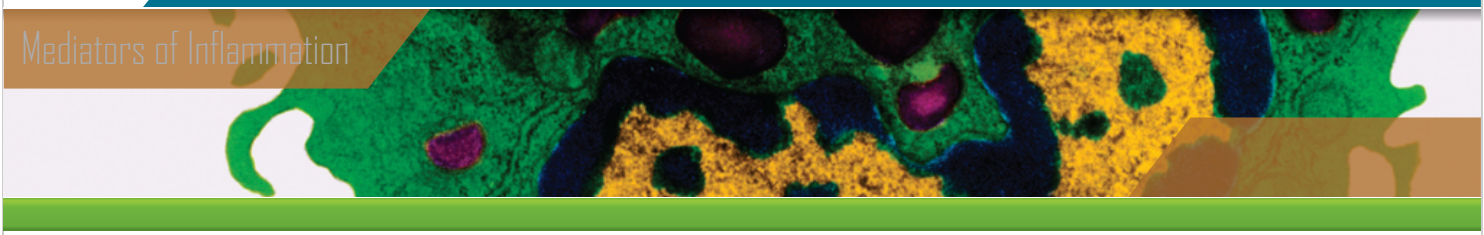

Mediators of Inflammation
Volume 2013 (2013), Article ID 714653, 13 pages
http://dx.doi.org/10.1155/2013/714653

Review Article

The Role of Oxidized Low-Density Lipoproteins in Atherosclerosis: The Myths and the Facts

Giuseppe Maiolino, Giacomo Rossitto, Paola Caielli, Valeria Bisogni, Gian Paolo Rossi, and Lorenzo A. Calò

Department of Medicine (DIMED), Internal Medicine 4, University of Padova, Via Giustiniani 2, 35128 Padova, Italy

Received 10 June 2013; Accepted 28 August 2013

Academic Editor: Ishak Tekin

Abstract

The oxidative modification hypothesis of atherosclerosis, which assigns to oxidized low-density lipoproteins (LDLs) a crucial role in atherosclerosis initiation and progression, is still debated. This review examines the role played by oxidized LDLs in atherogenesis taking into account data derived by studies based on molecular and clinical approaches. Experimental data carried out in cellular lines and animal models of atherosclerosis support the proatherogenic role of oxidized LDLs: (a) through chemotactic and proliferating actions on monocytes/macrophages, inciting their transformation into foam cells; (b) through stimulation of smooth muscle cells (SMCs) recruitment and proliferation in the tunica intima; (c) through eliciting endothelial cells, SMCs, and macrophages apoptosis with ensuing necrotic core development. Moreover, most of the experimental data on atherosclerosis-prone animals benefiting from antioxidant treatment points towards a link between oxidative stress and atherosclerosis. The evidence coming from cohort studies demonstrating an association between oxidized LDLs and cardiovascular events, notwithstanding some discrepancies, seems to point towards a role of oxidized LDLs in atherosclerotic plaque development and destabilization. Finally, the results of randomized clinical trials employing antioxidants completed up to date, despite demonstrating no benefits in healthy populations, suggest a benefit in high-risk patients. In conclusion, available data seem to validate the oxidative modification hypothesis of atherosclerosis, although additional proofs are still needed.

1. Introduction

Recent postulates on atherosclerosis designate the appearance of qualitative changes on endothelial cells, triggered by "irritative" stimuli (e.g., hypertension, dyslipidemia, and cigarette smoking), as an early pathogenic event [1]. This process occurs at specific segments of the arterial tree, mainly branching points and bifurcations, characterized by disturbed laminar blood flow, probably owing to differences in arteries regional development [2] and to the loss of the atheroprotective effect of laminar shear stress [3]. In this setting, the endothelium expresses adhesion and chemotactic molecules and acquires an increased permeability to macromolecules, which modifies the composition of the subendothelial extracellular matrix. Hence, the entry of low-density lipoprotein (LDL) particles in the arterial wall followed by their retention through the binding of apolipoprotein B100 to proteoglycans of the extracellular matrix [4] is held to be a key-initiating factor in early atherogenesis [5]. The LDL particles trapped in the subintimal extracellular matrix are mildly oxidized by resident vascular cells [6]. They retain the capability of binding to the LDL receptor [6, 7] and to exert their proatherogenic effects [8–10], including stimulation of the resident vascular cells to produce monocyte chemotactic protein-1, granulocyte, and macrophage colony-stimulating factors. These molecules promote monocytes recruitment and their differentiation into macrophages, which are able to further promote the oxidation of LDLs [11] through myeloperoxidase and reactive oxygen species. Completely oxidized LDLs, characterized by an increased apolipoprotein B100 negative charge, are recognized by scavenger receptors on macrophages and internalized to form foam cells [12], the hallmark of the atherosclerotic lesion. Furthermore, macrophages play a key role in atherogenesis through their proinflammatory action, which involves the production of interleukin-1β and tumor necrosis factor (Figure 1).

NATURE PUBLISHING GROUP LICENSE
TERMS AND CONDITIONS

Jul 07, 2017

This Agreement between Elizabeth LeMaster ("You") and Nature Publishing Group ("Nature Publishing Group") consists of your license details and the terms and conditions provided by Nature Publishing Group and Copyright Clearance Center.

License Number	4143940681756
License date	Jul 07, 2017
Licensed Content Publisher	Nature Publishing Group
Licensed Content Publication	Nature Reviews Molecular Cell Biology
Licensed Content Title	The multiple faces of caveolae
Licensed Content Author	Robert G. Parton and Kai Simons
Licensed Content Date	Mar 1, 2007
Licensed Content Volume	8
Licensed Content Issue	3
Type of Use	reuse in a dissertation / thesis
Requestor type	academic/educational
Format	print and electronic
Portion	figures/tables/illustrations
Number of figures/tables/illustrations	1
High-res required	no
Figures	Figure 3.1: Caveolae formation at the plasma membrane.
Author of this NPG article	no
Your reference number	
Title of your thesis / dissertation	Synergistic effect of hemodynamic environment and dyslipidemia on endothelial biomechanics
Expected completion date	Jul 2017
Estimated size (number of pages)	150
Requestor Location	Elizabeth LeMaster 909 South Wolcott St. Rm 3100 CHICAGO, IL 60612 United States Attn: Elizabeth LeMaster
Billing Type	Invoice
Billing Address	Elizabeth LeMaster 909 South Wolcott St. Rm 3100 CHICAGO, IL 60612 United States Attn: Elizabeth LeMaster

Total 0.00 USD

Terms and Conditions

Terms and Conditions for Permissions

Nature Publishing Group hereby grants you a non-exclusive license to reproduce this material for this purpose, and for no other use,subject to the conditions below:

1. NPG warrants that it has, to the best of its knowledge, the rights to license reuse of this material. However, you should ensure that the material you are requesting is original to Nature Publishing Group and does not carry the copyright of another entity (as credited in the published version). If the credit line on any part of the material you have requested indicates that it was reprinted or adapted by NPG with permission from another source, then you should also seek permission from that source to reuse the material.

2. Permission granted free of charge for material in print is also usually granted for any electronic version of that work, provided that the material is incidental to the work as a whole and that the electronic version is essentially equivalent to, or substitutes for, the print version.Where print permission has been granted for a fee, separate permission must be obtained for any additional, electronic re-use (unless, as in the case of a full paper, this has already been accounted for during your initial request in the calculation of a print run).NB: In all cases, web-based use of full-text articles must be authorized separately through the 'Use on a Web Site' option when requesting permission.

3. Permission granted for a first edition does not apply to second and subsequent editions and for editions in other languages (except for signatories to the STM Permissions Guidelines, or where the first edition permission was granted for free).

4. Nature Publishing Group's permission must be acknowledged next to the figure, table or abstract in print. In electronic form, this acknowledgement must be visible at the same time as the figure/table/abstract, and must be hyperlinked to the journal's homepage.

5. The credit line should read:
   Reprinted by permission from Macmillan Publishers Ltd: [JOURNAL NAME] (reference citation), copyright (year of publication)
   For AOP papers, the credit line should read:
   Reprinted by permission from Macmillan Publishers Ltd: [JOURNAL NAME], advance online publication, day month year (doi: 10.1038/sj.[JOURNAL ACRONYM].XXXXX)

   Note: For republication from the *British Journal of Cancer,* the following credit lines apply.
   Reprinted by permission from Macmillan Publishers Ltd on behalf of Cancer Research UK: [JOURNAL NAME] (reference citation), copyright (year of publication)For AOP papers, the credit line should read:
   Reprinted by permission from Macmillan Publishers Ltd on behalf of Cancer Research UK: [JOURNAL NAME], advance online publication, day month year (doi: 10.1038/sj.[JOURNAL ACRONYM].XXXXX)

6. Adaptations of single figures do not require NPG approval. However, the adaptation should be credited as follows:

   Adapted by permission from Macmillan Publishers Ltd: [JOURNAL NAME] (reference citation), copyright (year of publication)

   Note: For adaptation from the *British Journal of Cancer,* the following credit line applies.
   Adapted by permission from Macmillan Publishers Ltd on behalf of Cancer Research UK: [JOURNAL NAME] (reference citation), copyright (year of publication)

7. Translations of 401 words up to a whole article require NPG approval. Please visit http://www.macmillanmedicalcommunications.com for more information.Translations of up to a 400 words do not require NPG approval. The translation should be credited as follows:

Copyright Permission Policy

These guidelines apply to the reuse of articles, figures, charts and photos in the , and the .

For authors reusing their own material:

Authors need contact the journal to obtain rights to reuse their own material. They are automatically granted permission to do the following:

- Reuse the article in print collections of their own writing.
- Present a work orally in its entirety.
- Use an article in a thesis and/or dissertation.
- Reproduce an article for use in the author's courses. (If the author is employed by an academic institution, that institution also may reproduce the article for teaching purposes.)
- Reuse a figure, photo and/or table in future commercial and noncommercial works.
- Post a copy of the paper in PDF that you submitted via BenchPress.
- Link to the journal site containing the final edited PDFs created by the publisher.
- Authors who published their papers under the "Author's Choice" option may post the final edited PDFs created by the publisher to their own/departmental/university Web sites immediately upon publication. All other authors may do so 12 months after publication.

EXCEPTION: If authors select the Author's Choice publishing option:

- The final version of the manuscript will be covered under the Creative Commons Attribution license (CC BY), the most accommodating of licenses offered. Click here for details.
- The final version of the manuscript will be released immediately on the publisher's website and PubMed Central.

Please note that authors must include the following citation when using material that appeared in an ASBMB journal:

"This research was originally published in Journal Name. Author(s). Title. . Year; Vol:pp-pp. © the American Society for Biochemistry and Molecular Biology."

For other parties using material for noncommercial use:

Other parties are welcome to copy, distribute, transmit and adapt the work — at no cost and without permission — for noncommercial use as long as they attribute the work to the original source using the citation above.

Examples of noncommercial use include:

- Reproducing a figure for educational purposes, such as schoolwork or lecture presentations, with attribution.
- Appending a reprinted article to a Ph.D. dissertation, with attribution.

For other parties using material for commercial use:

Navigate to the article of interest and click the "Request Permissions" button on the middle navigation bar. (See diagram at right.) It will walk you through the steps for obtaining permission for reuse.

Examples of commercial use by parties other than authors include:

- Reproducing a figure in a book published by a commercial publisher.
- Reproducing a figure in a journal article published by a commercial publisher.

Personal and Institutional Repositories:

- The "paper-in-press", ie, manuscript version of the article can be deposited at any time. The final, copyedited version of the article may not be deposited until 12 months after publication, unless the article is an Author's Choice article. Author's Choice articles may be deposited upon publication.
- An institution may deposit only articles published by individuals employed by or students attending the institution. The normal procedure is for the author to make the deposit.
- A link back to the article on the journal website should be provided.

Updated December 14, 2016

Title:	Endothelial Membrane Modulation by OxLDL: Molecular-Scale Effects of Oxidation Products on Model Membranes
Author:	Manuela A. Ayee,Elizabeth LeMaster,Belinda S. Akpa,Irena Levitan
Publication:	Biophysical Journal
Publisher:	Elsevier
Date:	16 February 2016

Review Order

Please review the order details and the associated terms and conditions.

No royalties will be charged for this reuse request although you are required to obtain a license and comply with the license terms and conditions. To obtain the license, click the Accept button below.

Licensed Content Publisher	Elsevier
Licensed Content Publication	Biophysical Journal
Licensed Content Title	Endothelial Membrane Modulation by OxLDL: Molecular-Scale Effects of Oxidation Products on Model Membranes
Licensed Content Author	Manuela A. Ayee,Elizabeth LeMaster,Belinda S. Akpa,Irena Levitan
Licensed Content Date	16 February 2016
Licensed Content Volume	110
Licensed Content Issue	3
Licensed Content Pages	1
Type of Use	reuse in a thesis/dissertation
Portion	figures/tables/illustrations
Number of figures/tables/illustrations	1
Format	both print and electronic
Are you the author of this Elsevier article?	Yes
Will you be translating?	No
Original figure numbers	Figure 5
Title of your thesis/dissertation	Synergistic effect of hemodynamic environment and dyslipidemia on endothelial biomechanics
Expected completion date	Jul 2017
Estimated size (number of pages)	150
Requestor Location	Elizabeth LeMaster 909 South Wolcott St. Rm 3100 CHICAGO, IL 60612 United States Attn: Elizabeth LeMaster
Publisher Tax ID	98-0397604
Total	0.00 USD

Edit Order Details

Edit Requestor Location This location may be used to determine your tax liability.

☑ I agree to these terms and conditions.

I understand this license is for reuse only and that no content is provided.

Customer Code (if supplied) APPLY

BACK DECLINE ACCEPT

Please click accept only once.